AD NUMBER

**AD913413**

LIMITATION CHANGES

TO:

**Approved for public release; distribution is unlimited.**

FROM:

**Distribution authorized to U.S. Gov't. agencies only; Test and Evaluation; SEP 1973. Other requests shall be referred to Naval Ship Research and Development Center, Bethesda, MD 20034.**

AUTHORITY

**USNSRDC Itr, 27 Aug 1976**

Report 4153

# NAVAL SHIP RESEARCH AND DEVELOPMENT CENTER

Bethesda, Md. 20034

ARCTIC SURFACE EFFECT VEHICLE PROGRAM

## PRELIMINARY PROPULSION AND LIFT-POWER TRADEOFF FOR A LARGE SURFACE EFFECT VEHICLE

by

Rolf K. Muench

Sponsored by

ADVANCED RESEARCH PROJECTS AGENCY
ARPA Order No. 1676
Program Code No. 0N10





PROPULSION AND AUXILIARY SYSTEMS DEPARTMENT
Annapolis

RESEARCH AND DEVELOPMENT REPORT

September 1973

Report 4153

Preliminary Propulsion and Lift-Power Tradeoff for a Large Surface Effect Vehicle

The Naval Ship Research and Development Center is a U. S. Navy center for laboratory effort directed at achieving improved sea and air vehicles. It was formed in March 1967 by merging the David Taylor Model Basin at Carderock, Maryland with the Marine Engineering Laboratory at Annapolis, Maryland.

Naval Ship Research and Development Center
Bethesda, Md. 20034

## MAJOR NSRDC ORGANIZATIONAL COMPONENTS

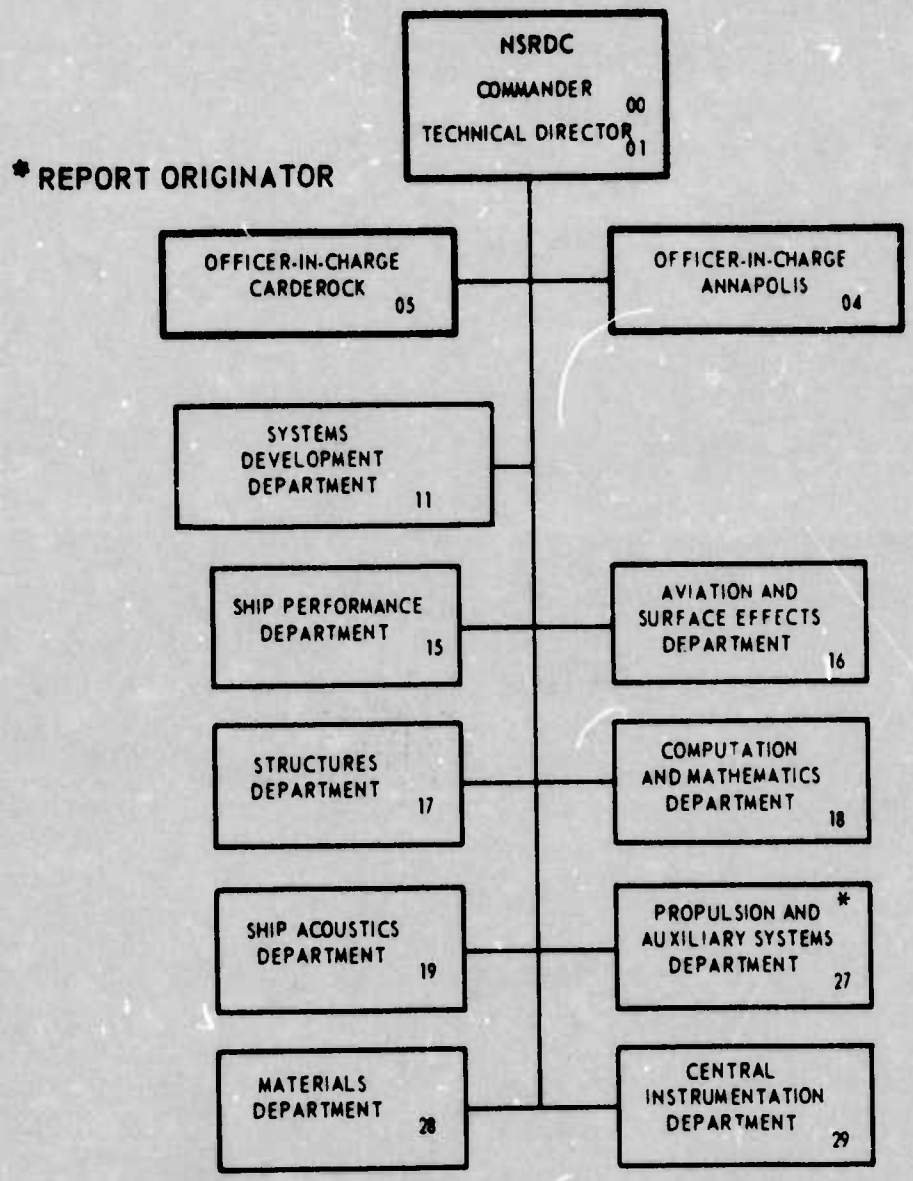

DEPARTMENT OF THE NAVY

NAVAL SHIP RESEARCH AND DEVELOPMENT CENTER

BETHESDA, MD. 20034

# ARCTIC SURFACE EFFECT VEHICLE PROGRAM

# PRELIMINARY PROPULSION AND LIFT-POWER TRADEOFF FOR A LARGE SURFACE EFFECT VEHICLE

by
Rolf K. Muench


This research was supported by the Advanced Research Projects Agency of the Department of Defense and was monitored by the Arctic SEV Program Office, Systems Development Department.



September 1973 27-497 Report 4153

## ABSTRACT

To determine the desirable speed and cushion pressure operating region of large surface effect vehicles, a propulsion and lift-power tradeoff study has been made for both overland and overwater operation. In addition, range has been examined as it is related to the associated fuel fraction and cargo-carrying capacity. The power tradeoff study examines the effect of the various drag components and efficiencies at the minimum power. The cargo-carrying study considers the effect of the available payload area and payload weight as a function of cushion pressure. The thrust margin study examines the impact on power requirement of the low-speed wave drag hump. The results generally indicate that cargo-carrying considerations restrict the maximum cushion pressure due to space and the maximum velocity due to cost consideration, while the overwater thrust margin study restricts the vehicle to low cushion pressure and high maximum velocity capability.

## ADMINISTRATIVE INFORMATION

This study was conducted for the Arctic Surface Effect Vehicle Program Office of the Naval Ship Research and Development Center through support provided by the Defense Advanced Research Projects Agency of the Department of Defense. The work was accomplished in the Gas Turbines Branch of the Power Systems Division, Propulsion and Auxiliary Systems Department under Work Unit 1-1130-272-20, ARPA Order 2251, Program Code 3N10.

TABLE OF CONTENTS

## NOTATION

| | |
|---|---|
| $b$ | Overall beam width (ft) |
| $c_F$ | Specific fuel consumption (lb/hph) |
| $C_c$ | Cost factor |
| $C_D$ | Aerodynamic drag coefficient = $D_A/qS_c$ |
| $C_M$ | Cushion momentum coefficient |
| $C_p$ | Cushion pressure coefficient |
| $C_T$ | Thrust coefficient = $T_t/qS$ |
| $d_p$ | Propeller diameter (ft) |
| $d_f$ | Lift fan diameter (ft) |
| $D$ | Total drag (lb) |
| $D_A$ | Aerodynamic drag (lb) |
| $D_M$ | Momentum drag (lb) |
| $D_s$ | Specific diameter of lift fan (ft) |
| $D_T$ | Total drag (lb) |
| $D_W$ | Wave drag (lb) |
| $\mathcal{D}_c$ | Cushion discharge coefficient |
| $E$ | Energy (hph) |
| $Fr$ | Froude number = $V/\sqrt{\ell g}$ |
| $g$ | Acceleration of gravity = 32.2 ft/s$^2$ |
| $k$ | Speed parameter = $\frac{1/2\rho V^2}{p_c}$ |
| $k_c$ | Speed parameter at cruise |
| $k_G$ | Speed parameter at the initial velocity and gross weight |
| $K_f$ | Fan area parameter |
| $\ell$ | Overall craft length (ft) |
| $m_H$ | Thrust margin at wave drag hump |
| $m_C$ | Thrust margin at cruise conditions |

| | |
|---|---|
| $\dot{m}$ | Mass flow rate (slugs/s) |
| $N_s$ | Specific speed of lift fan |
| $p_c$ | Cushion pressure ($lb/ft^2$) |
| $p_c/\ell$ | Cushion pressure/cushion length ratio ($lb/ft^3$) |
| $p$ | Static pressure, ($lb/ft^2$) |
| $p_f$ | Peripheral fan exit static pressure ($lb/ft^2$) |
| $p_f^o$ | Fan exit total pressure ($lb/ft^2$) |
| $p_s^o$ | Supply total pressure ($lb/ft^2$) |
| $p_x$ | Reference pressure ($lb/ft^2$) |
| $P_L$ | Lift power (ft-lbf/s) |
| $P_T$ | Total power (ft-lbf/s) |
| $P_{PR}$ | Propulsion power (ft-lbf/s) |
| $P/W_G V$ | Specific power |
| $q$ | Dynamic pressure ($lb/ft^2$) = $\frac{1}{2} \rho V^2$ |
| $Q$ | Fan volume flow rate of air ($ft^3/s$) |
| $R$ | Range (nautical miles) |
| $S_c$ | Cushion area ($ft^2$) |
| $S_E$ | Engine platform area ($ft^2$) |
| $S_f$ | Fan platform area ($ft^2$) |
| $S_{fr}$ | Fan rotor area ($ft^2$) |
| $S_g$ | Peripheral daylight gap area ($ft^2$) |
| $t$ | Time (s) |
| $t_j$ | Peripheral-jet thickness (ft) |
| $T$ | Propeller thrust (lb) |
| $T_C$ | Propeller thrust at cruise (lb) |
| $T_{CM}$ | Maximum propeller thrust at cruise (lb) |
| $T_H$ | Propeller thrust at wave drag hump (lb) |

| | |
|---|---|
| $T_S$ | Propeller thrust static (lb) |
| $V$ | Vehicle speed relative to surface (kn) |
| $V_C$ | Vehicle cruise speed, relative to surface (kn) |
| $V_e$ | Characteristic cushion escape velocity (ft/s) |
| $V_H$ | Craft speed relative to surface at hump (kn) |
| $V_I$ | Initial vehicle velocity (kn) |
| $V_M$ | Maximum craft speed relative to surface (kn) |
| $V_T$ | Fan tip speed (ft/s) |
| $V_\infty$ | Free stream velocity (ft/s) |
| $w_M$ | Machinery specific weight (lb/hp) |
| $W$ | Vehicle weight (lb) |
| $W_{EQ}$ | Equipment and miscellaneous weight (lb) |
| $W_F$ | Fuel weight (lb) |
| $W_{FP}$ | Fuel and power plant weight (lb) |
| $W_G$ | Gross weight (all-up weight) (lb) |
| $W_L$ | Lift system weight (lb) |
| $W_M$ | Machinery weight (lb) |
| $W_P$ | Payload weight (lb) |
| $W_{PR}$ | Propulsion system weight (lb) |
| $W_S$ | Structural weight (lb) |
| $\overline{W}_E$ | Energy specific weight including tankage (lb/hph) |
| $\overline{W}_L$ | Lift system specific weight (lb/hp) |
| $\overline{W}_{PR}$ | Propulsion system specific weight (lb/hp) |
| $X_{ER}$ | Equipment fraction = $W_{EQ}/W_G$ |
| $X_F$ | Fuel fraction = $W_F/W_G$ |
| $X_{FP}$ | Fuel plus power plant fraction = $W_{FP}/W_G$ |
| $X_M$ | Machinery fraction = $W_M/W_G$ |

| | |
|---|---|
| $X_P$ | Payload fraction = $W_P/W_G$ |
| $X_S$ | Structural fraction = $W_S/W_G$ |
| $\beta$ | Lift-propulsion specific weight ratio |
| $\eta_f$ | Fan efficiency |
| $\eta_{fd}$ | Fan-duct efficiency |
| $\eta_{PR}$ | Propulsion efficiency |
| $\phi$ | Lift-propulsion system specific weight ratio $W_L/W_{PR}$ |
| $\pi_C$ | Cargo loading ($lb/ft^2$) |
| $\pi_E$ | Engine area parameter ($ft^2/hp$) |
| $\theta$ | Jet inclination angle (from vertical) (degrees) |
| $\rho$ | Air mass density ($slugs/ft^3$) |
| $\rho_W$ | Water mass density ($slugs/ft^3$) |
| $\ell/b$ | Craft length/beam ratio |

Subscripts

| | |
|---|---|
| C | Cruise |
| p-j | Peripheral-jet-type cushion |
| p | Plenum-type cushion |
| I | Initial conditions |
| G | Gross weight conditions |
| x | Reference condition |
| FP | Free propeller |
| SP | Shrouded propeller |

## INTRODUCTION

During the conceptual design of any vehicle, one of the first problems which must be faced is the power requirement, usually as a function of other yet undefined vehicle parameters. For established vehicle systems, this means following a standard procedure which is aided by design guidelines. Unfortunately, this is not the case for any vehicle using the air cushion concept. For this relatively recent concept, very little guidance can be found from previous approaches. In addition, the power plant for this vehicle must supply power for both lift and propulsion.

It is therefore not surprising that any analyis of the power requirement raises more questions than it answers. In an earlier report based on this study,[1] minimum power and vehicle fuel fraction were addressed. This raised the question of cushion pressure limits, since power optimizes at relatively high cushion pressure. Therefore, the present report will attempt to treat additional areas. The three areas which will be discussed are: (1) propulsion and lift-power tradeoff and the associated fuel fraction, (2) cargo-loading considerations, and (3) thrust margin during overwater operation.

The propulsion and lift-power tradeoff is similar to the earlier work.[1] Some of the parameters have been redefined to make a more meaningful presentation. The question of the fuel fraction will be treated in some detail. For instance, the fuel fraction will be evaluated under three conditions: (1) constant velocity, (2) constant-propulsion/constant-lift power, and (3) constant total power/constant daylight clearance. The results will be compared with Breguet range equation results. An approximate method for the two constant power cases is developed in appendix A.

A speed-range tradeoff at constant fuel fraction is not necessarily the best approach. Power increases with speed which, in turn, increases power plant weight. It might therefore be more meaningful to perform the speed-range tradeoff at constant fuel plus power plant fraction. This consideration will be treated in the Power-Energy section. The name "power-energy" is derived from the manner in which this tradeoff will be presented.

Usually the payload parameter is a density such as pounds of payload per unit payload volume. This is certainly acceptable for a bulk carrier but not for a surface effect vehicle. High-speed vehicles require a cargo handling system which is compatible with their short transit time. For this reason,

---

[1] Superscripts refer to similarly numbered entries in the Technical References at the end of the text.

containers and pallets are likely to be used, to prepackage the cargo for rapid loading and unloading. Furthermore, if military hardware is transported, it may include battle-ready tracked or wheeled vehicles. Even military supplies are prepackaged in vans or on pallets. Scientific cargoes would also be contained in vans, which might even be self-sufficient to the point where they could be deposited on the ice pack. It is therefore expected that the Arctic surface effect vehicle (SEV) will carry containerized, palletized, tracked, or wheeled cargo which can be unloaded quickly. In this case, it is more expedient to characterize the payload in terms of cargo weight per unit cargo area or as referred to in this report as "cargo loading."

The thrust margin for overwater operation is an important consideration, even for a vehicle which operates mostly over Arctic land and ice. The vehicle must operate with acceptable performance over the small amount of open water it encounters in the Arctic region and the extensive ocean area it will encounter during its ferry missions from a more temperate climate. This requires that the vehicle have an acceptable thrust margin at the wave drag hump the vehicle encounters at a relatively low speed. It would be unfortunate if the vehicle did not have a sufficient thrust margin to surpass the wave drag hump at 20 knots in order to reach its 100-knot design speed.

The objective of this report is therefore to generally treat these five considerations and then to summarize them and to determine the operating regime of an Arctic SEV in terms of velocity and cushion pressure.

## ANALYSIS

This section summarizes the theory needed for the five areas mentioned in the Introduction. In the Propulsion and Lift-power subsection, the necessary equations for the tradeoff are developed. This section parallels the analysis of earlier work,[1] but it treats both the optimistic peripheral-jet and more realistic plenum-cushion assumption. This analysis is augmented in the subsequent subsections for relationships between cargo loading, thrust margin, and cushion pressure.

### PROPULSION AND LIFT POWER

To minimize the amount of data, the attempt will be made to employ nondimensional groups of terms whenever possible. One of the most important dimensionless parameters in this analysis is the speed parameter (k) defined in the following manner:

$$k = \frac{1/2\rho V^2}{p_c}. \qquad (1)$$

This parameter has been used previously by Mantle[2] in the same form but called pressure number and by Chaplin and Ford[3] in a velocity ratio form ($V/\sqrt{p_c}$). Barrett, et al,[4] refer to the speed parameter (k) as the dynamic head coefficient. The inverse of the speed parameter has also been used, but it was awkward to relate this inverse to the velocity.[1]

Under the assumption that the vehicle gross weight is supported on a rectangular cushion of length ($\ell$) and beam (b) (see figure 1), the speed parameter (k) can be related to the vehicle weight in the following manner:

$$k = \frac{1/2\rho V^2}{p_c} = \frac{\ell b q}{W} = \frac{\ell^2 q}{W\ell/b} \quad . \tag{2}$$

This assumes that the vehicle aerodynamic lift and the vertical cushion momentum contribution are negligible compared to the cushion lift. A general expression including the aerodynamic lift could also be written if required. It should be noted here that the vehicle velocity, weight, and therefore cushion pressure might change with time as fuel is used up or speed changed.

The power needed to propel the vehicle at a given speed (V) with a total drag ($D_T$) is the propulsion power ($P_{PR}$). The non-dimensional form of this is the specific propulsion power ($P_{PR}/WV$). The total vehicle drag is assumed to consist of the vehicle aerodynamic and cushion momentum drag. The specific propulsion power ($P_{PR}/WV$) is then equal to:

$$\frac{P_{PR}}{WV} = \frac{DV}{\eta_{PR}} \frac{1}{WV} = \frac{D}{W} \frac{1}{\eta_{PR}} \quad . \tag{3}$$

Wave drag will be included in a later section, when performance over water will be examined.

The aerodynamic drag to weight ratio ($D_A/W$) needed for the above equation is:

$$\frac{D_A}{W} = \frac{C_D S_c q}{W} = C_D k \quad , \tag{4}$$

where the drag coefficient is based on the cushion area rather than the usual frontal area.

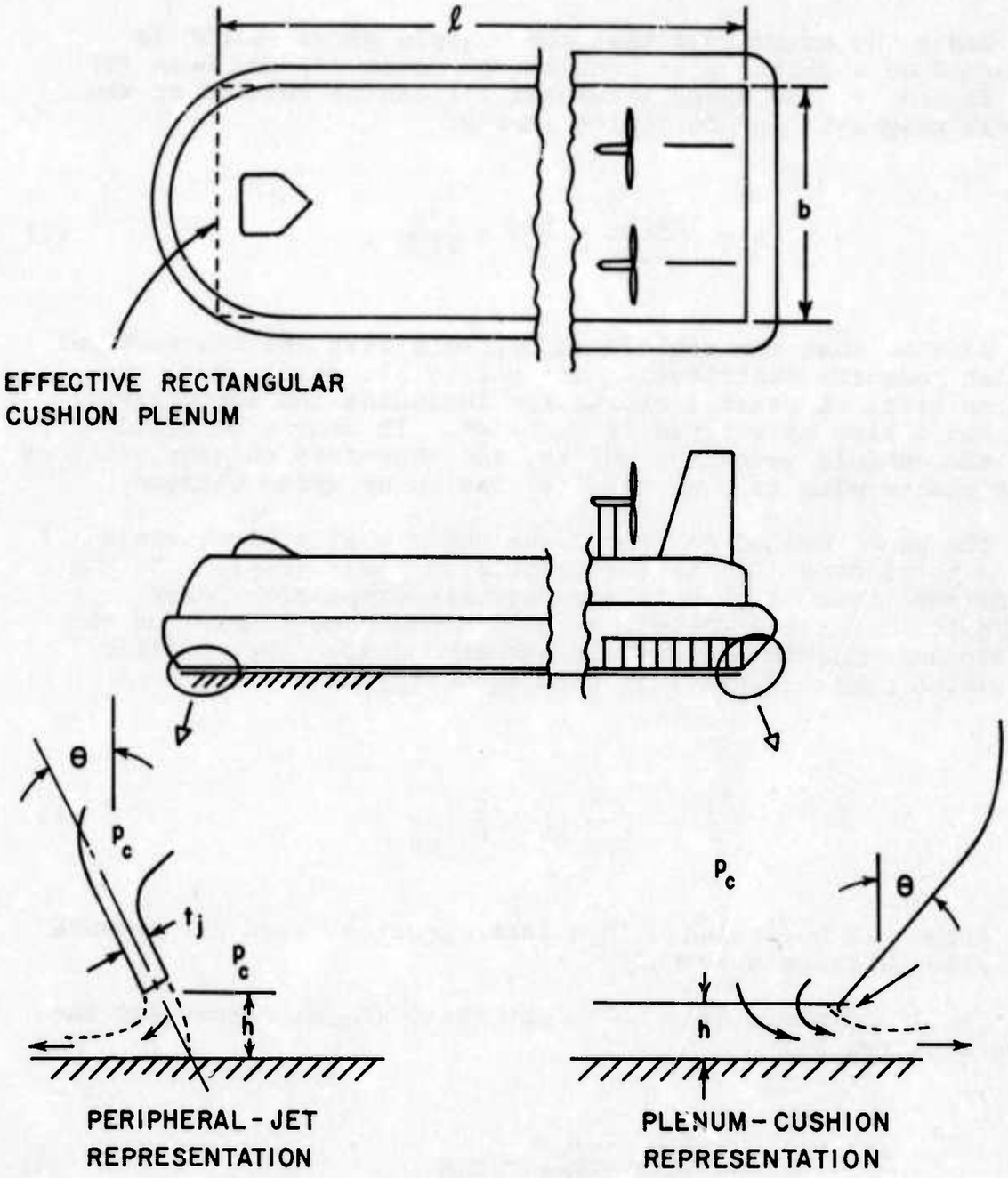


Figure 1
Surface Effect Vehicle

The cushion momentum drag is due to the deceleration of the cushion airflow from some given velocity relative to the vehicle to zero or:

$$\frac{D_M}{W} = \frac{\dot{m}_C V}{W} \quad .$$

The cushion airflow can now be expressed in terms of the air cushion pressure ($p_c$), the area due to the daylight clearance ($S_g$), and a discharge coefficient ($\mathcal{D}_c$):

$$\dot{m}_C = \mathcal{D}_c \rho V_e S_g = \mathcal{D}_c \sqrt{2\rho p_c}\ S_g, \tag{5}$$

where the characteristic cushion escape velocity ($V_e$) was related to the cushion pressure by Bernoulli s equation. Combining the two equations results in the following equation for the momentum drag to weight ratio in terms of the pressure parameter:

$$\frac{D_M}{W} = \frac{\mathcal{D}_c \sqrt{2\rho p_c}}{p_c} \frac{S_g}{S_c} V = 2\mathcal{D}_c \frac{S_g}{S_c} k^{1/2}. \tag{6}$$

Usually the daylight clearance area ($S_g$) is expressed in terms of an average daylight clearance (h) (see figure 1). Thus, the above area ratio can be rewritten in the following form:

$$\frac{S_g}{S_c} = \frac{2h(\ell + b)}{\ell b} = 2\,\frac{h}{\ell}\,(\ell/b + 1) \quad . \tag{7}$$

The above discharge ceofficient ($\mathcal{D}$) is a function of the type of cushion assumed. It can range from the low discharge coefficient possible with the theoretical peripheral-jet air cushion to a more realistic plenum-chamber type of air cushion (see figure 1). To show this range of possibilities, the necessary equation for both cushion models will be shown after the development of the lift-power equations below.

The total lift power can be determined from the power into the lift fan system:

$$P_L = \frac{p_f^o \dot{m}_c}{\rho \eta_f}$$

where $p_f^o$ is the total pressure developed by the fan and $\eta_f$ is the fan efficiency. Converting the lift power to specific power and substituting the previously shown cushion mass flow equation and the daylight clearance/cushion area ratio equation results in:

$$\frac{P_L}{WV} = \frac{\mathcal{D}_c}{\eta_f} \frac{p_f^o}{p_c} \sqrt{\frac{p_c}{1/2\rho V^2}} \frac{S_g}{S_c} = 2 \frac{\mathcal{D}_c}{\eta_f} \frac{1}{p_c/p_f^o} \frac{h}{\ell} (\ell/b + 1) \frac{1}{k^{1/2}} . \quad (8)$$

In addition to the discharge coefficient ($\mathcal{D}_c$), the cushion fan pressure ratio ($p_c/p_f^o$) is also a function of the air cushion type.

To calculate the cushion discharge coefficients and the cushion fan pressure ratio for both the plenum and peripheral-jet-type cushion, it is best to follow the development given by Chaplin and Ford.[3] The discharge coefficient for the peripheral-jet cushion, as derived by Chaplin and Ford, is:

$$\mathcal{D}_c = \overline{\mathcal{D}}_c \left\{ \tanh \left[ \frac{t_j/h}{2\overline{\mathcal{D}}^2 (1 + \sin \theta)} \right] \right\}^{1/2} ,$$

Where $\overline{\mathcal{D}}_c$ is the discharge coefficient of an equivalent two-dimensional orifice similar to the discharge from a plenum type cushion, or:

$$\overline{\mathcal{D}}_c = 1/2 \left[ 1 + \frac{\cos \theta}{\frac{\pi + 2}{\pi - 2} (1 + \sin \theta) - \sin \theta \cos \theta} \right] .$$

In addition, $t_j/h$ is the jet thickness daylight clearance ratio and $\theta$ is the peripheral jet inclination angle, as shown in figure 1.

The above discharge coefficient is a slight function of $\theta$, decreasing from 0.61 for $\theta = 90°$ to 0.50 for $\theta = 0°$. The equation for the discharge coefficient can be simplified by using an average discharge coefficient of 0.55, resulting in:

$$\mathcal{D}_c \Big|_{p\text{-}j} = 0.55 \left[ \tanh \frac{1.66\ t_j/h}{1 + \sin \theta} \right]^{1/2} \quad (9a)$$

for the discharge coefficient of a peripheral-jet-type cushion. For the plenum-type cushion, the discharge coefficient is simply:

$$C_d\Big|_p = 0.55. \tag{9b}$$

The cushion fan pressure ratio ($p_c/p_f^o$) for a peripheral-jet cushion can be expanded in the following manner:

$$\frac{p_c}{p_f^o} = \frac{p_c}{p_s^o}\,\frac{p_s^o}{p_f^o}.$$

The first ratio on the right side is determined from an analysis of the flow out of the peripheral jet. A relatively simple approach (referred to as the exponential theory[3]) gives:

$$\frac{p_c}{p_s^o} = 1 - e^{-2t_j/h(1 + \sin\theta)}.$$

The second ratio is just an efficiency of collecting the airflow from the fans and ducting it to the periphery or:

$$\frac{p_s^o}{p_f^o} = \eta_f.$$

In summary, the pressure ratio ($p_c/p_f^o$) for the peripheral-jet-type cushion can be expressed as:

$$\frac{p_c}{p_f^o}\Big|_{p\text{-}j} = \eta_D\left[1 - e^{-2t_j/h(1 + \sin\theta)}\right]. \tag{10a}$$

The pressure ratio for the plenum-type cushion can be expressed in the following manner:

$$\frac{p_c}{p_f^o} = \frac{p_x}{p_f^o} \frac{p_c}{p_x}$$

where $p_x$ is the pressure at some convenient point between the fan and the cushion. If the fan is located in its own plenum, then the fan plenum pressure would be a convenient reference point. The two pressure ratios in the above equations will be replaced by efficiencies. The first pressure ratio ($p_x/p_f^o$) will be referred to as the fan-duct efficiency ($\eta_{fd}$), expressing the loss in pressure between the fan exit and the arbitrary reference point. The second pressure ratio ($p_c/p_x$) is a cushion efficiency ($\eta_c$), representing the pressure loss between the reference point and the cushion. The equation for the cushion fan pressure ratio for the plenum-type cushion is then:

$$\left.\frac{p_c}{p_f^o}\right|_p = \eta_{fd}\, \eta_c \,. \tag{10b}$$

Summarizing the above equations for the total specific power ($P_T/WV$) and redefining terms:

$$\frac{P_T}{WV} = \frac{C_D}{\eta_{PR}} k + \frac{C_M}{\eta_{PR}} k^{1/2} + \frac{C_M C_P}{k^{1/2}} \tag{11a}$$

where the cushion momentum and cushion pressure coefficients are defined, respectively, in the following manner:

$$C_M = 4\mathcal{D}_c \frac{h}{\ell} (\ell/b + 1), \tag{11b}$$

$$C_p = \frac{1}{2\eta_f\, p_c/p_f^o} \,. \tag{11c}$$

The various coefficients as their names imply can be identified with aerodynamic drag ($C_D$), momentum drag ($C_M$), and lift system power, since power is equal to mass flow times pressure ($C_M C_p$).

VEHICLE FUEL FRACTION

Now that the total specific power has been defined, the question of fuel requirement can be attacked. The Breguet range

equation is not strictly correct, since the total specific power ($P_T/WV$) does not necessarily remain constant as the vehicle uses up fuel. Therefore, a range equation will be developed from basic considerations. The incremental fuel consumed during an incremental time interval is:

$$dW_F' = \frac{P_T}{WV} c_F WV \, dt, \tag{12}$$

where $c_F$ is the specific fuel consumption of the power plant which is usually expressed in pounds of fuel per shaft horsepowerhour. The prime will be used to differentiate the above fuel weight (fuel consumed during some time interval) from the fuel weight carried by the vehicle. The change in fuel weight equals the decrease in vehicle weight, since the fuel is carried on board, or:

$$dW_F' = -dW.$$

The range is equal to:

$$dR = V dt.$$

Substituting these two expressions into equation (12), rearranging, and integrating from the initial weight which is assumed to equal the vehicle gross weight ($W_G$) to its final value ($W_G - W_F$) yields:

$$R = -\frac{1}{c_F} \int_{W_G}^{W_G - W_F} \frac{1}{\frac{P_T}{WV}} \frac{dW}{W}$$

where $W_F$ is the fuel weight carried by the vehicle. This equation will result in the Breguet range equation under the assumption that the total specific power is constant:

$$R = - \frac{\ln(1 - X_F)}{C_F \left(\frac{P_T}{WV}\right)} ,$$

where $X_F$ is the vehicle fuel fraction ($W_F/W_G$). This equation can be cast into a more systematic form:

$$X_F = 1 - e^{-RC_F \frac{P_T}{WV}} . \qquad (13)$$

The exponent in the above equation determines the fuel fraction of a vehicle and will therefore be referred to as the fuel fraction parameter. Analysis using different assumptions will yield different results which can still be correlated in terms of this fuel fraction parameter. In that case, the weight is equal to the gross weight ($W_G$) and the velocity equal to the initial velocity ($V_I$). It should be noted here that the vehicle gross or all-up weight ($W_G$) can only be realized at the beginning of the mission. At any other time the vehicle weight is W, or more precisely:

$$W = W_G - W_F' .$$

Similarly the initial velocity ($V_I$) will be defined as the velocity at the beginning of the mission.

One simple expression for the fuel fraction can be derived under the assumption of constant velocity, but first it will be of interest to write a general differential equation for the fuel fraction in terms of the independent fuel fraction parameter. From equation (12) and subsequent equations, the following equation can be written:

$$\frac{dW}{W_G} = - \frac{\left(\frac{P_T}{WV}\right)}{\left(\frac{P_{TI}}{W_G V_I}\right)} \frac{W}{W_G} d\left[C_F R \left(\frac{P_{TI}}{W_G V_I}\right)\right] . \qquad (14)$$

This equation can be rewritten in the following differential form:

$$\frac{dX_F}{d\left[C_F R \left(\frac{P_{TI}}{W_G V_I}\right)\right]} = \frac{\left(\frac{P_T}{WV}\right)}{\left(\frac{P_{TI}}{W_G V_I}\right)} (1 - X_F) . \qquad (15)$$

Under the assumption that the velocity is constant, the specific power equation (11) can be rewritten in the following form:

$$\frac{P_T}{WV} = \frac{C_D}{\eta_{PR}} k_G \left(\frac{W}{W_G}\right)^{-1} + \frac{C_M}{\eta_{PR}} k_G^{1/2} \left(\frac{W}{W_G}\right)^{-1/2} + \frac{C_M C_P}{k_G^{1/2}} \left(\frac{W}{W_G}\right)^{1/2}, \qquad (16)$$

where the special speed parameter ($k_G$) is the value of the speed parameter at the beginning of the mission when the weight of the vehicle is equal to its gross weight or:

$$k_G = \frac{1/2\ \rho\ V_I^2\ S_C}{W_G}.$$

This is related to the speed parameter at any other speed and weight by:

$$k_G = k\ \frac{W}{W_G} \left(\frac{V}{V_I}\right)^{-2}. \qquad (17)$$

Substituting equation (16) into equation (15) results in the following differential equation which can be easily integrated with the aid of numerical methods:

$$\frac{dX_F}{d\left[C_F R \left(\frac{P_{TI}}{W_G V_I}\right)\right]} = \left[\frac{C_D k_G}{\eta_{PR}} + \frac{C_M k_G^{1/2}}{\eta_{PR}} (1 - X_F)^{1/2} + \frac{C_M C_P}{k_G^{1/2}} (1 - X_F)^{3/2}\right] \Bigg/ \left(\frac{P_{TI}}{W_G V_I}\right). \qquad (18)$$

The above equation is actually simpler to interpret than it first appears. The individual terms in the numerator on the right-hand side divided by the denominator represent the fraction of the total power due to the aerodynamic, momentum, and lift considerations, respectively. The fuel fraction is therefore only a function of the fuel fraction parameter and the initial proportioning of the total power.

Constant velocity was not the only assumption utilized in the above derivation. In writing equation (16), it was also

assumed that $C_D$, $C_M$, $C_P$, and $\eta_{PR}$ remain constant. Holding the momentum coefficient ($C_M$) constant implies that the daylight clearance (h) remains constant.

One can easily argue that a constant velocity assumption is not a very representative case, since the power will have to be cut back as the vehicle uses up fuel. Therefore, a constant total power assumption might represent an interesting case. It is not possible to approach this derivation in the manner shown above, since the velocity ratio ($V/V_I$) cannot be eliminated from the differential equation. Another approach is to integrate equation (14) in the following form:

$$c_F R \frac{P_{TI}}{W_G V_I} = -\int_1^{\frac{W_G - W_F}{W_G}} \frac{\left(\frac{P_{TI}}{W_G V_I}\right)}{\left(\frac{P_T}{WV}\right)} \frac{dW}{W_G} \Big/ \frac{W}{W_G} = -\int_1^{\frac{W_G - W_F}{W_G}} \left(\frac{V}{V_I}\right) \frac{dW}{W_G} \qquad (19)$$

and then substitute for $W/W_G$ in terms of $V/V_I$. The easiest case to handle is the subcase of constant-propulsion/constant-lift power. This is the case of a separated lift and propulsion system, where decreasing vehicle weight is taken in terms of increasing daylight gap and changing velocity.

The general equation of the specific propulsion power is:

$$\frac{P_{PR}}{WV} = \frac{C_D}{\eta_{PR}} k + \frac{C_M}{\eta_{PR}} k^{1/2} . \qquad (20)$$

It should be remembered that the momentum coefficient is not constant but related to the vehicle weight via the specific lift-power equation:

$$\frac{P_L}{WV} = \frac{C_M C_P}{k^{1/2}} . \qquad (21)$$

This equation can be rewritten in terms of initial values for the specific lift power ($P_{LI}/W_G V_I$), speed parameter ($k_G$), and weight ratio ($W/W_G$):

$$\frac{P_{LI}}{W_G V_I} = \frac{C_P C_M}{k_G^{1/2}} \left(\frac{W}{W_G}\right)^{3/2} = \text{constant.} \qquad (22)$$

Since $C_M = C_{MI}$ when $W = W_G$, $V = V_I$, and $k = k_G$, then:

$$\frac{C_M}{C_{MI}} = \left(\frac{W}{W_G}\right)^{-3/2} . \qquad (23)$$

Now equation (20) can be rewritten similarly to equation (22), and substituting for $C_M$ from equation (23):

$$\frac{P_{PR}}{W_G V_I} = \frac{C_D}{\eta_{PR}} k_G \left(\frac{V}{V_I}\right)^3 + \frac{C_{MI}}{\eta_{PR}} k_G^{1/2} \left(\frac{W}{W_G}\right)^{-1} \left(\frac{V}{V_I}\right)^2 . \qquad (24)$$

This equation is linear in the weight ratio ($W/W_G$) and can therefore easily be solved.

$$\frac{W}{W_G} = \frac{\left(\frac{V}{V_I}\right)^2}{1 + \frac{C_D}{C_{MI}} k_G^{1/2} \left[1 - \left(\frac{V}{V_I}\right)^3\right]} . \qquad (25)$$

This equation indicates that the velocity ratio ($V/V_I$) decreases with decreasing weight ratio ($W/W_G$), since, at constant lift power, the daylight clearance increases, and therefore the momentum drag also increases with decreasing weight ratio ($W/W_G$). The fuel fraction parameter [$R_{CF}(P_T/WV)$] can now be found by differentiating equation (25) with respect to ($V/V_I$). Substituting into equation (19) and integrating between 1.0 and some reference velocity ratio ($V_X/V_I$), the result is:

$$R_{C_F}\left(\frac{P_{TI}}{W_G V_I}\right) = 1 - \frac{\left(\frac{V_X}{V_I}\right)^3}{1 + \frac{C_D}{C_{MI}} k_G^{1/2} \left[1 - \left(\frac{V_X}{V_I}\right)^3\right]}$$

$$- \frac{1}{3} \frac{C_{MI}}{C_D k_G^{1/2}} \ln \left\{1 + \frac{C_D}{C_M} k_G^{1/2} \left[1 - \left(\frac{V_X}{V_I}\right)^3\right]\right\} , \qquad (26)$$

where the velocity ratio ($V_X/V_I$) is also used to relate the above equation to the fuel fraction. The fuel fraction is calculated from equation (25):

$$X_F = 1 - \frac{W}{W_G} = 1 - \frac{\left(\frac{V_X}{V_I}\right)^2}{1 + \frac{C_D}{C_M} k_G^{1/2} \left[1 - \left(\frac{V_X}{V_I}\right)^3\right]} . \qquad (27)$$

In this case the fuel fraction is only a function of the fuel fraction parameter and the initial aerodynamic to momentum drag ratio ($C_D k_G^{1/2}/C_M$) or aerodynamic/momentum power ratio.

The constant total power/constant daylight clearance case cannot be handled in the manner shown above. This case is of interest since it represents an integrated system which requires power to be shifted from the lift system to the propulsion system with decreasing vehicle weight. Upon further examination the above analysis (constant propulsion and lift power) shows that the resulting changes in the vehicle velocity are small and therefore a valid solution can be found by linearizing the velocity ratio ($V/V_I$). Appendix A shows the derivation of these two cases under this assumption. The result for the constant-propulsion and lift-power case is:

$$Rc_F\left(\frac{P_{TI}}{W_G V_I}\right) \cong X_F + \frac{1}{3\left(\frac{C_D}{C_M} k_G^{1/2}\right)} \left\{ X_F + \frac{3\left(\frac{C_D}{C_M} k_G^{1/2}\right) + 2}{3\left(\frac{C_D}{C_M} k_G^{1/2}\right)} \right.$$

$$\left. \times \ln\left[1 - \frac{3\left(\frac{C_D}{C_M} k_G^{1/2}\right)}{3\left(\frac{C_D}{C_M} k_G^{1/2}\right) + 2} X_F\right] \right\} \qquad (28a)$$

and

$$\frac{V_X}{V_I} = 1 - \frac{X_F}{3\frac{C_D}{C_M} k_G^{1/2} (1 - X_F) + 2} . \qquad (28b)$$

It is shown in appendix A that this approximation agrees quite well with the previous derivation. The results for the constant total power/constant daylight clearance case are:

$$c_F R \frac{P_{TI}}{W_G V_I} = X_F + \frac{1}{4} \frac{1 + 3 \frac{C_P \eta_{PR}}{k_G}}{2 + 3 \frac{C_D}{C_M} k_G^{1/2}} X_F^2 \left[ 1 + \frac{1}{2} \left( \frac{1}{2 + 3 \frac{C_D}{C_M} k_G^{1/2}} \right.\right.$$

$$\left.\left. - \frac{1 + 3 \frac{C_D}{C_M} k_G^{1/2}}{2 + 3 \frac{C_D}{C_M} k_G^{1/2}} \frac{1 + 3 \frac{C_P \eta_{PR}}{k_G}}{2 + 3 \frac{C_P}{C_M} k_G^{1/2}} + \frac{1}{4} \frac{1 - 3 \frac{C_P \eta_{PR}}{k_G}}{1 + 3 \frac{C_P \eta_{PR}}{k_G}} \right) X_F \right] \quad (29a)$$

and

$$\frac{V}{V_I} = 1 + \frac{1}{2} \frac{1 + 3 \frac{C_P \eta_{PR}}{k_G}}{2 + 3 \frac{C_D}{C_M} k_G^{1/2}} X_F + \left[ 1 + \frac{3}{4} \left( \frac{1}{2 + 3 \frac{C_D}{C_M} k_G^{1/2}} \right.\right.$$

$$\left.\left. - \frac{1 + 3 \frac{C_D}{C_M} k_G^{1/2}}{2 + 3 \frac{C_D}{C_M} k_G^{1/2}} \frac{1 + 3 \frac{C_P \eta_{PR}}{k_G}}{2 + 3 \frac{C_D}{C_M} k_G^{1/2}} + \frac{1}{4} \frac{1 - 3 \frac{C_P \eta_{PR}}{k_G}}{1 + 3 \frac{C_P \eta_{PR}}{k_G}} \right) X_F \right]. \quad (29b)$$

Equations (28) which is an approximation of equation (27), contain the same ratio of initial aerodynamic drag to momentum drag. Equations (29), which do not require that the lift power remain constant, contain the additional lift to momentum/power ratio ($C_P \eta_{PR}/k_G$) similar to equation (18).

POWER-ENERGY

The above fuel fraction analysis will allow the examination of range as a function of vehicle fuel fraction or vice versa. It might also be of interest to examine the range as a function

of vehicle power plant specific weight and energy content of the fuel.[5] These two parameters are basic; they are essentially determined by the type of power plant or fuel. The analysis is essentially an extension of the above fuel fraction analysis and a modification of the analysis covering the SEV case.[5] The basis for this power-energy analysis is the energy and power per unit power plant and fuel weight. This energy/weight ratio in horsepowerhours per pound is related to the total power ($P_T$) and time ($t_x$) by:

$$\frac{E}{W_{FP}} = \frac{1}{W_{FP}} \int_0^{t_x} P_T \, dt. \tag{30}$$

The total power is not necessarily constant, and the above equation cannot be integrated. Recalling equation (12), which gives the weight change due to burning up of fuel:

$$dW_F' = c_F P_T \, dt.$$

Substituting this equation into equation (30) for $P_T dt$ yields:

$$\frac{E}{W_{FP}} = \frac{1}{W_{FP}} \int_0^{W_F} \frac{dW'}{c_F} F ,$$

which can be integrated under the assumption that the specific fuel consumption is constant to yield:

$$\frac{E}{W_{FP}} = \frac{1}{c_F} \frac{W_F}{W_{FP}} = \frac{1}{c_F} \frac{X_F}{X_{FP}} . \tag{31}$$

This then relates the previous fuel fraction analysis with the propulsion plant energy/weight ratio. The equation represents the vehicle requirement since it is generally a function of vehicle-related parameters.

The power plant requirement is obtained from a summation of the fuel weight, propulsion, and lift power plant weight, or:

$$W_{FP} = W_F + W_{PR} + W_L = E\bar{W}_E + \bar{W}_{PR}P_{PR} + \bar{W}_L P_L, \qquad (32)$$

where the three specific weights are:

$\bar{W}_E$ = energy specific weight including tankage, lb/hph*

$\bar{W}_{PR}$ = propulsion system specific weight, lb/hp

$\bar{W}_L$ = lift system specific weight, lb/hp.

Usually the lift system is heavier than the propulsion system, and therefore the following factor will be introduced:

$$\beta = \frac{\bar{W}_L}{\bar{W}_{PR}} .$$

Substituting this into equation (32) and eliminating the lift power with the aid of the total power yields:

$$W_{FP} = \bar{W}_E E + \left[ \frac{P_{PR}}{P_T} + \left( 1 - \frac{P_{PR}}{P_T} \right) \beta \right] \bar{W}_{PR} P_T ,$$

which finally can be written in the form:

$$\frac{E}{W_{FP}} = \frac{1}{\bar{W}_E} + \left[ \frac{P_{PR}}{P_T} + \left( 1 - \frac{P_{PR}}{P_T} \right) \beta \right] \frac{\bar{W}_{PR}}{\bar{W}_E} \frac{P_T}{W_{FP}} , \qquad (33)$$

where the propulsion/total power ratio is strictly a function of the speed parameter ($k_G$). Simple layouts, such as shown in figure 2, and preliminary performance and weight calculations have shown that the propulsion system specific weight ($\bar{W}_{PR}$) can be as light as 2 lb/hp with a more conservative estimate of 3 lb/hp for the Arctic SEV. The lift/propulsion specific weight ratio ($\beta$) is in the range from 1.5 to 2.0. For the Arctic SEV a realistic figure might be 1.75. The energy specific weight,

*Abbreviations used in this text are from the GPO Style Manual, 1973, unless otherwise noted.

including tankage for a gas turbine-type fuel, is given as 0.6 kWh/lb.[5] This converts to 0.447 hph/lb. The power/weight ratio is also known from the above fuel fraction analysis since:

$$\frac{P_T}{W_{FP}} = \left(\frac{P_{TI}}{W_G V_I}\right) \frac{V_I}{X_{FP}} = \left(\frac{P_{TI}}{W_G V_I}\right) \frac{\sqrt{\kappa_G}}{\sqrt{1/2\rho}} \frac{\sqrt{p_{cI}}}{X_{FP}} \quad . \tag{34}$$

This allows both constant velocity and constant pressure data to be generated.

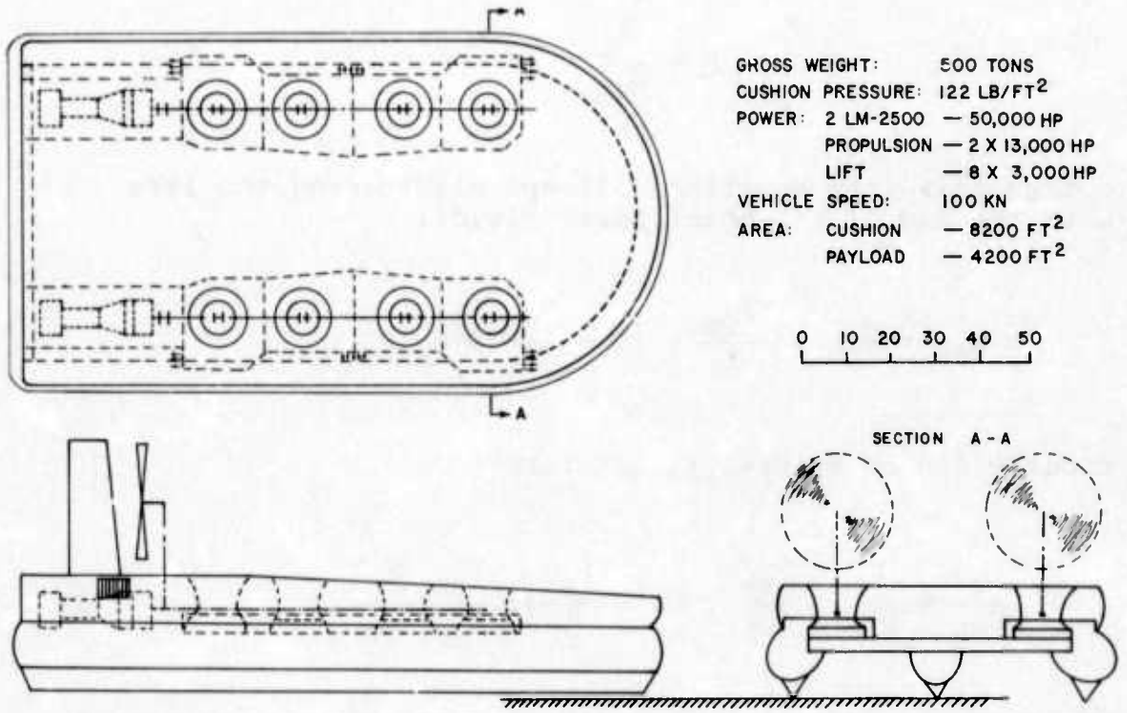


Figure 2
Surface Effect Vehicle Machinery

CARGO LOADING

As pointed out in the Introduction, cargo loading (weight per unit cargo area) rather than payload density is the important parameter to consider here. Obviously, the calculation of this

parameter is very much dependent on the assumptions. Keeping these assumptions simple and direct will be attempted so that the results will be of a general nature.

The following assumptions are needed to start off this portion of the analysis:

- The useful deck area is located on one level above the craft's air cushion and buoyancy tank or other structural section. Bilevel arrangements do not appear feasible for vehicles of less than 1000 tons.

- The useful deck area is allotted to engines for the main power and the lift system fans. The remaining area is available for payload. Thrusters, air distribution, and other items are located elsewhere.

- The useful deck area is equal to the cushion area.

- The axis of the lift fan is positioned perpendicular to the cushion.

Even for other arrangements, this approach should yield a reasonable estimate of the fan area requirement.

Figure 2 is a schematic for the machinery in a 500-ton surface effect vehicle. The configuration provides a single drive-through cargo space at the expense of two separate machinery spaces. The schematic is consistent with the assumptions made above. Also, many current large surface effect vehicles (British SRN4 and the U. S. Navy-sponsored Amphibious Assault Landing Craft) have a similar layout of machinery and cargo space.

The area required for the engine should be proportional to the engine planform area. In figure 3 engine planform area is plotted as a function of the engine's horsepower for various marine gas turbine engines. The engine area requirement (maximum length times maximum diameter) can be expressed in terms of a single parameter (engine area parameter ($\pi_E$)):

$$\pi_E = \frac{S_E}{P_T} . \tag{35}$$

A reasonable value for $\pi_E$ is approximately 0.02 $ft^2/hp$. This is twice the engine planform area, as shown in figure 3, and thus includes a margin for engine accessories and access to the engine for maintenance and inlet and exhaust ducting. The fraction of the cushion area required for the engine can be calculated from:

$$\frac{S_E}{S_C} = \frac{\pi_E P_T}{S_C} = \pi_E \left(\frac{P_T}{WV}\right) p_c V = \pi_E \left(\frac{P_T}{WV}\right) \frac{q}{k} V. \qquad (36)$$

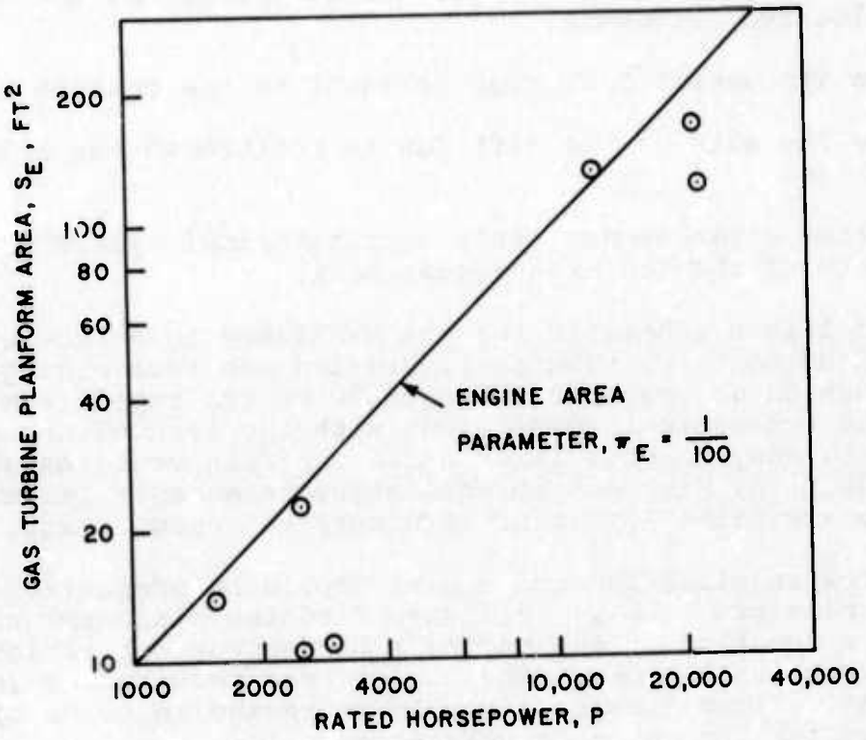


Figure 3
Marine Gas Turbine Planform Area
Correlation

The area required for the fan system should be some function of the vehicle airflow requirement. Purnell[6] summarizes the correlation of optimum axial and centrifugal fans by Cordier and Baljé. Their correlation is based upon the specific speed and specific diameter parameter, but it can also be presented in terms of fan flow and pressure coefficient or a combination of any two of these. The fan rotor area is:

$$S_{fr} = U \frac{\pi}{4} d_f^2 ,$$

where U represents the number of fan units of diameter $d_f$. Introducing the fan tip speed, which is a limiting parameter, in the following manner:

$$V_T = \frac{n_f d_f}{2} .$$

The above equation becomes:

$$S_{fr} = U \frac{\pi}{8} \frac{n_f d_f^3}{V_T} .$$

Now, normalizing this fan area by the fan flow coefficient:[6]

$$\phi = \frac{Q_f}{n_f d_f^3} \tag{37}$$

yields the following fan rotor area equation:

$$S_{fr} = U \frac{\pi}{8} \frac{Q_f}{V_T \phi} = \frac{\pi}{8} \frac{Q_c}{V_T \phi} . \tag{38}$$

This equation shows that the fan rotor area is not only a function of the cushion airflow but also the fan tip speed and fan flow coefficient. The tip speed for centrifugal fans is usually limited to approximately 500 ft/s due to structural considerations, and the axial fan is limited to 650 ft/s due to noise considerations. The fan flow coefficient can vary over an appreciable range, but the above-mentioned Cordier-Baljé correlation restricts the flow coefficient to a narrow range. Figure 4 shows a plot of the flow coefficient as a function of the fan's specific speed based upon Baljé's correlation.[7] Specific speed is a basic fan characteristic which is used to classify fans. Centrifugal fans have a specific speed of 0.5 to 1.85, while axial fans range from 1.6 on up.[6] For the present analysis a constant fan flow coefficient of 0.05 will be used. This falls within ±10% of the optimum line for axial and most

centrifugal fans, as shown in figure 4. Figure 4 suggests the possibility of trading off fan size for efficiency, which will not be attempted in this preliminary study.

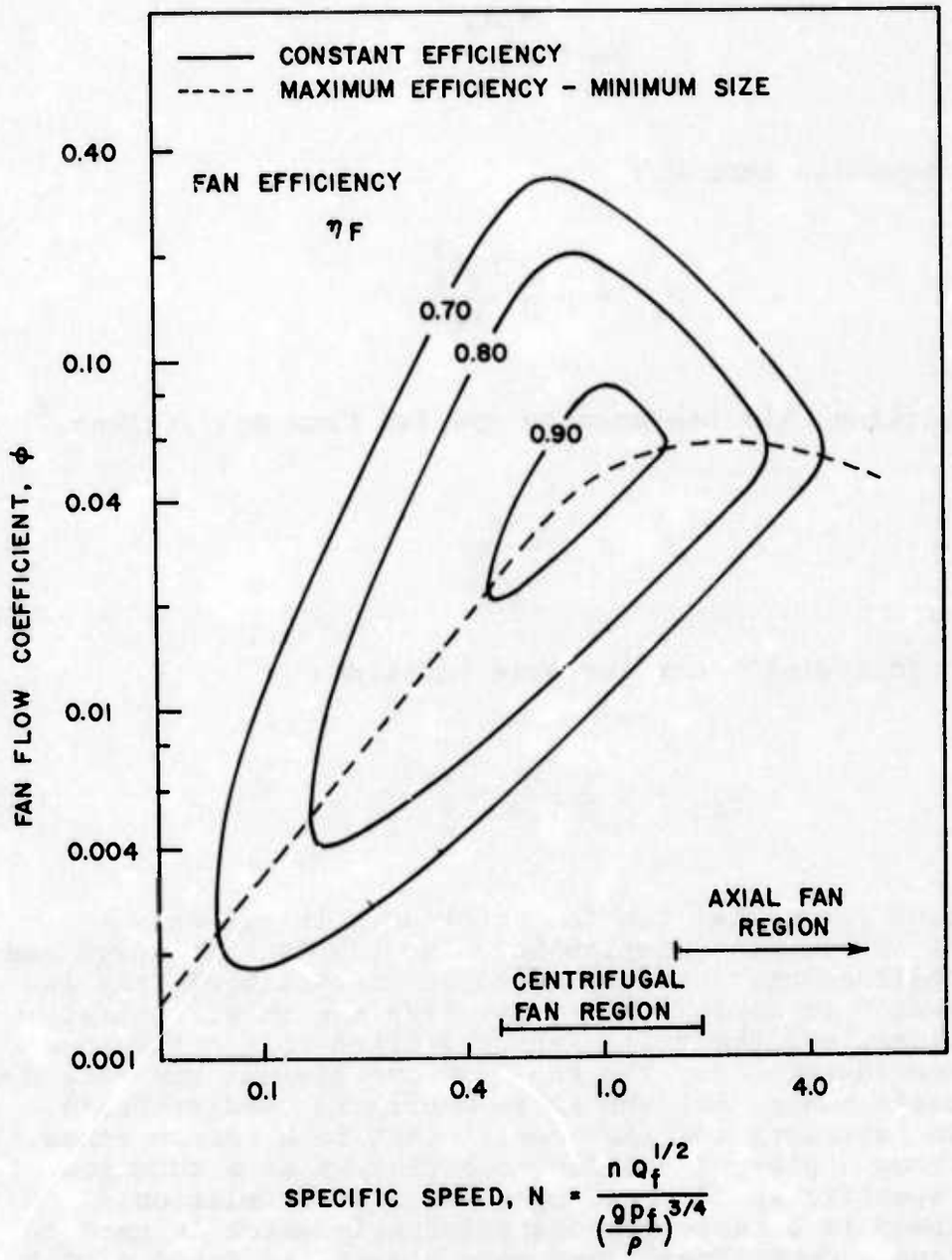


Figure 4
Baljé Fan Correlation

Besides the fan-rotor area, floor space must be allotted to fan diffusers and/or scrolls. For a centrifugal fan the scroll can be as large as 400% of the fan-rotor area. Therefore, equation (38) will be multiplied by a fan-area factor $K_f$ to account for this additional area. The equation for the fan area ($S_f$) thus becomes:

$$S_f = \frac{\pi}{8} \frac{1}{0.05} K_f \frac{Q_c}{V_T} = 7.85 K_f \frac{Q_c}{V_T} . \quad (39)$$

The fan-area factor ($K_f$) is assumed to be 2.0 for axial fans and 5.0 for centrifugal fans. Normalizing the above equation with the cushion area ($S_c$) and substituting for the cushion airflow rate from equations (5) and (7) results in:

$$\frac{S_f}{S_c} = 7.85 K_f \frac{\mathcal{D}_c}{V_T} \sqrt{\frac{2p_c}{\rho}} 2 \frac{h}{\ell} \left( \frac{\ell}{b} + 1 \right),$$

which can be further simplified to yield:

$$\frac{S_f}{S_c} = 3.93 K_f C_M \frac{V}{V_T} \frac{1}{k^{1/2}} . \quad (40)$$

Finally, from the before-mentioned assumption, the area remaining for the payload is:

$$\frac{S_p}{S_c} = 1 - \frac{S_f}{S_c} - \frac{S_E}{S_c} . \quad (41)$$

The fraction of the gross weight available for the payload is the portion left over after subtracting the machinery, fuel, structural, and miscellaneous equipment weight fraction, or:

$$X_P = 1 - X_M - X_F - X_S - X_{EQ} . \quad (42)$$

The machinery weight can be calculated from the total specific power in the following manner:

$$X_M = \frac{W_M}{W_G} = \left(\frac{P_T}{WV}\right) V \bar{W}_M \tag{43}$$

where $\bar{W}_M$ is the specific weight of the total machinery. This is a simplification of the separate propulsion and lift specific weight used in the power-energy relationship. The specific machinery for this type of vehicle might range from 2.5 to 4.0 lb/hp. The calculation of the fuel fraction was similarly simplified by using the Breguet range equation. These two assumptions offset each other to some extent, since the fuel fraction will be lower at low value of the speed parameters but the machinery fraction will be higher and vice versa at higher values of the speed parameter. The structural weight fraction as a function of the cushion pressure[8] is:

$$X_S = \frac{W_S}{W_G} = \frac{2.36}{p_c^{0.481}} = 2.36 \left(\frac{k}{q}\right)^{0.481} . \tag{44}$$

Finally, the equipment fraction is just a constant, assumed to equal 5%.

The cargo loading can now be defined simply as the payload or cargo weight per unit cargo area:

$$\pi_c = \frac{W_S}{S_P} = \frac{W_P}{W_G} \frac{S_c}{S_P} \frac{1}{p_c} = \frac{X_P q}{S_p/S_c \, k} . \tag{45}$$

Both the cargo fraction and the fuel fraction can vary widely in this analysis. In order to define an optimum operating point, a parameter proportional to the operating fuel cost of costs per ton-mile will be defined. This cost factor is:

$$C_c = \frac{W_F}{W_P} \frac{1000}{R} = \frac{X_F}{X_P} \frac{1000}{R} . \tag{46}$$

The multiplication factor has been introduced in order to generate some reasonably sized number. It will not affect the conclusions. It should be cautioned that this cost factor only includes the fuel cost and makes no attempt to include other operating and fixed costs.

OVERWATER THRUST MARGIN

The vehicle will operate not only over land and ice but also over water. For waterborne operation wave drag must be included in estimating the total drag on the vehicle. Figure 5 shows, as a function of speed, the three components of drag considered for this portion of the analysis

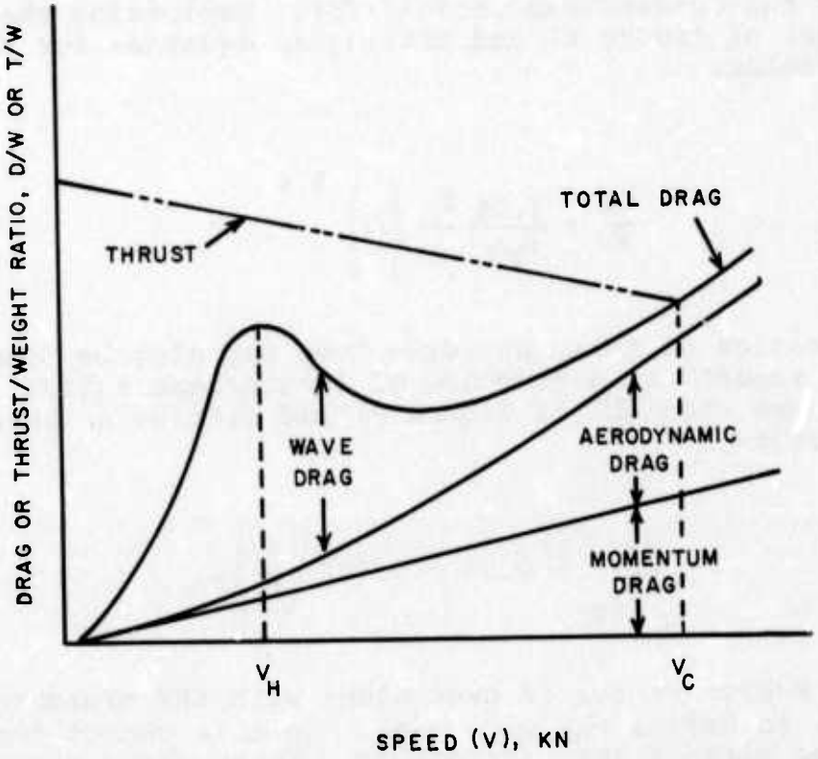


Figure 5
Drag and Thrust Characteristic
of a Surface Effect Vehicle

Also shown is the available thrust as a function of speed. It can be seen that at the wave drag hump, the thrust margin can be quite small. In fact, this margin can be negative, since the wave drag at the hump increases with cushion pressure and sea state. In this analysis the effect of the sea state is neglected.

The aerodynamic and momentum drag curves are known as a function of the speed parameter (k). Combining the aerodynamic and momentum drag equation developed previously:

$$\frac{D}{W} = C_D k + 4\mathcal{D}_c \frac{h}{\ell}\left(\frac{\ell}{b} + 1\right) k^{1/2} = C_D k + C_M k^{1/2}. \qquad (47)$$

The wave drag is a complex function of speed, cushion pressure vehicle length, etc. Inclusion of the full wave drag analysis would result in unnecessary complexity for this preliminary analysis. It was therefore decided to concentrate on the magnitude and location of the wave drag hump and the behavior of the wave drag for Froude number larger than 1.0. Ford[9] shows in his figure 4 that the magnitude of the wave drag peaks is only a function of the length/beam ratio ($\ell/b$). Replotting these data (see item (a) of figure 6) and fitting an equation for the wave drag hump yields:

$$\frac{D_W}{W} = \frac{3.08}{\rho_W g} \frac{p_c}{\ell} \left(\frac{\ell}{b}\right)^{-0.4} . \qquad (48)$$

The location of this wave drag hump can also be determined from Ford's report[9] as a function of length/beam ratio. Replotting these data (see item (b) of figure 6) and fitting a linear equation results:

$$Fr\Big|_W = 0.53 + 0.058 \left(\frac{\ell}{b}\right). \qquad (49)$$

Usually the Froude number is used along with the pressure/length ratio ($p_c/\ell$) to define the wave drag. In this report the speed parameter has already been introduced. These three parameters are not independent, and one will have to be eliminated. Usually the pressure/length ratio is quoted for surface effect vehicles and ships. It will therefore be used along with the speed parameter to eliminate the Froude number from the above equation:

$$Fr = \frac{V}{\sqrt{g\ell}} = \sqrt{\frac{2}{\rho}} \sqrt{k \frac{p_c}{\ell}} . \qquad (50)$$

The wave drag in the higher Froude number region (see figure 4 of Ford[9]) is a function of both the length/beam ratio and the Froude number. A relatively simple fit to these data can be accomplished with the following equation:

Item (a)
Maximum Wave Drag

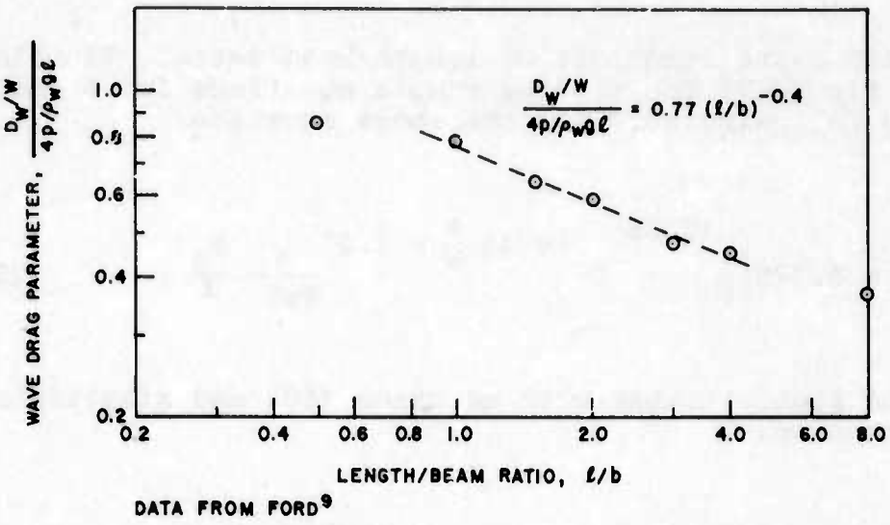


Item (b)
Location of Maximum
Wave Drag

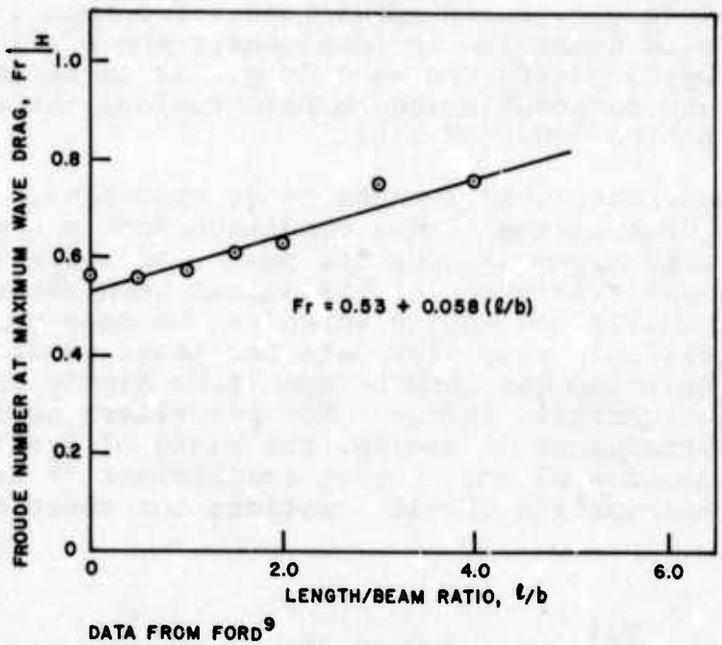


Figure 6
Maximum Wave Drag for
a Rectangular Pressure Source

$$\frac{D_W/W}{4p_c/\rho_w g \ell} = A\ F^m \ ,$$

where both A and m are functions of length/beam ratio. Plotting the data (see figure 7) and fitting simple equations for A and m results in the following form for the above equation:

$$\frac{D_W}{W} = 0.275\left(\frac{\ell}{b}\right)^{0.38} Fr^{+0.15\ \frac{\ell}{b} - 1.87}\ \frac{4}{\rho_w g}\ \frac{p_c}{\ell} \ . \qquad (51)$$

Eliminating the Froude number with equation (50) and simplifying the above expression:

$$\frac{D_W}{W} = \frac{1.1}{\rho_w g}\left(\frac{\ell}{b}\right)^{0.38}\ \frac{p_c}{\ell}\left(\frac{2}{\rho g}\ k\ \frac{p_c}{\ell}\right)^{0.075\ \frac{\ell}{b} - 0.93} \ . \qquad (52)$$

The wave drag can now be combined with the aerodynamic and momentum drag to give the total drag at the wave drag hump and over a large portion of the supercritical wave drag region, which hopefully will include the cruise conditions. For this study no attempt was made to determine in this manner the error encountered with approximating the wave drag. It is estimated that for $F_r > 1.0$ and reasonable length/beam ratios, the approximation should be on the order of ±10%.

The thrust characteristic remains to be specified. The thrust matches the drag at the cruise condition and is assumed to vary linearly with speed at constant power, as shown in figure 5. This linear variation of thrust has been shown[10] to be the most reasonable assumption which can be made consistent with the limited available propeller data for these conditions. The thrust characteristics can then be specified simply in terms of the ratio of static/cruise thrust. For propellers designed to yield optimum performance at cruise, the ratio of static/cruise thrust is only a function of the thrust coefficient,[10] as shown in figure 8. The appropriate simple equations for these data are:

$$\left.\frac{T_S}{T_C}\right|_{FP} = 1.6\ C_T^{-0.20} \qquad (53a)$$

and

$$\left.\frac{T_S}{T_C}\right|_{SP} = 2.1\ C_T^{-0.24} \tag{53b}$$

for the free and shrouded propellers respectively. The data and equation confirm the fact that the shrouded propeller has a better static performance than the free propeller.

The thrust coefficient is defined in the following manner:

$$C_T = \frac{T_C}{1/2\ \rho\ V_C^2\ S_P} . \tag{54}$$

In specifying the thrust coefficient, the weight of the vehicle must be introduced. Up to this point it was possible to avoid this. In the preceding sections only the propeller efficiency was needed. It was assigned independent of any other parameter but could have been specified as a function of the thrust coefficient. The thrust coefficient can be rewritten in terms of the speed parameter (k) and drag/weight ratio:

$$C_T = \frac{D}{W}\frac{S_C}{S_P}\frac{p_c}{1/2\ \rho\ V_C^2} = \frac{D}{W}\frac{S_C}{S_P}\frac{1}{k} . \tag{55}$$

The determination of the thrust coefficient is now only a matter of calculating the cushion/propeller area ratio. It will be assumed that the vehicle is propelled by two maximum diameter ($D_{max}$) propellers. These propellers are positioned side by side. The area ratio can then be approximated by:

$$\frac{S_C}{S_P} = \frac{\ell b}{2\ \frac{\pi}{4}\ D_{max}^2} = \frac{\ell}{b}\frac{b^2}{D_{max}^2}\frac{2}{\pi} . \tag{56}$$

It will be necessary to introduce the vehicle weight in order to eliminate the beam from the above equation. Solving the relationship of weight, cushion pressure, and area (see equation (2)) for the beam (b) results in:

$$b = \left[\frac{W_G}{\left(\frac{\ell}{b}\right)^2\ \frac{p_c}{\ell}}\right]^{1/3} . \tag{57}$$

Item (a) - Constant

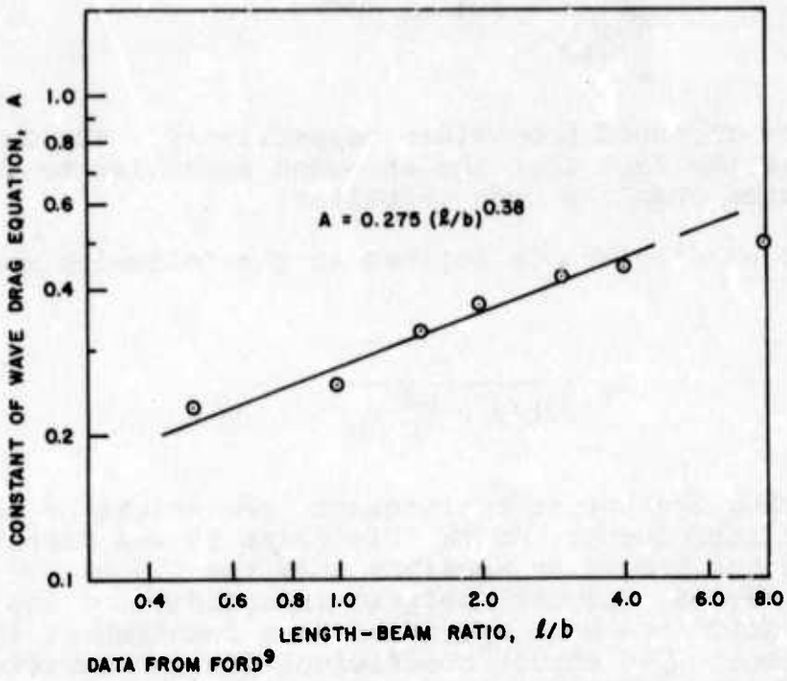


Item (b) - Exponent

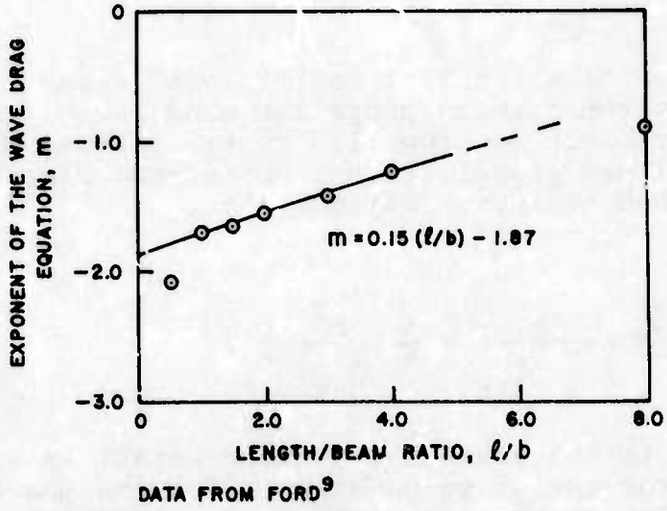


Figure 7
Constant and Exponent of the
Supercritical Wave Drag

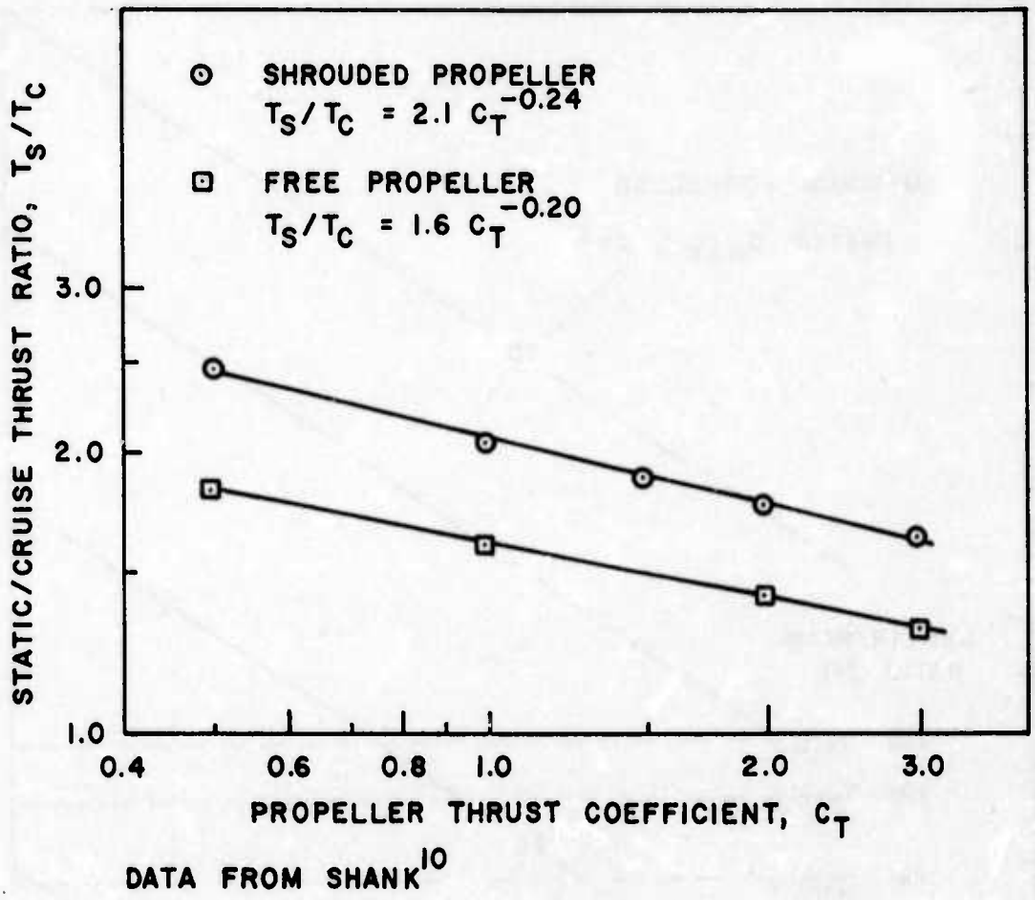


Figure 8
Static/Cruise Thrust Correlation

Finally, substituting this into equation (56), the area ratio becomes:

$$\frac{S_C}{S_P} = \frac{2}{\pi} \frac{1}{D_{max}^2} \left[ \frac{W_G}{\left(\frac{\ell}{b}\right)^{1/2} \frac{p_c}{\ell}} \right]^{2/3} . \qquad (58)$$

This area ratio is plotted in figure 9 as a function of parameter in the parentheses. Also plotted in this figure is the minimum area ratio when twice the propeller diameter is equal to the beam.

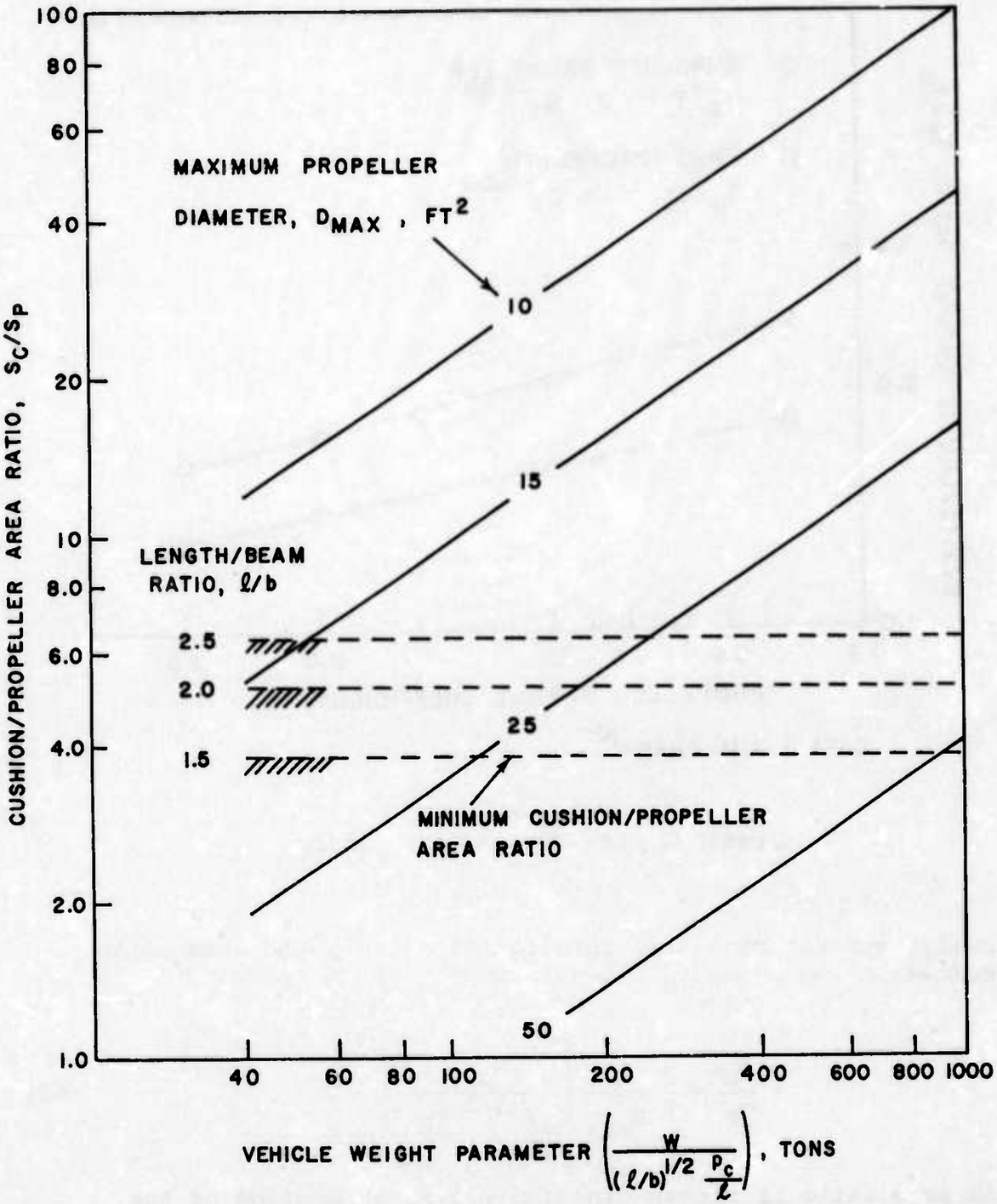


Figure 9
Cushion/Propeller Area Ratio Correlation

It can be seen that 50-foot-diameter propellers are applicable for vehicles in excess of 1000 tons and 25-foot-diameter propellers for vehicles in exesss of 170 tons for a length/beam ratio of 2. For the present analysis it will be assumed that the maximum propeller diameter is 25 feet.

Other assumptions could have been made for the propeller arrangement, but it is believed that no more than two propellers will span the vehicle. It might be desirable to use two propeller planes with two propellers each, but how to treat this tandem arrangement simply is not known at present.

As mentioned above it is assumed that the thrust at constant power varies linearly with the speed between static and cruise conditions. The thrust at any speed can then be written as:

$$\frac{T}{T_C} = \frac{T_S}{T_C} - \left(\frac{T_S}{T_C} - 1\right)\frac{V}{V_C} \quad ,$$

or, in terms of the speed parameter:

$$\frac{T}{T_C} = \frac{T_S}{T_C} - \left(\frac{T_S}{T_C} - 1\right)\sqrt{\frac{k}{k_c}} \quad . \tag{59}$$

The thrust margin at the wave drag hump is now defined in the following manner:

$$m_H = \frac{\frac{T_H}{W} - \frac{D_H}{W}}{\frac{D_H}{W}} = \frac{\frac{T_H}{W}}{\frac{D_H}{W}} - 1 \quad . \tag{60}$$

The above margin assumes that the thrust and drag are matched at the cruise condition. Usually a vehicle does not cruise at its maximum power but at a lower power setting. In that case the maximum thrust at the cruise condition is more than the drag, or there exists a cruise thrust margin ($m_c$). If this margin is defined in the following manner:

$$m_c = \frac{T_{CM} - D}{D} = \frac{T_{CM}}{D} - 1 \quad , \tag{61}$$

then the hump thrust margin with a cruise thrust margin ($m_H'$) can be calculated from:

$$m_H' = (m_H + 1)m_c - 1 \quad . \tag{62}$$

## DISCUSSION AND RESULTS

Each of the more significant results of the foregoing analysis will be discussed individually. Then an attempt will be made to summarize these individual results in a total picture which will reflect the desirable operating regime of the vehicle from the standpoint of machinery and cargo carrying.

### TOTAL SPECIFIC POWER

In the previous section the total specific power was derived as a function of the speed parameter (k) and propulsive efficiency ($\eta_{PR}$) and aerodynamic drag ($D_A$), momentum ($C_M$), and pressure ($C_p$) coefficients (see equation (11a)). The simplicity and compactness of this equation is worth noting. The equation is independent of vehicle weight (W), velocity (V), cushion area ($S_c$), or cushion pressure ($p_c$). These parameters appear implicitly in the speed parameter (k) via equation (1) or (2).

Figure 10 shows the total specific power and its components under both the plenum- and peripheral-jet cushion assumptions as a function of the speed parameter. The values of the different parameters used to calculate the results in figure 10 appear in table 1. These values are reasonable and consistent with work carried out by others. As can be seen from equation (11a), and demonstrated in figure 10, the propulsion specific power increases with increasing speed parameter (k). This is due to increasing aerodynamic and momentum drag of a fixed vehicle with speed. It can also be thought of as the increasing power that is needed to propel vehicles of larger size and given weight and speed, since by equation (2) the speed parameter (k) is proportional to planform area. On the other hand, the lift specific power decreases with increasing speed parameter (k), since the lift system pressure requirement decreases in proportion to the vehicle weight for a given vehicle size, and the air mass flow increase is only proportional to the square root of the vehicle weight. As a result of these two opposing trends (propulsion and lift power), there occurs a minimum total specific power point at a speed parameter of 0.25 and 0.15 under the plenum and peripheral-jet assumptions, respectively. This demonstrates that the total power is not just an addition of the various components but a tradeoff. The 150% increase in lift power which resulted with the plenum-cushion over the peripheral-jet assumption not only resulted in a 90% increase in power but also a 60% shift in the

speed parameter for minimum specific power. Similar tradeoffs will be encountered for changes in the lift or propulsion power or their components, such as drag coefficient ($C_D$), length/beam ratio, etc.

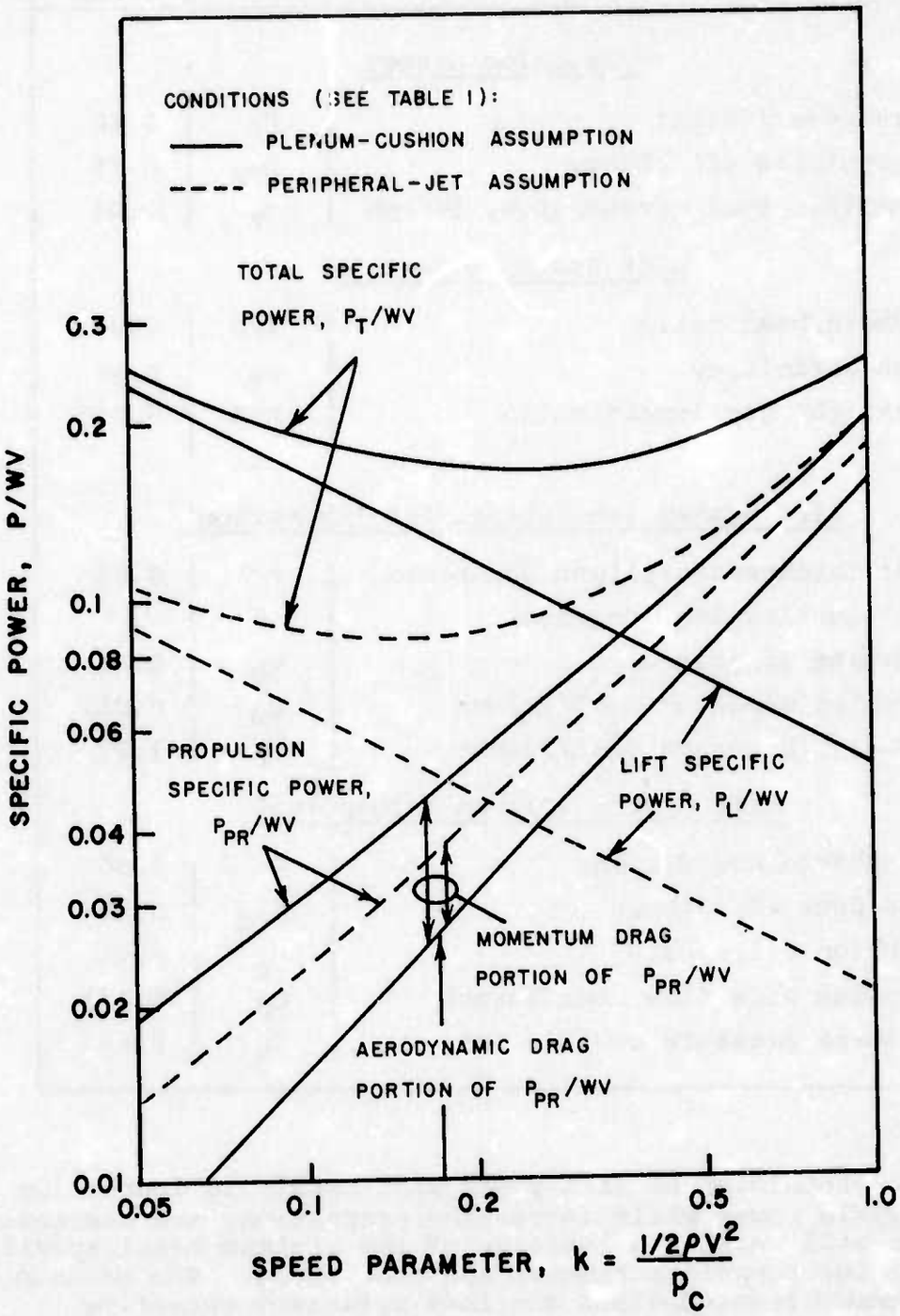


Figure 10
Specific Power Comparison

TABLE 1
STANDARD CONDITIONS

| Description | Symbol | Assumed Value |
|---|---|---|
| **Propulsion System** | | |
| Drag coefficient | $C_D$ | 0.10 |
| Propulsion efficiency | $\eta_{PR}$ | 0.65 |
| Specific fuel consumption, lb/hph | $c_F$ | 0.45 |
| **Lift System (General)** | | |
| Length/beam ratio | $\ell/b$ | 2.0 |
| Fan efficiency | $\eta_F$ | 0.80 |
| Daylight gap/length ratio | $h/\ell$ | 0.005 |
| **Lift System (Peripheral-Jet Assumption)** | | |
| Jet thickness/daylight gap ratio | $t/h$ | 0.03 |
| Jet inclination, degrees | $\theta$ | 45 |
| Ducting efficiency | $\eta_D$ | 0.80 |
| Cushion momentum coefficient | $C_M$ | 0.017 |
| Cushion pressure coefficient | $C_P$ | 1.22 |
| **Lift System (Plenum Assumption)** | | |
| Discharge coefficient | $\mathcal{D}$ | 0.55 |
| Fan-duct efficiency | $\eta_{fd}$ | 0.80 |
| Cushion efficiency | $\eta_c$ | 0.50 |
| Cushion mass flow coefficient | $C_M$ | 0.033 |
| Cushion pressure coefficient | $C_P$ | 1.56 |

Increasing propulsion or lift power will result in increasing total specific power while increasing propulsion, and decreasing lift power will shift the location of the minimum total specific power to a lower speed parameter and vice versa. The minimum specific power point defines the most efficient operating condition.

At the minimum total specific power point shown in figure 10 the lift power is the larger component, representing 63% of the total power, while the power needed to overcome the aerodynamic drag is 24% and momentum drag is only 13%. This is rather surprising since one usually thinks of a 50/50 propulsion/lift power split. The 50/50 power split can be realized at a speed parameter of 0.47 where the total specific power is 0.182 or 10% above its minimum value. At higher speed parameters the lift portion of the total power decreases (at k = 1.0 the lift power is less than 20% and the momentum drag portion is less than 18%), while at lower speed parameters the aerodynamic portion of the propulsion power becomes small.

A desirable operating or cruise point for a surface effect vehicle would be the minimum or optimum specific power point as shown in figure 10. The only problem is that this point can correspond to a high cushion pressure for fast vehicles. Under the plenum-cushion assumption the optimum condition requires a cushion pressure which is four times the free stream dynamic pressure or 135 and 194 $lb/ft^2$ for a 100- and 120-knot cruise speed, respectively. For the peripheral-jet assumption the optimum cushion is more than six times the free stream dynamic pressure. Since these high cushion pressures might not be desirable from other standpoints, it will be of interest to sacrifice some additional power for lower cushion pressure. As shown in figure 11, increasing the total specific power by 10% (plenum-cushion assumption) will almost double the speed parameter (k). Increasing the total power even more will not buy significantly larger reductions in cushion pressure, since the power required for propulsion increases significantly above this point. At the lower speed parameter, the specific power increase is relatively small, but this region requires higher cushion pressures and is therefore not of interest. Since a small sacrifice in total power is acceptable for some flexibility in cushion pressure, the optimum operating region from a total power standpoint will be defined as the region from the point of minimum total specific power to a point at higher speed parameter where the total power is 10% higher than minimum.

Figure 11 shows that the behavior of power for the peripheral-jet cushion assumption away from the minimum point is essentially the same as under the plenum-cushion assumption. The only difference is the magnitude and location of the minimum points. This suggests a way of examining the effect of each of the independent variables which make up the total specific power equation. Figure 12 shows that the behavior is very little different for the minimum or 10% higher specific power points under the plenum-cushion assumption and, as figure 11 suggests, the peripheral-jet cushion assumption would differ very little from the plenum-cushion results shown in figure 12. The total specific power is most sensitive to the cushion mass flow ($C_M$) and pressure parameter ($C_p$). A 10% improvement (decrease) of either of these can result in up to 8% decrease in total specific power. Surprisingly, the total specific power is not very sensitive to

changes in the drag coefficient. A 10% improvement (decrease) results in only 2% decrease in specific power. The split in power between propulsion and lift is insensitive to the change of the independent variables.

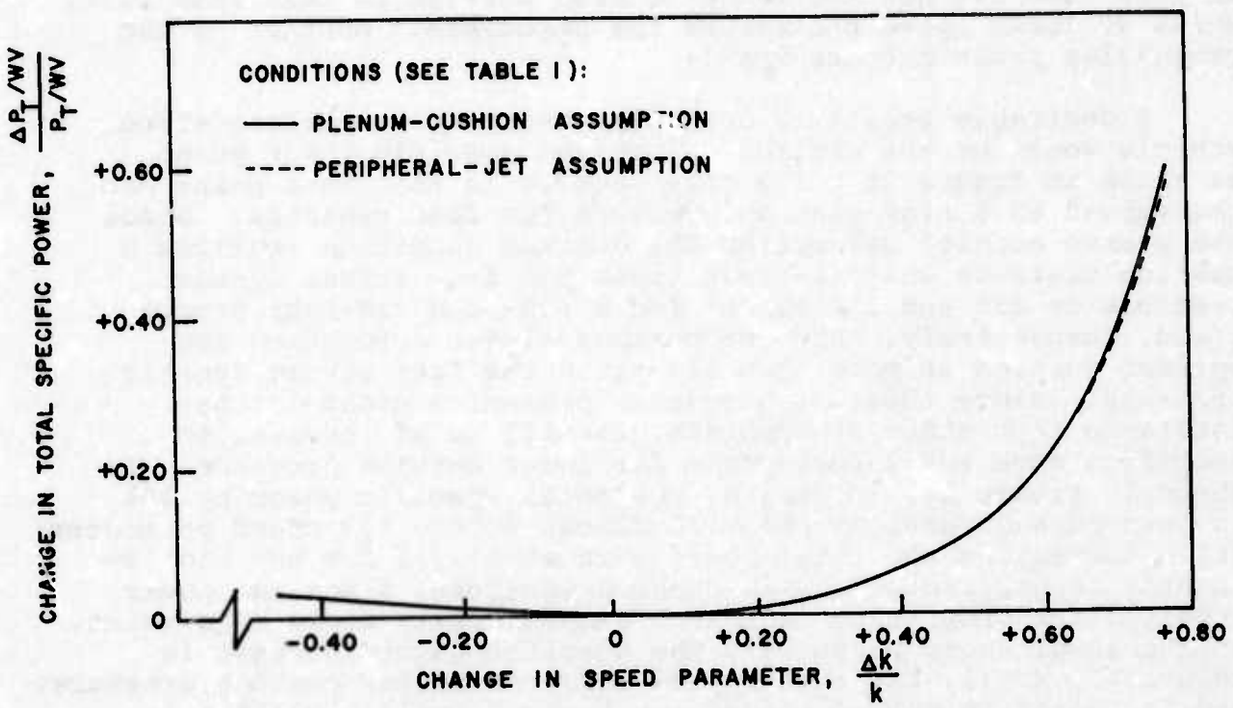


Figure 11
Sensitivity of Total Specific Power to
Changes in Speed Parameter

It was shown above that the power split is quite sensitive to speed parameter (k). The effect of the independent variable change on the speed parameter is about the same for the four variables shown in figure 12. Increasing the drag coefficient will shift the speed parameters to lower values, while increasing the other three variables will shift the specific speed parameter to higher values. This effect is a result of the opposing trends of the lift and propulsion power, which was discussed in conjunction with figure 10. According to their definitions, the cushion flow and pressure coefficients are a function of several variables. The cushion flow coefficient ($C_M$) can be improved by changes in the discharge coefficient ($\mathcal{D}_C$). The only way to accomplish this is to use more sophisticated cushion concepts such as a peripheral-jet cushion.

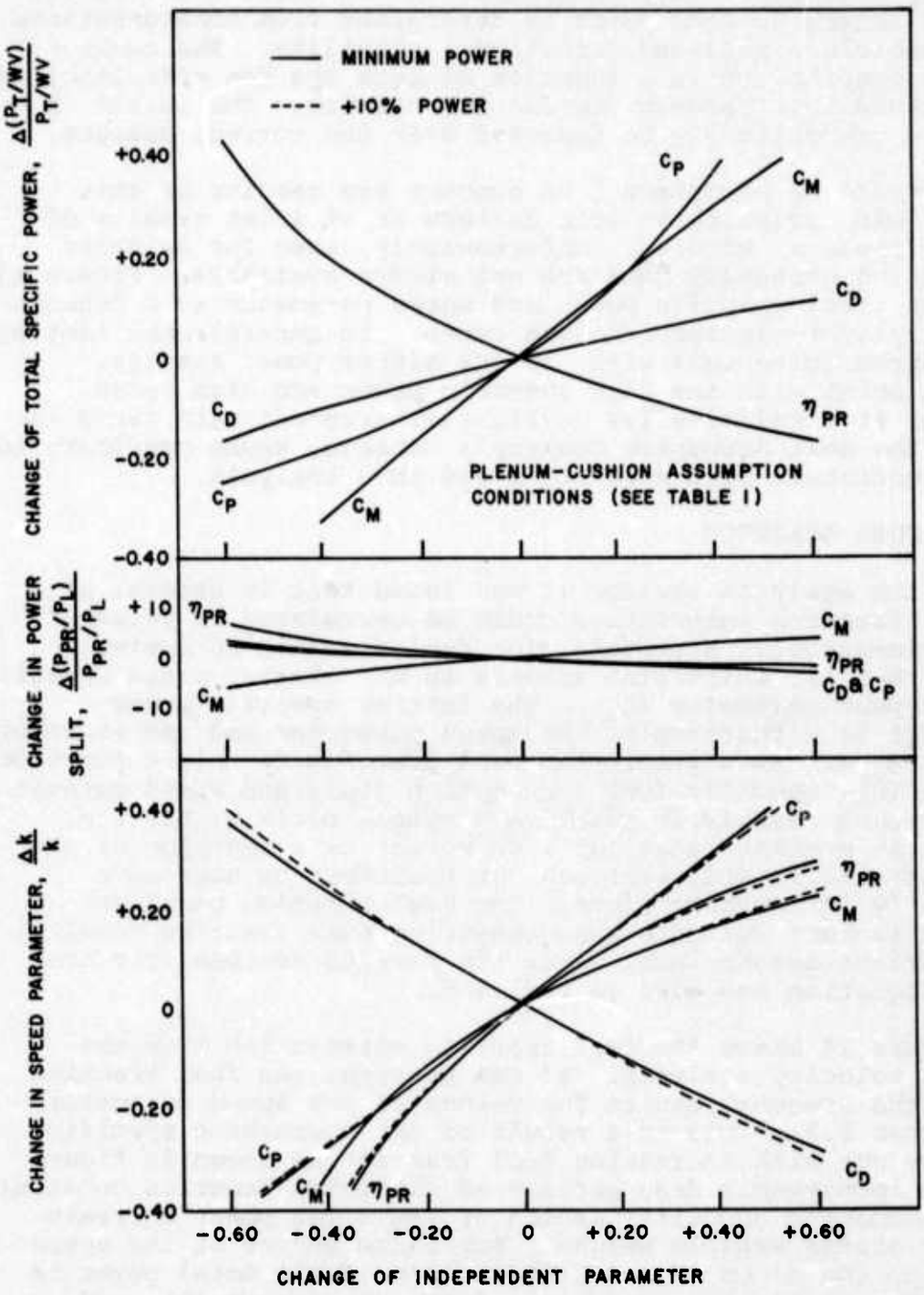


Figure 12
Total Specific Power Sensitivity

This approach will sacrifice the maintainability of the cushion. The other parameters which enter into the cushion flow coefficient are the ratio of daylight gap to vehicle length which is primarily determined from considerations of skirt wear and the ratio of length to beam which is determined from considerations of the vehicle's roll and directional stability. The cushion pressure coefficient is a function of both the fan efficiency and the pressure loss between the fan and cushion. The latter of these two can certainly be improved over the current designs.

It would be of interest to compare the results of this analysis with existing vehicle designs or at least results of detailed powering studies. Unfortunately, even for existing vehicles the necessary data are not always available. Figure 13 shows the total specific power and speed parameter as a function of the daylight-clearance/length ratio. In general, the limited data all agree quite well with the 10% higher power results. The data point with the high specific power and high speed parameter at a relative low daylight clearance/length ratio is that of the Bell Aerospace Company's Carabou, whose configuration is not consistent with most SEV's and this analysis.

## VEHICLE FUEL FRACTION

In the analysis section it was found that in general all the fuel fraction information could be correlated in terms of two nondimensional parameters, the fuel fraction parameter $(R c_F (P_{TI}/W_G V_I))$, which also appears in the Breguet range equation, and the speed parameter $(k_G)$. The initial specific power $(P_{TI}/W_G V_I)$ is a function of the speed parameter and can therefore be eliminated. As a result the fuel fraction is only a function of range (R), specific fuel consumption $(c_F)$, and speed parameter. This approach results in relatively simple plots of the fuel fraction at a given range (or vice versa) as a function of the speed parameter. This approach can therefore be used more efficiently for working plots. The fuel fraction parameter approach is more suitable when comparing fuel fraction results under various assumptions, since the results derived from the Breguet equation can also be included.

Figure 14 shows the fuel fraction correlation from the constant velocity analysis. As can be seen, the fuel fraction exceeds the Breguet results for values of the speed parameter larger than 0.2. This is a result of the increasing specific power $(P_T/WV)$ with increasing fuel fraction as shown in figure 15. The aerodynamic drag portion of the total power is constant, but the momentum and lift portion of the total power decrease with decreasing vehicle weight. For large values of the speed parameter, the momentum and lift portion of the total power is small compared to the aerodynamic drag (see figure 10), and therefore the total specific power ratio essentially increases proportionally with the inverse of the weight ratio $(W/W_G)$.

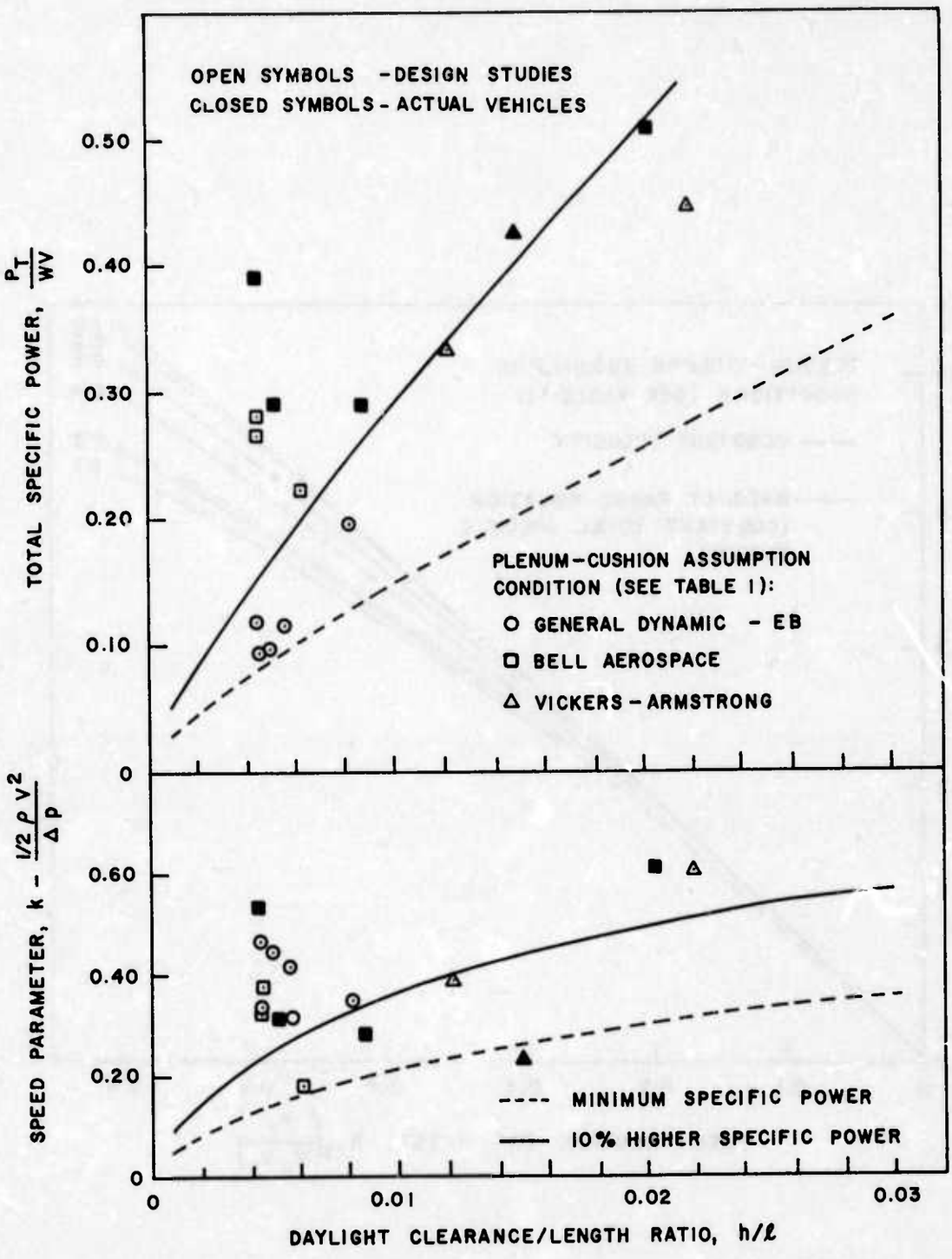


Figure 13
Comparison of Parametric Results with Vehicle Data

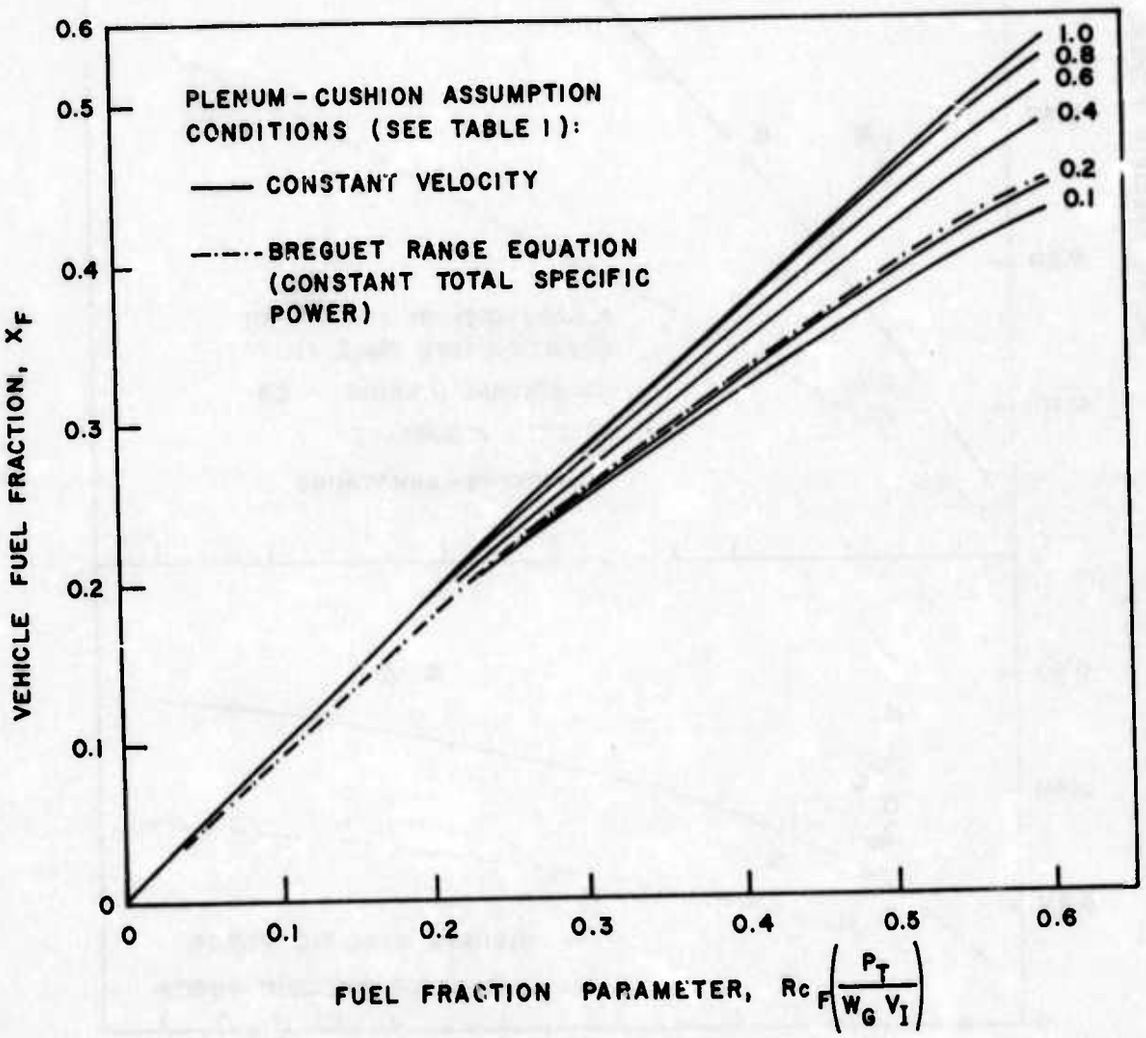


Figure 14
Constant Velocity Fuel Fraction Correlation

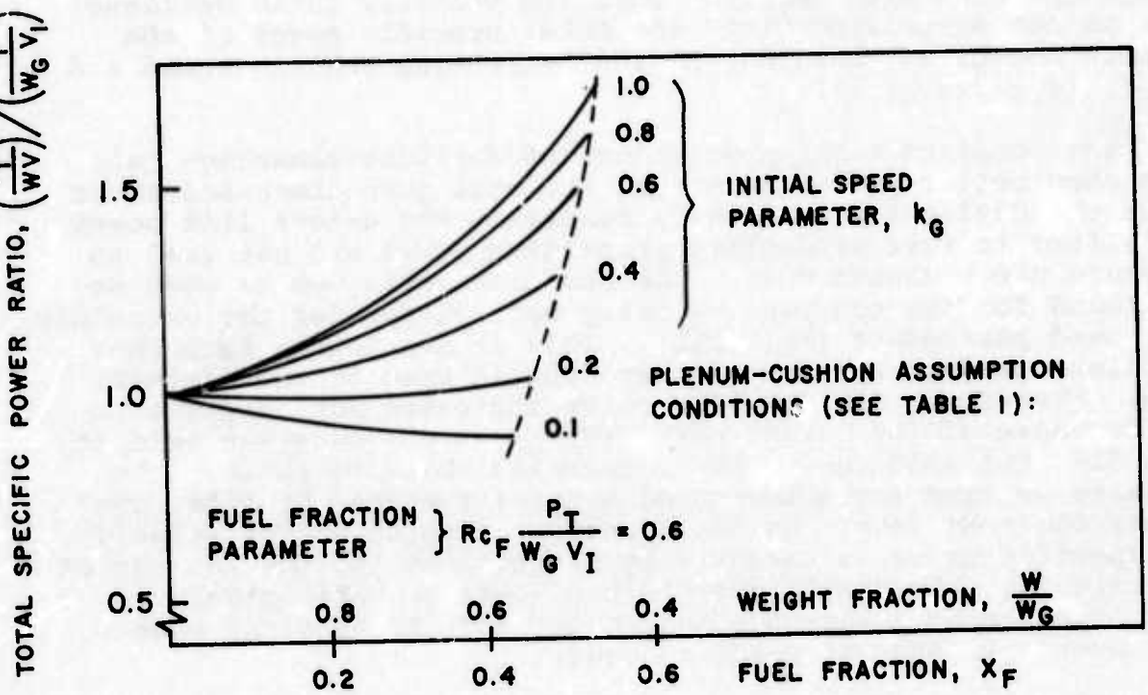


Figure 15
Specific Power Change at Constant Velocity

At a very small speed parameter the opposite is the case. The lift power is the largest contributor to the total power and, since it is proportional to $(W/W_G)^{3/2}$, the specific power $(P_T/WV)$ varies essentially as $(W/W_G)^{1/2}$.

It should be noted that the constant velocity assumption requires that the total power be decreased as the fuel is used up and might therefore not represent an interesting case. The more meaningful constant power fuel fraction correlation is shown in figure 16. The constant-propulsion/constant-lift power case has the worst fuel fraction compared to Breguet results. This is a result of the increased momentum drag with increasing daylight clearance which also requires that the velocity ratio decrease. This is not surprising since the total specific power of the vehicle increases, both due to the decreasing vehicle speed and weight (see figure 17).

The constant total power/constant daylight-clearance case does show better performance than the case just discussed above. Since the daylight clearance is constant, the excess lift power is shifted to more productive propulsion power and not used to increase the momentum drag. The performance is not as good as was found for the constant velocity case except for the extremely low-speed parameters ($k_G \leq 0.1$). This is due to the fact that for high-speed parameters the aerodynamic drag is the dominant term. Therefore, the specific power increases not only due to the decrease of the weight ratio $(W/W_G)$ as the constant velocity case did, but also due to the increasing velocity ratio. The opposite is true for a low-speed parameter where the lift power is the dominant term. As lift power is independent of velocity the specific power is essentially proportional to the inverse of the velocity. This will result in a lower specific power and fuel fraction at a low-speed parameter for the constant power case over the constant velocity case.

The constant total-power/constant daylight-clearance case therefore results in a slightly higher fuel fraction at the larger speed parameters and most likely a slightly lower fuel consumption at the lower speed parameters than in the constant velocity case. Both the constant total-power/constant daylight-clearance and constant-velocity cases show lower fuel fractions for lower speed parameters. Thus, when the fuel fraction is plotted as a function of speed parameter, the minimum fuel fraction point should occur at a lower speed parameter than the minimum specific power point shown in figure 10. Figure 18 shows this type of behavior for the constant velocity case. The minimum fuel fraction does indeed occur at lower speed parameters with increasing range. The locus of these minimum fuel fractions intersects the ordinate of the figure at the speed parameter where the minimum specific power is found.

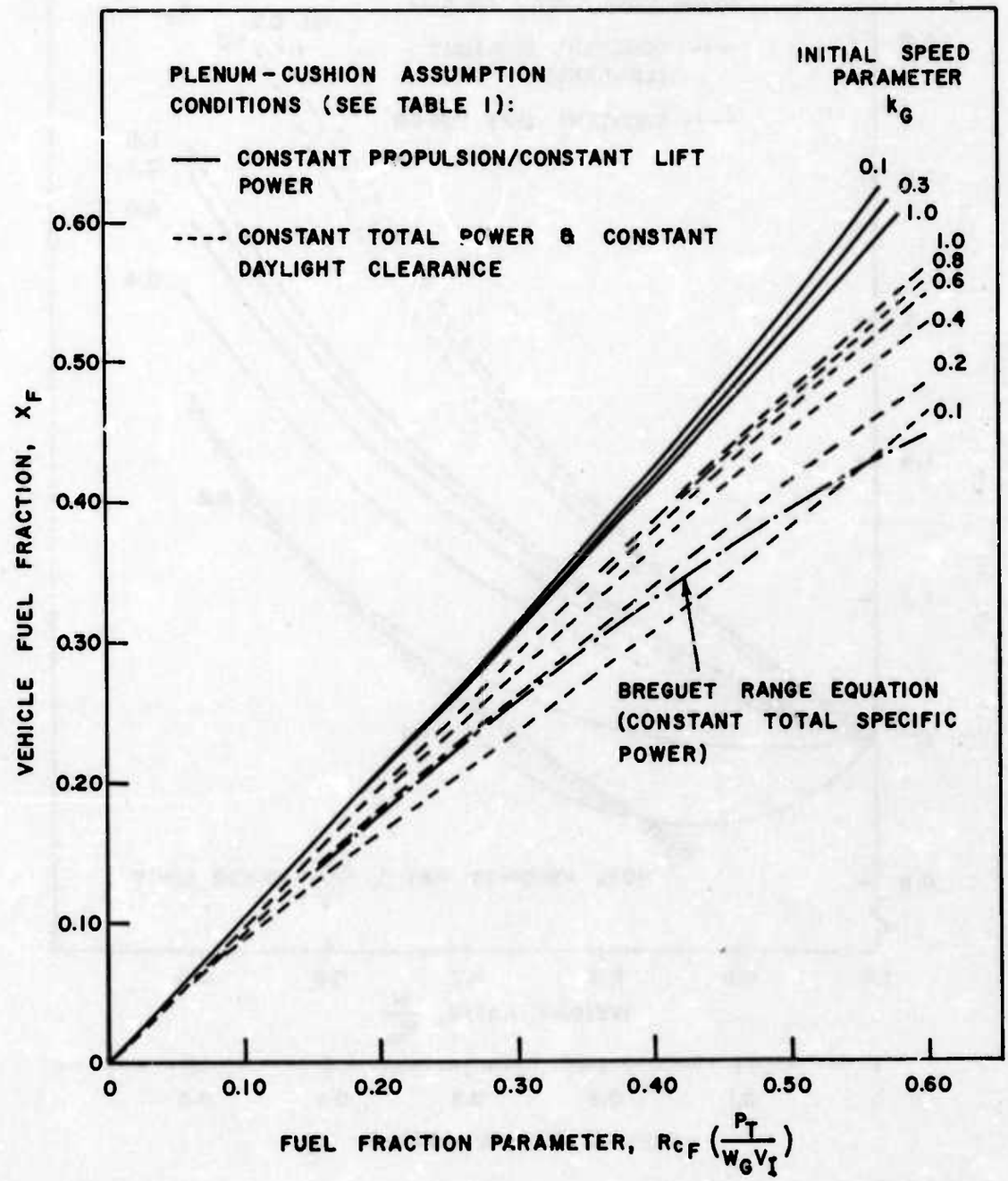


Figure 16
Constant Power Fuel Fraction Correlation

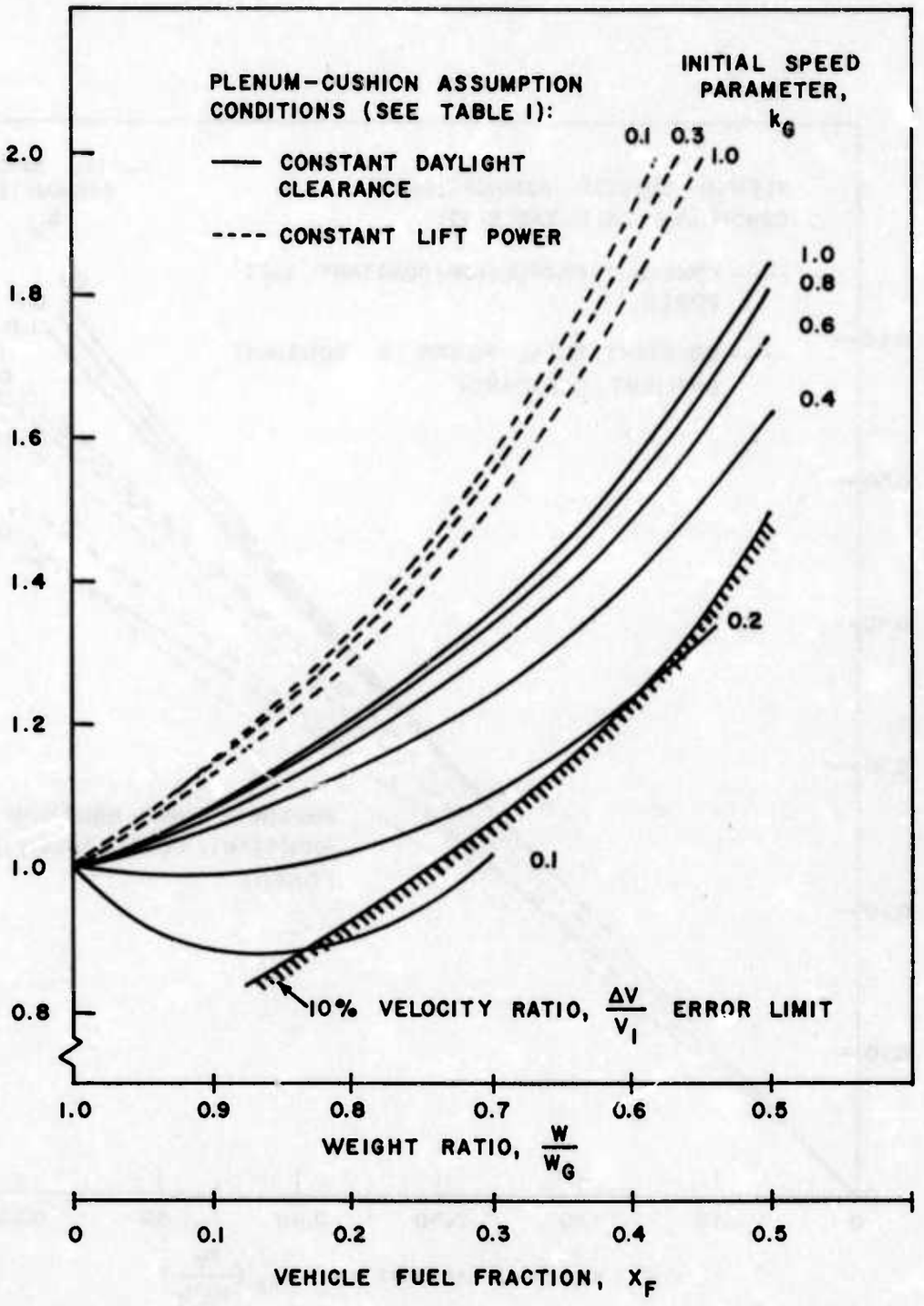


Figure 17
Specific Power Change at Constant Total Power

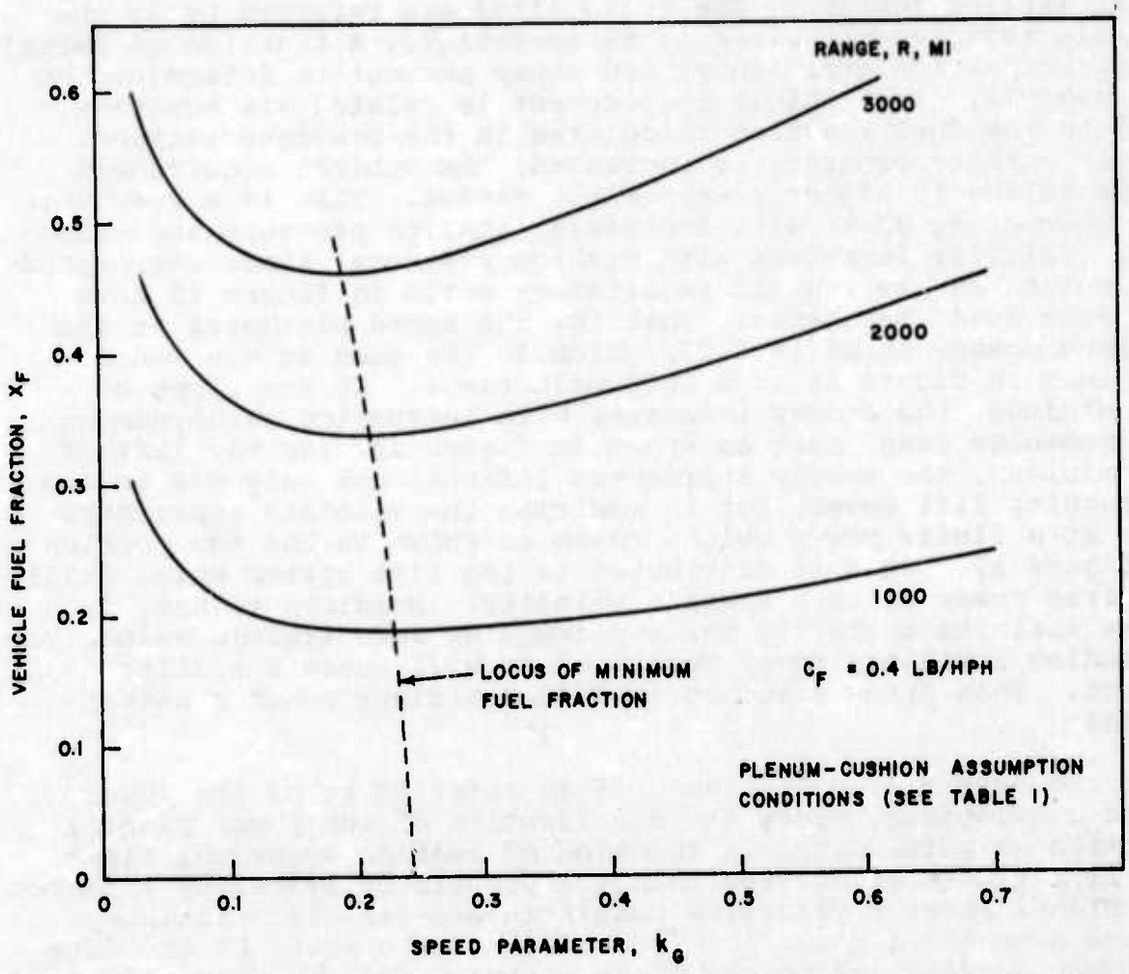


Figure 18
Fuel Fraction as a Function of Speed Parameter
(Constant Velocity)

POWER-ENERGY

Basically, this section differs from the previous section in that the power plant weight is included in the tradeoff along with the fuel weight. By including the power plant weight, the higher velocities and cushion pressures are penalized more than in the preceding fuel fraction section. The result is that the tradeoff is shifted to lower velocities and cushion pressures

Energy is simply proportional to the fuel fraction as shown in equation (31). In fact, in this analysis where only one fuel is considered, it might have been easier to talk in terms of fuel

fraction. The power refers to the total propulsion and lift power, and the reference weight includes both the machinery and fuel weight. Figure 19 presents a power-energy plot similarly to an earlier report.[5] The solid lines are referred to as the vehicle requirement, since it is essentially a function of vehicle drag, propulsion efficiency, and other parameters determined by the vehicle. The vehicle requirement is related via equation (31) to the fuel fraction calculated in the previous section. As the cushion pressure is increased, the vehicle requirement curve shifts to higher power/weight ratios. This is a result of the increasing power with increasing cushion pressure and velocity. Velocity increases with cushion pressure, since corresponding points on the vehicle requirement curve in figure 19 have the same speed parameter. That is, the speed parameter at the minimum energy point is 0.23, which is the same as was found for them in figure 18 at a 1000-mile range. To the right of the minimum, the energy increases with increasing aerodynamics and momentum drag, just as shown in figure 10. To the left of the minimum, the energy approaches infinity not only due to the increasing lift power, but in addition the velocity approaches zero at a finite power weight ratio as shown in the top portion of figure 19. This is attributed to the lift system which still requires power at zero vehicle velocity. Needless to say, it takes infinite energy to get any range at zero vehicle velocity. Including auxiliary power requirements will cause a similar effect. This study does not include auxiliary power considerations.

The dashed line in figure 19 is referred to as the power plant requirement, since it is a function of the power plant's specific weights. It is a function of cushion pressure, since the lift system is heavier than the propulsion system by a factor $\beta$. Higher cushion pressures result in heavier lift machinery at the same total power level, resulting in a shift of the data to lower energy/ and power/weight ratios. This is also reflected in the intersection of the power plant requirement with the ordinate. The intersection is the inverse of the power plant specific weight,[5] just as the intersection of the abscissa is the inverse of the energy specific weight. As pointed out[5] these are basic quantities and can only be improved by going to higher energy fuels and lighter machinery configurations, both of which are improbable for this application. Actually the power plant requirements for nonzero cushion pressures will not intersect the abscissa, but the locus of the zero velocity points will intersect the correct point on the abscissa.

The intersection of the vehicle and power plant requirements represents the possible,operating points of the vehicle. There usually exist two intersections for each cushion pressure corresponding to a lift- or propulsion-dominated system (left or right intersection, respectively). The figure indicates that higher cushion pressure will result in higher power/weight ratios due to the higher velocities.

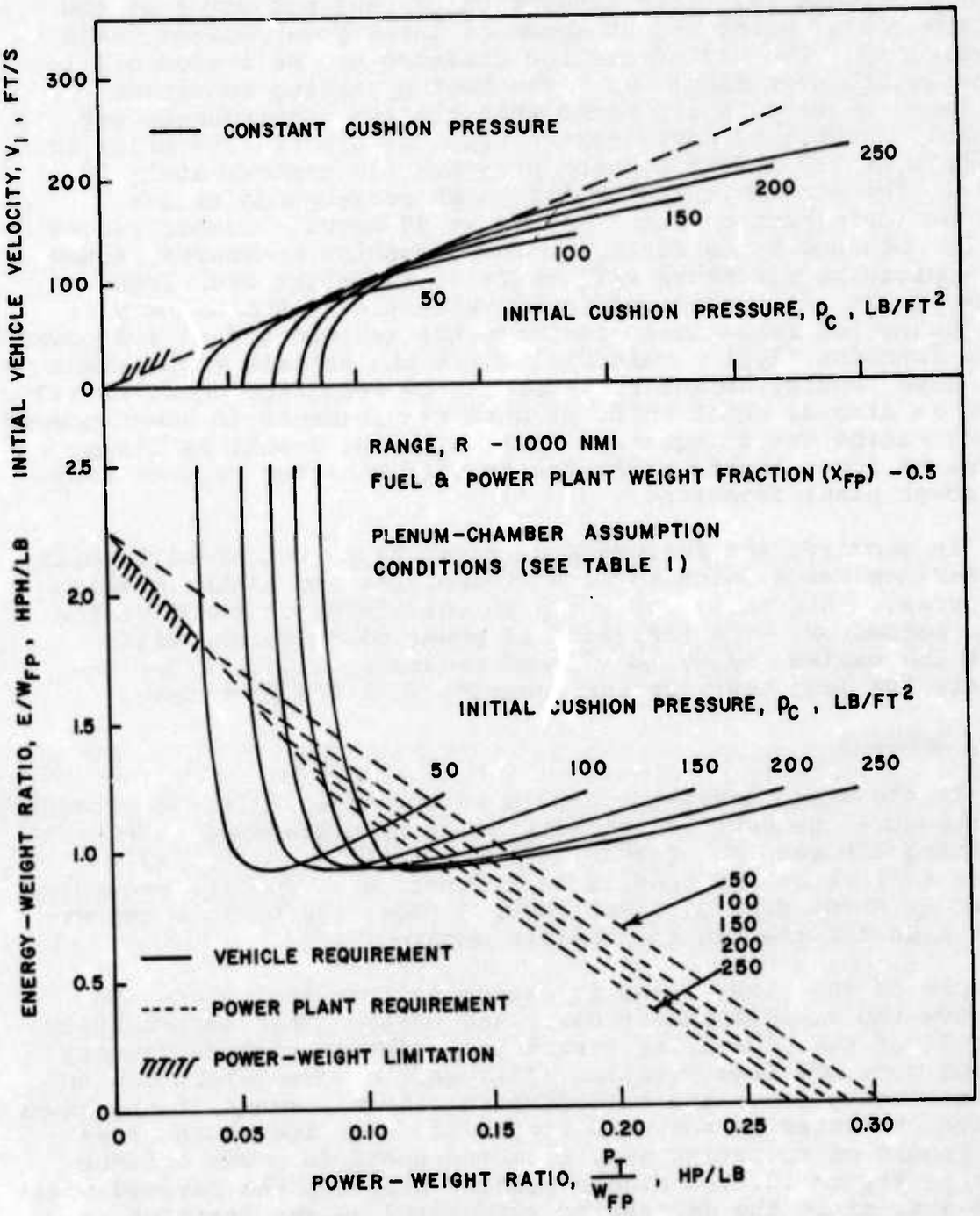


Figure 19
Power-Energy Tradeoff as a Function of Initial Cushion Pressure

The vehicle and power plant requirements are tangent at a cushion pressure of about 280 $lb/ft^2$. This represents the maximum cushion pressure the vehicle can operate at for the conditions shown in figure 19. This tangent point does not occur at the minimum energy point but at somewhat lower power/weight ratio or velocity. The higher cushion pressure can be traded off for range as shown in figure 20. The best operating condition (maximum range) is again found when the two requirements are tangent. Figure 20 shows that a range of almost 1500 miles is possible at 150 $lb/ft^2$ cushion pressure and approximately 70 knots. The minimum energy point which corresponds to the minimum fuel fraction point occurs at 90 knots. Longer ranges can be obtained by operating at lower cushion pressures, since the vehicle requirements will shift to the right with lower pressures at the expense of lower velocities. Another way of increasing the range is to increase the vehicle's fuel and power plant fraction ($X_{PP}$). This will shift the vehicle requirement to a lower energy/weight ratio as can be seen from equation (33). There is also an equal shift of both requirements to lower power/weight ratios due to equation (34). The net result is longer ranges at lower power/weight ratios with a higher vehicle fuel and power plant fraction.

In summary, the inclusion of power plant weight will shift the maximum range point to lower velocities and higher cushion pressures. This shift can again be correlated in terms of the speed parameter. The inclusion of power plant weight will shift the maximum range to a speed parameter which is approximately 10% less than for the constant fuel fraction case.

## CARGO LOADING

In the cargo loading analysis of the vehicle it was necessary to introduce the vehicle velocity or cushion pressure. In examining the results of this analysis it will be initially easier to look at the results as a function of cushion pressure. Figure 21 shows some of these results under the various assumptions made for the fan and the air cushion.

One of the first items to notice is that at low cushion pressure the vehicle cannot carry any cargo. This is primarily a result of the increasing structural fraction with decreasing cushion pressure (see equation (44)) and to some extent due to the increasing power and therefore fuel requirements at the lower cushion pressures as shown in figure 22. The increasing power is a result of operating away from the specific power optimum shown in figure 10. At higher cushion pressure the payload again decreases, since the decreasing structural weight fraction is over shadowed by the increasing machinery and fuel weight fraction. This increasing machinery and fuel weight is again a result of operating away from the optimum specific power point. The cargo loading parameter ($\pi_C$), also shown in figure 21, represents the distribution of the payload over the entire area available for that purpose (see equation (45) for the definition of this term).

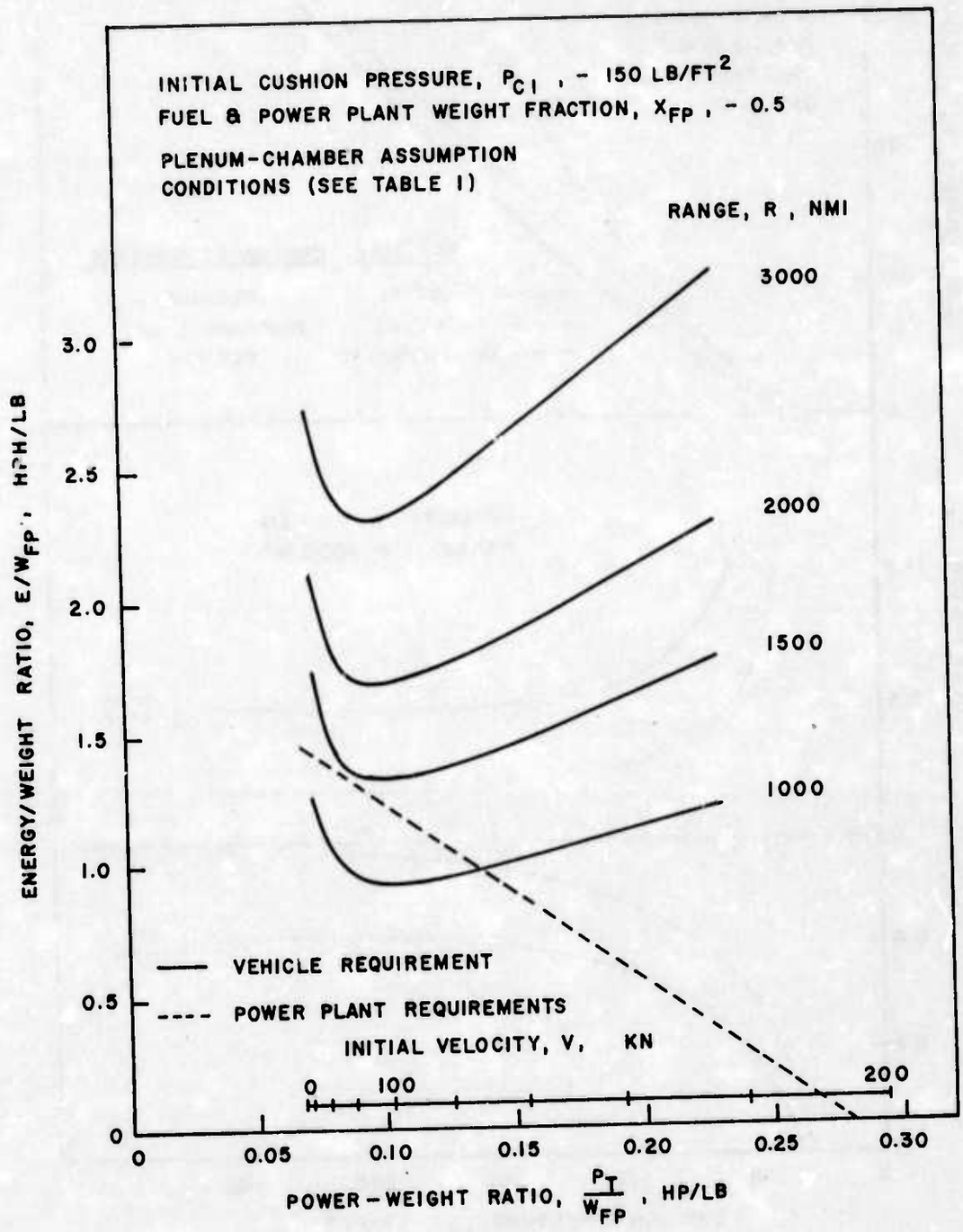


Figure 20
Power-Energy Tradeoff at Constant Range and Initial Cushion Pressure

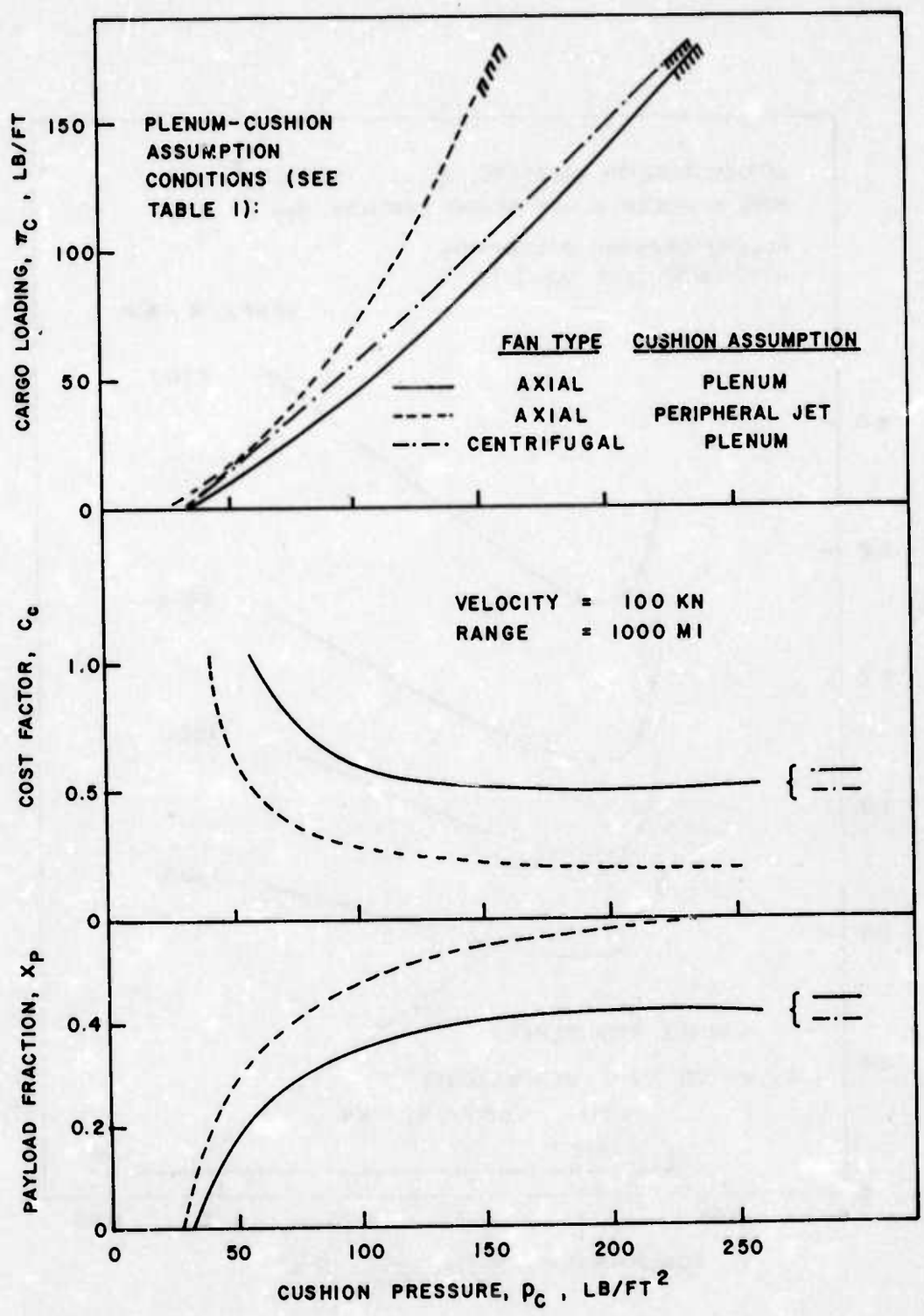


Figure 21
Effect of Fan Type and Cushion Assumption on
Cargo-Carrying Capacity

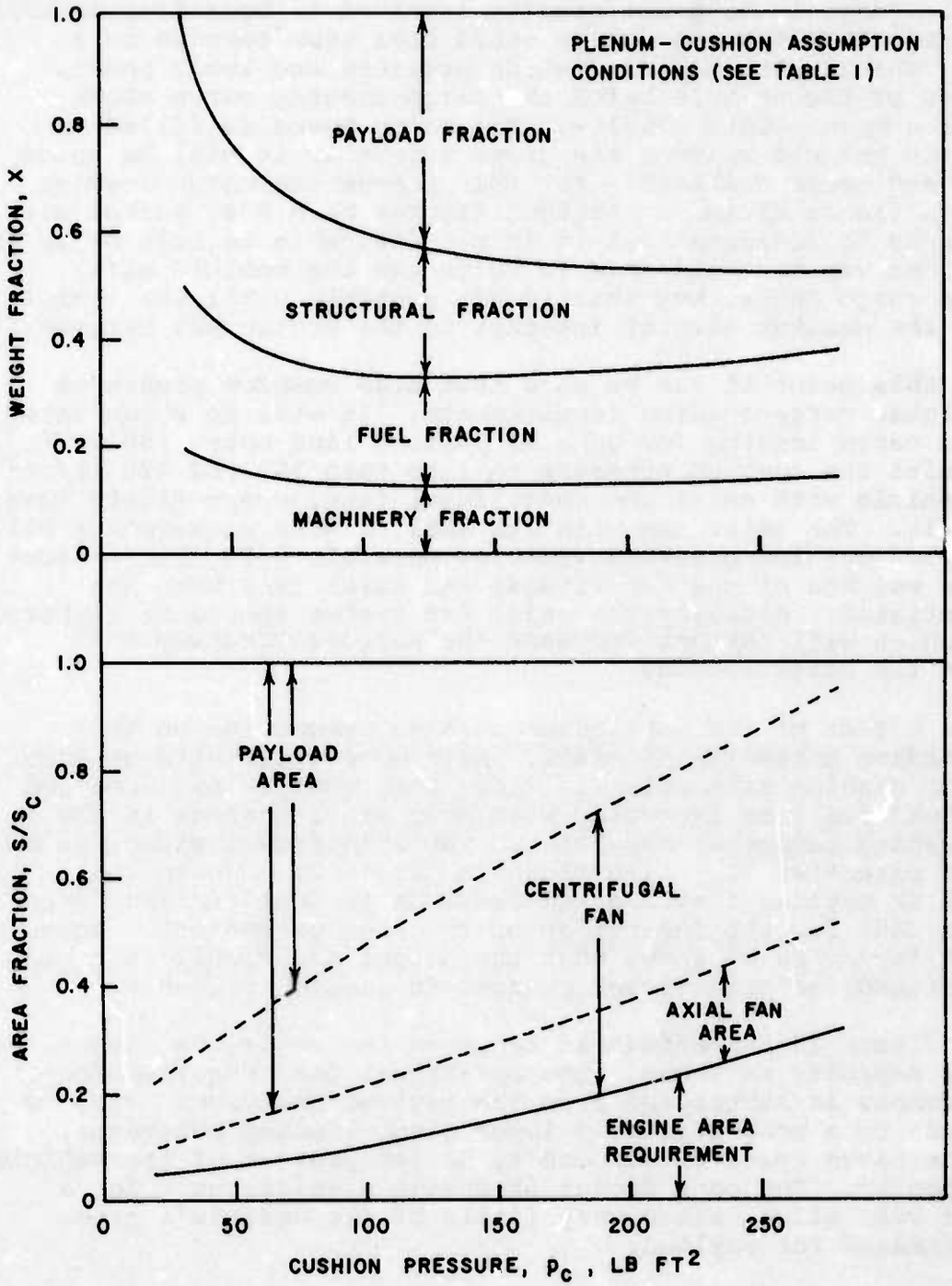


Figure 22
Variation of Vehicle Weight and Area Fraction
as a Function of Cushion Pressure

Carrying cargo whose loading exceeds the line shown in the figure means that the vehicle will encounter its weight limitation before the entire cargo space is filled or the vehicle is weight limited. There is no great penalty involved in operating in this mode except that the same cargo could have been carried on a smaller vehicle with higher cushion pressure and lower power. Operation of the vehicle below the cargo-loading curve shown presents a more severe penalty. The cargo space is filled up before the vehicle reaches its gross weight or it will be space limited and under utilized. For this reason the cargo loading curves in figure 21 and subsequent figures have been marked with hatch marks to indicate that it is not desirable to work below this curve. One way to avoid this is to design the vehicle with multiple cargo decks, but this is not possible until the vehicle exceeds the maximum size of interest to the Arctic SEV Program.

At this point it can be said that high cushion pressures force higher cargo-loading requirements. It will be shown later that the cargo loading for general payload lies below 100 $lb/ft^2$. This limits the cushion pressure to less than 165 and 120 $lb/ft^2$ for a vehicle with axial and centrifugal fans, respectively (see figure 21). The axial fan with its smaller area requirement will make higher cushion pressure vehicles possible. In this present analysis weights of the ce trifugal and axial fans were not differentiated. Actually the axial fan system should be lighter, a fact which will further increase the payload fraction and increase the cargo loading.

The effect of the particular cushion assumption on the cargo-loading parameter is small. As a more optimistic or more efficient cushion assumption is made, both the payload area and the payload fraction increase, with only small changes in the cargo-loading parameter resulting. The significant effect is on the cost parameter ($C_c$) also shown in figure 21, due to the increase in payload fraction and decrease in fuel fraction (see equation (46) for the definition of the cost parameter). Again, the cost factor curve shows that the slight additional cost can be sacrificed for significant changes in cushion pressure.

In figure 23 the effect of range on the vehicle's cargo-carrying capacity is shown. The additional fuel required for longer ranges is subtracted from the payload fraction. This in turn leads to a proportionally lower cargo-loading parameter, since the cargo space is assumed to be independent of the vehicle fuel capacity. The cost factor increases significantly for a range of 3000 miles, since very little of the vehicle's gross weight remains for payload.

Figure 24 shows the effect of the speed on the vehicle's cargo-carrying capacity. The zero payload point moves to higher cushion pressures as the velocity increases, since the vehicle's machinery and fuel fraction increases with increasing velocity. The maximum payload fraction increases slightly and is located at higher cushion pressures with increasing vehicle velocity.

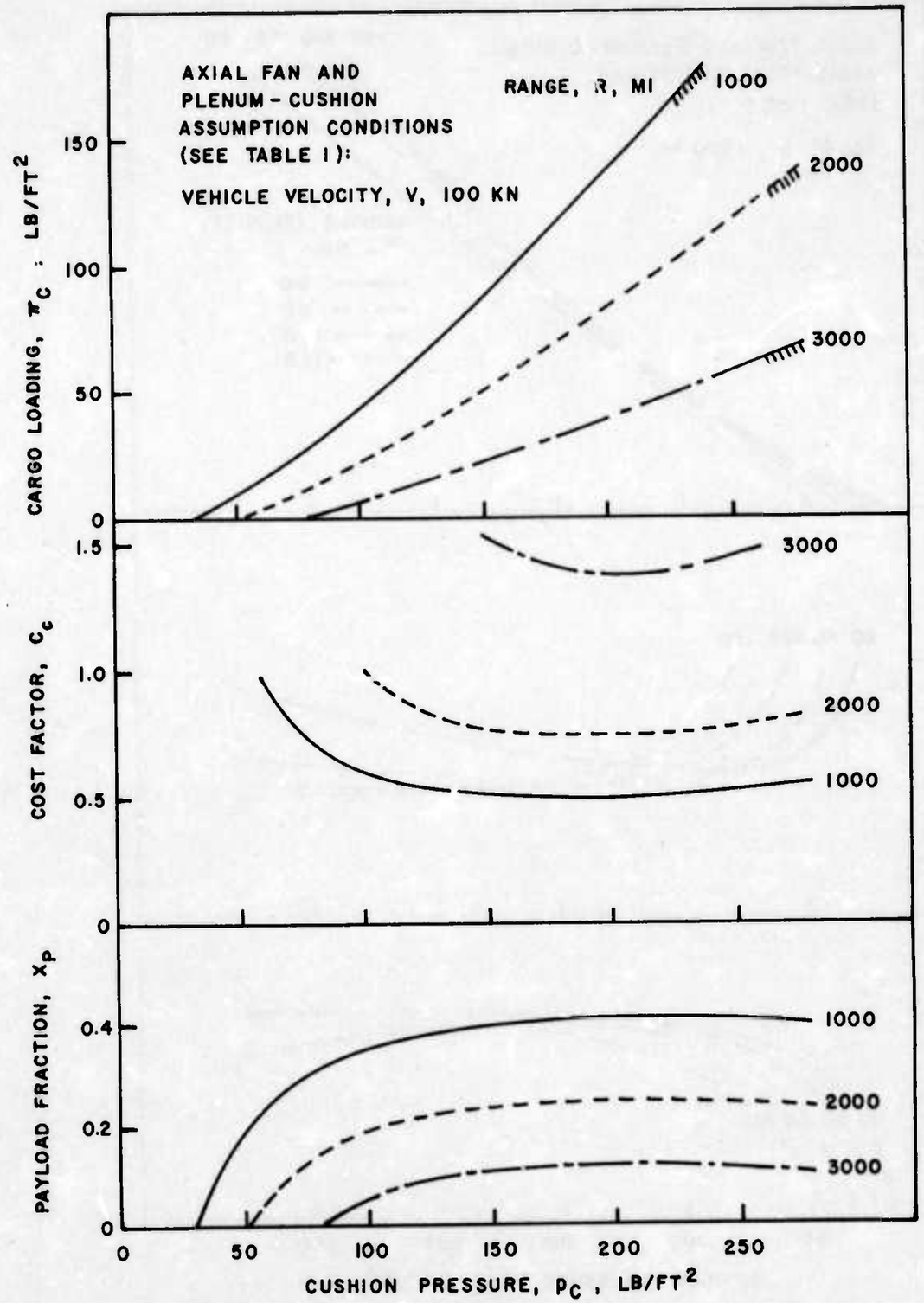


Figure 23
Effect of Range on Cargo-Carrying Capacity

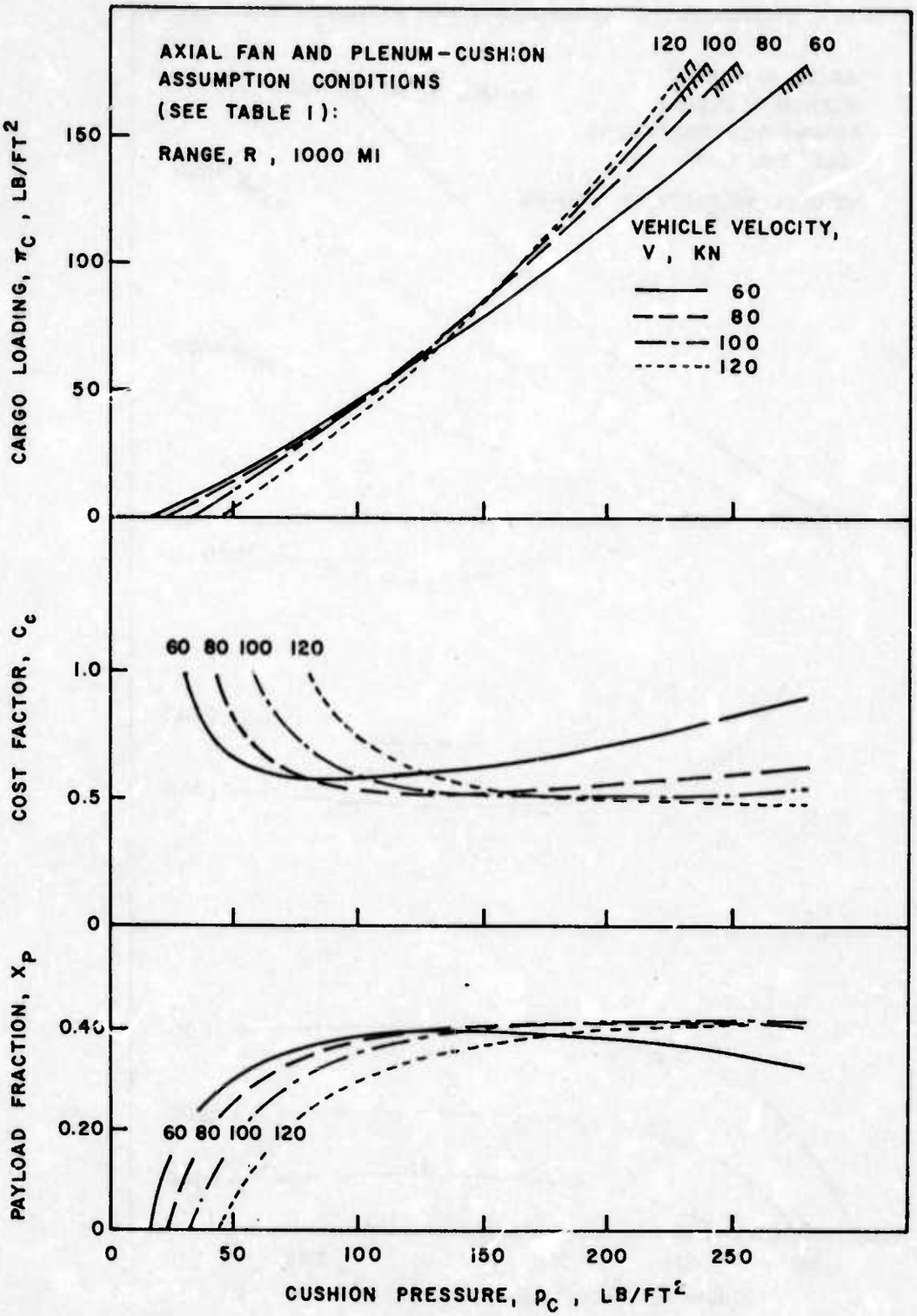


Figure 24
Effect of Vehicle Speed on Cargo-Carrying Capacity

This phenomenon is a result of the optimum specific power occurring at higher cushion pressure with increasing velocity and the lower structural fraction at these higher cushion pressures. The cargo-loading parameter does reflect the payload fraction behavior. At low cushion pressure the cargo-loading parameter is higher for low velocity conditions due to the higher payload fraction, while at higher cushion pressures the cargo-loading parameter is smaller for the low velocities partially due to the lower payload fraction and lower engine-space requirements. The cost factor minimizes at a cushion pressure which is lower than the one which yields the maximum payload fraction. This is a result of the increasing fuel fraction while the cargo fraction is still increasing.

Figure 24 suggests that the operating cost parameter can be correlated in terms of the speed parameter (k). That is, since the lower velocities optimize at lower cushion pressures, it might be possible to collapse all the data in terms of the speed parameter. Figure 25 shows that the speed parameter does indeed collapse these data. The minimum operating cost is found at a speed parameter between 0.14 and 0.19, with lower cargo loading and lower vehicle speeds producing the lower value of the quoted speed parameter. The 10% higher cost parameter is encountered at a 55% to 65% higher speed parameter than the minimum cost case. The operating region for cargo-carrying consideration will be defined as the range between minimum and 10% higher cost. Figure 26 shows the effect of range on the cargo-loading/speed-parameter correlation. Increased range shifts the operating region to lower speed parameter and cargo loading. The effect of the type of fan or cushion assumption on this operating region is shown in figure 27. The peripheral-jet-cushion assumption shifts the operating region to lower values of the speed parameter, but it should be remembered that this cushion assumption is overly optimistic. The effect of the fan type on the operating range is small.

It should be realized that, when collapsing the data in this manner, the effect of the cushion pressure is lost. Therefore, in figure 28 the cushion-pressure/cargo-loading relationship has been plotted for both axial and centrifugal fans. The immediate result is that the smaller size of the axial fans will allow higher cushion pressures for the same cargo loading compared to a centrifugal fan-equipped vehicle. This is especially noticeable at higher speeds, higher cargo loading, and longer ranges. In fact, it can be said that, even for an axial fan installation, vehicles with cushion pressures in excess of 310, 220 and 170 $lb/ft^2$ are not of interest for 3000-, 2000-, and 1000-mile vehicles. Under such conditions these vehicles cannot carry generalized cargo at a loading of 100 $lb/ft^2$. Again the curves in figure 28 have been hatch-marked to indicate the direction in which the vehicle encounters the cargo volume limitation. The effect of speed and cushion pressure and cargo loading shown in figure 28 has already been noted in previous figures.

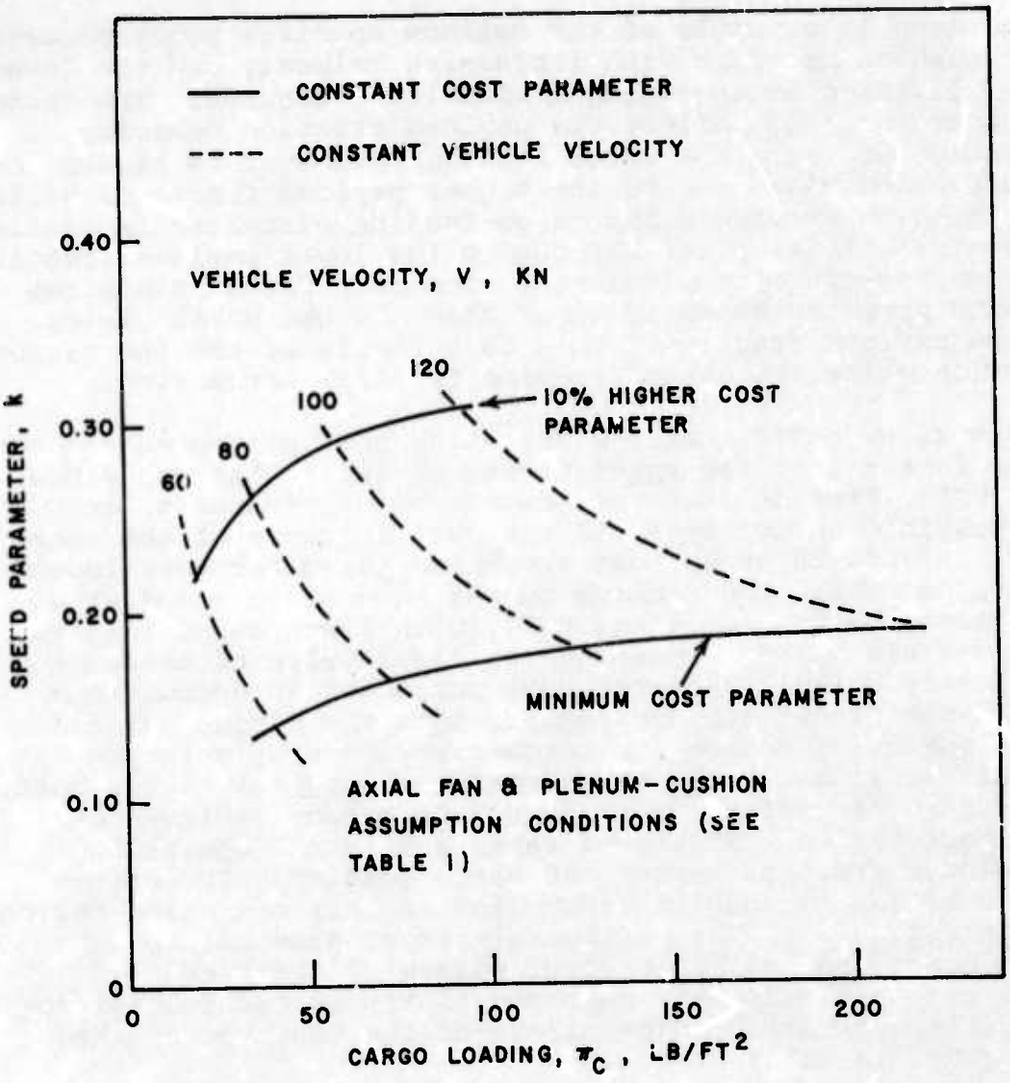


Figure 25
Cargo-Loading/Speed-Parameter Correlation
for a 1000-Mile Range

The effect of accepting 10% higher cost is a shift to both lower cushion pressures and lower cargo loading, as shown in figure 29. The shift to lower cushion pressure and cargo loading generally follows a constant range curve. Trading off additional cost for increased cushion pressure is not of interest, since it also will result in higher cargo-loading requirements. Again, one can operate below the constant velocity and to the right of the constant range lines without encountering the vehicle's cargo limitation. Above a 10% cost increase, the payoff is very little, since the cost increases rapidly, like the total specific power shown in figure 11.

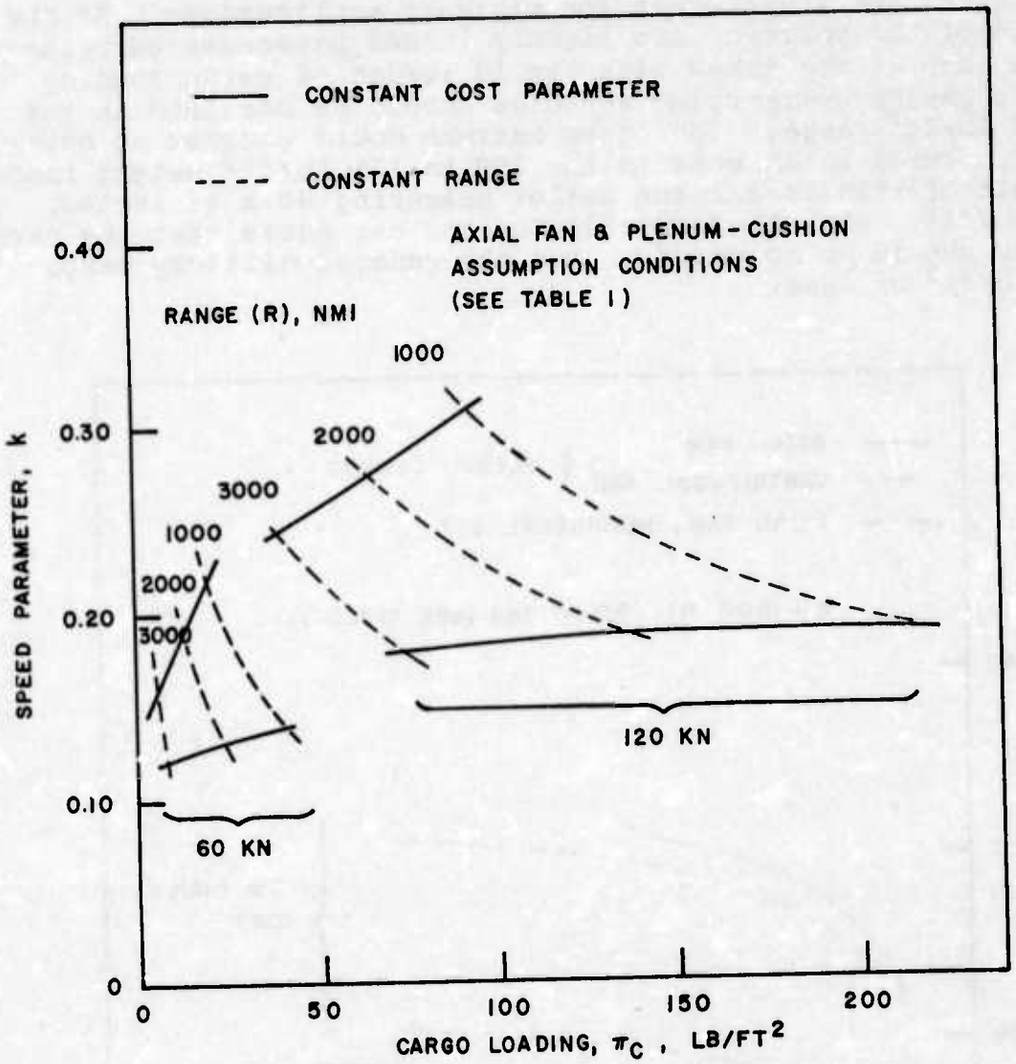


Figure 26
Cargo-Loading/Speed-Parameter Correlation
for 60 and 120 Knots

Also shown in figure 28 is the cargo loading and cushion pressures for a small number of vehicles for which this information was easily obtainable. In general, these data do agree with the present analysis. Most of the current vehicles have a small range and a low speed. The two amphibious assault landing craft (C-150) have a fairly high cargo loading and cushion pressure by present standards. This was forced by the constraints placed upon these vehicles by the dimensions of the landing ship well. A representative military application[12] such as deploying a battle-ready division will require a cargo loading of 71.5 lb/ft$^2$. Therefore, it can be expected that cargo loadings of 50

to 100 lb/ft$^2$ are of interest for military applications. At the lower end of the spectrum are lightly loaded passenger-carrying vehicles such as the SRN-4 with its 19 lb/ft$^2$ of cargo loading. Therefore passenger-carrying vehicles should be designed in the 20 to 30 lb/ft$^2$ range. The other extreme would consist of heavy palletized cargo which runs in the 150 to 175 lb/ft$^2$ weight range. An example of this is a 1-ton pallet measuring 40 x 48 inches, or 168 lb/ft$^2$. With these statistics one can guess that the cargo of an SEV should be no heavier than the general military cargo of 100 lb/ft$^2$ or less.

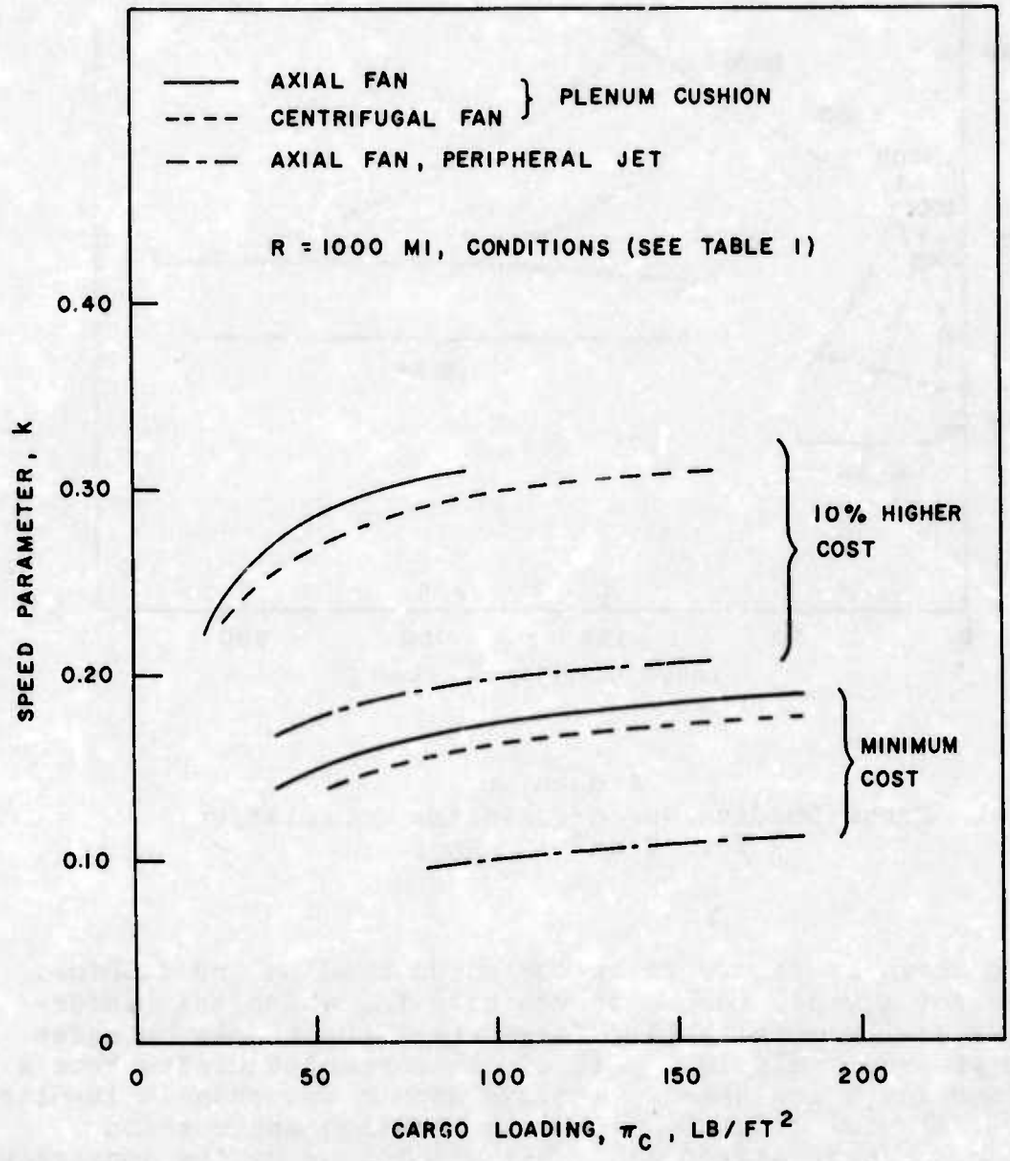


Figure 27
Effect of Fan Type and Cushion Assumption on Cargo Loading and Speed Parameter

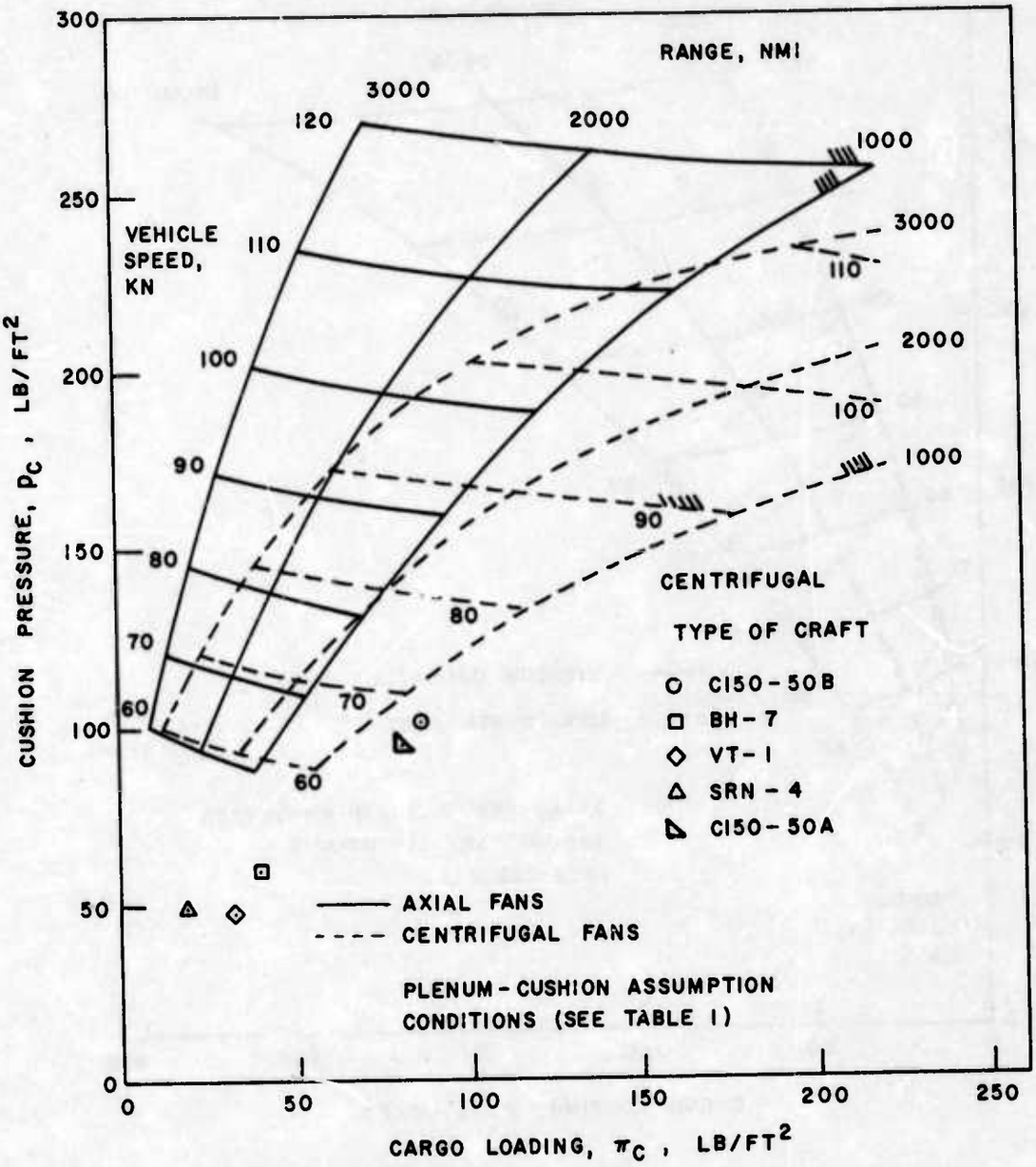


Figure 28
Cushion-Pressure/Cargo-Loading Correlation
for Axial and Centrifugal Fans

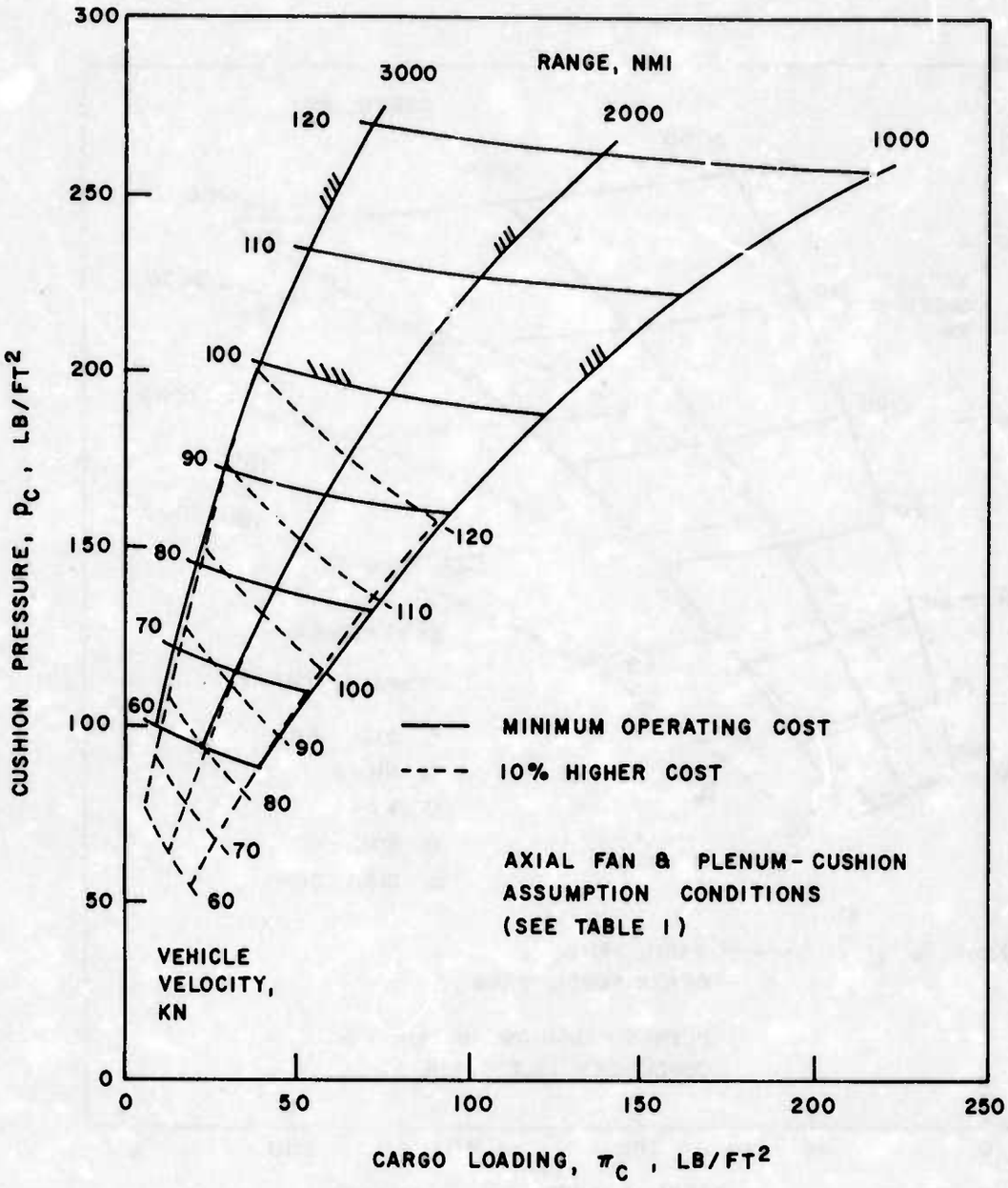


Figure 29
Effect of Operating Cost Parameter on
Cushion Pressure and Cargo Loading

THRUST MARGIN

The two additional parameters which are needed for this portion of the discussion are the pressure/length ratio ($p_c/\ell$) and the vehicle weight ($W_G$) or the propeller thrust coefficient ($C_T$). Pressure/length ratio is a convenient parameter for this discussion, but later it will be eliminated with the aid of the vehicle velocity and the speed parameter. Figure 30 shows the composite of the propeller thrust and the vehicle drag. The propeller characteristic is shown as a function of the thrust coefficient for a free propeller. The thrust is not linear, since the abscissa is proportional to the square of the velocity. As can be seen, the static thrust (and therefore the thrust at the wave drag hump) dependence on the thrust coefficient is appreciable. The thrust coefficient shown is approximately the range which is of interest for vehicles between 100 and 1000 tons under the assumptions of this analysis. In general, the contribution of the wave drag to the total drag above the wave drag hump is small. The dependence of the wave drag in this region is a nonlinear function of the pressure/length ratio (see equation (52)). Small values of the pressure/length ratio have a great effect on the wave drag, while the dependence in the region of interest ($(p_c/\ell)$ between 0.6 and 1.4) is very small. In the Analysis section it was mentioned that the supercritical wave drag approximation was within 10% for Froude numbers above 1.0. Figure 31 shows that this indeed covers the entire region above the minimum total drag point. The region between the wave drag hump and the minimum total drag point does not represent a stable operating region.

At the wave drag hump the total drag primarily consists of the wave drag with the pressure/length ratio being the important variable. The position of this hump is also slightly dependent on the pressure/length ratio. Figure 31 shows the slight effect of the length/beam ratio on the speed of the wave drag hump. The noteworthy item is that the magnitude of the wave drag hump decreases with increasing length/beam ratio, while the wave drag at the cruise condition does the opposite. In this region both momentum drag and wave drag increase with increasing length/beam ratio. The net result is that higher length/beam ratios will result in larger thrust margins not only due to a lower wave drag hump but also a higher drag at cruise. This is exactly demonstrated in figure 32, which shows the thrust margin as a function of the speed parameter for both the length/beam and pressure/length ratios. Both parameters have about the same influence on the thrust margin. As was found from the previous figures, the thrust margin increases with increasing length/beam ratios and decreasing pressure/length ratio. Generally, above a speed parameter of 0.2, one can obtain an acceptable 40% thrust margin.

The effect of vehicle weight and type of propeller is shown in figure 33. The larger vehicles have a lower thrust margin at the same speed parameter than the smaller vehicles.

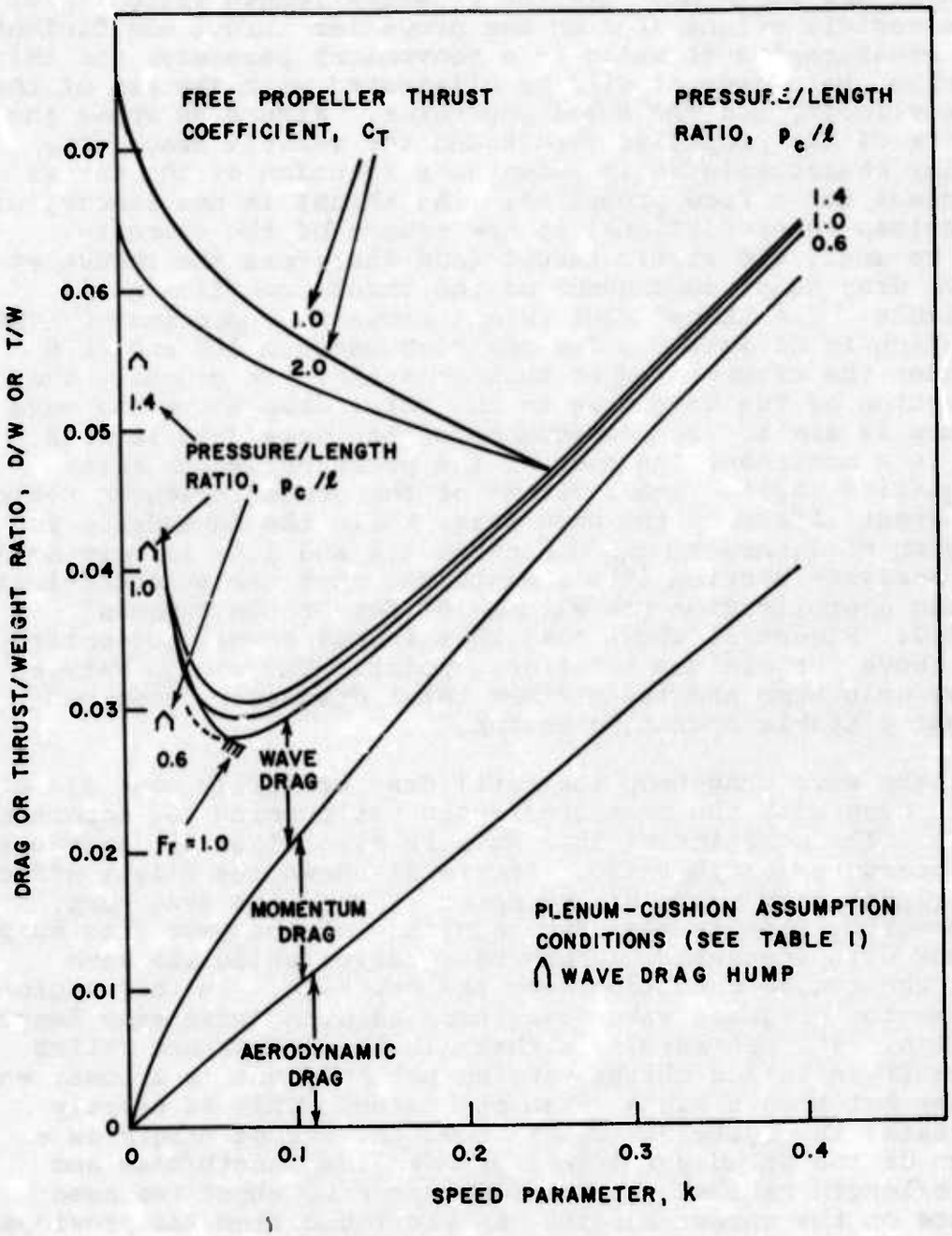


Figure 30
Thrust-Drag Profiles as a
Function of Pressure/Length Ratio

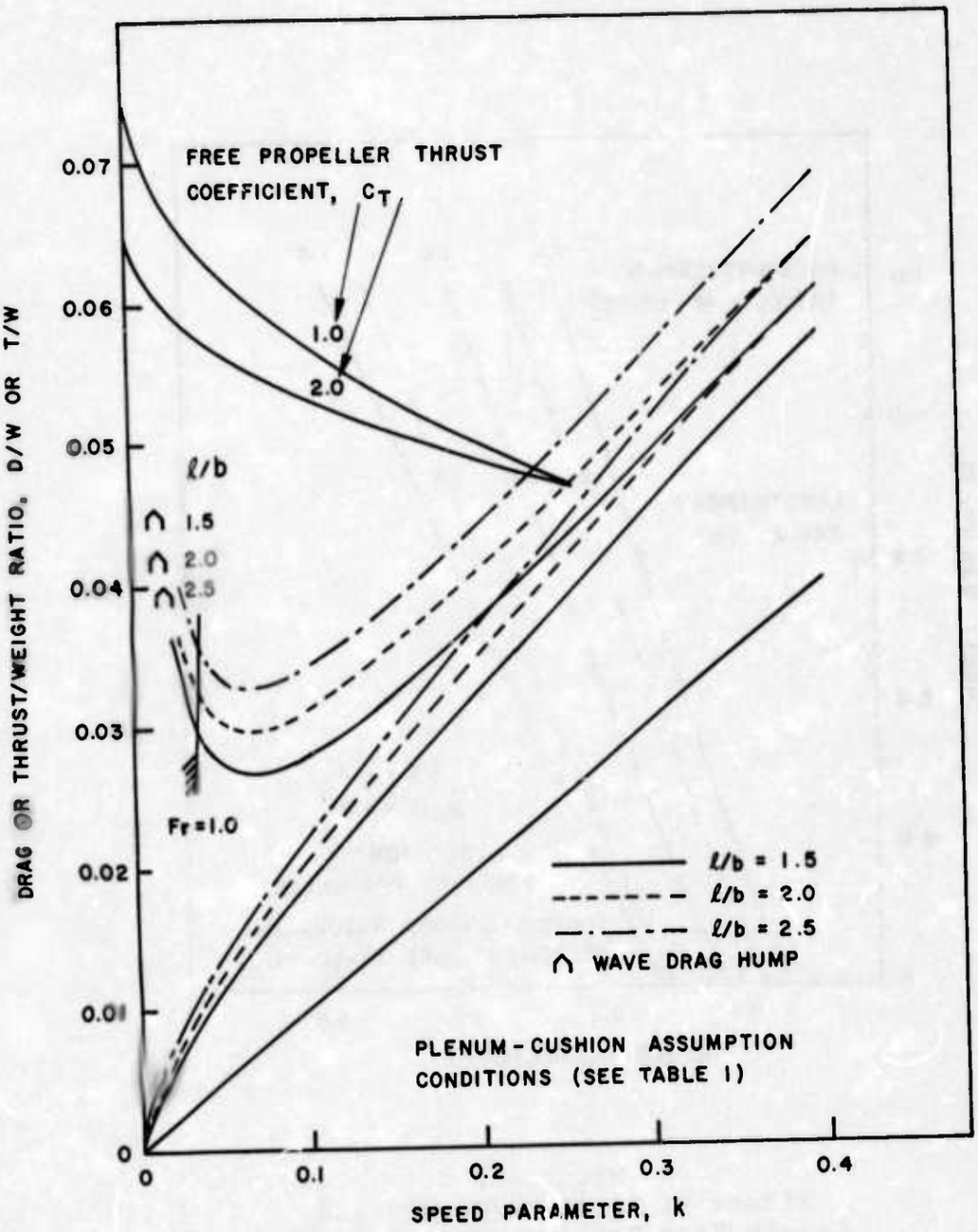


Figure 31
Thrust-Drag Profiles as a Function
of Length/Beam Ratio

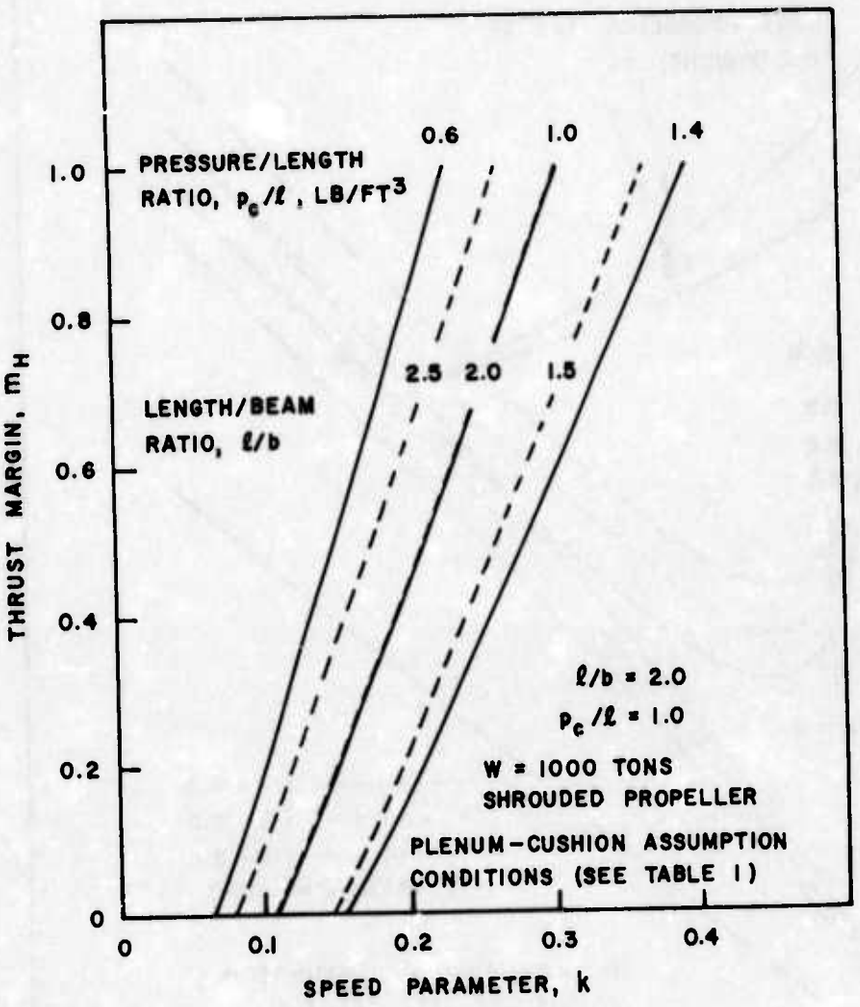


Figure 32
Effect of Pressure/Length and
Length/Beam Ratio on Thrust Margin

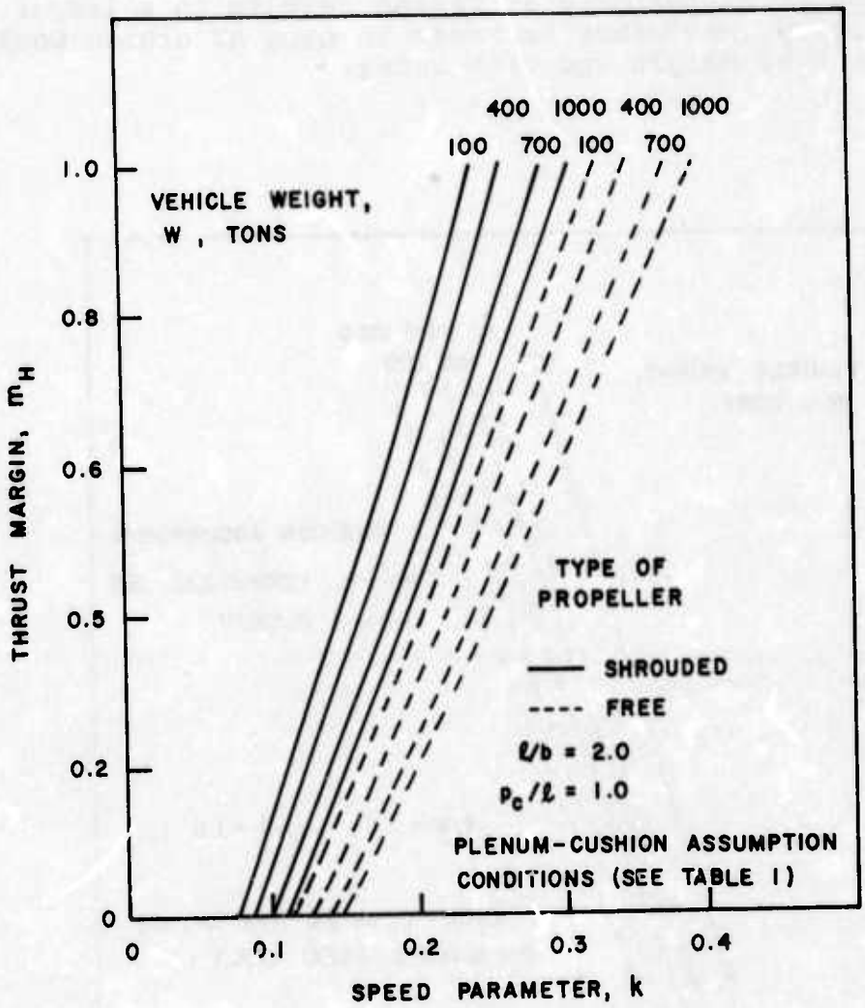


Figure 33
Effect of Vehicle Weight and
Propeller Type on Thrust Margin

This is a direct function of the higher thrust coefficient due to the higher cushion/propeller area ratio where the larger vehicles are forced to operate (see figure 9). The free propeller thrust margin is appreciably lower than that of shrouded propellers. If the shrouded propeller thrust margin is 50%, the thrust margin of a similarly installed free propeller would be only 35%. The effect of the cushion assumption is shown in figure 34. The lower efficiency plenum-chamber assumption with its higher momentum drag and therefore higher drag at cruise results in a larger thrust margin. Similarly, any other increase in drag at cruise would increase the thrust margin and vice versa.

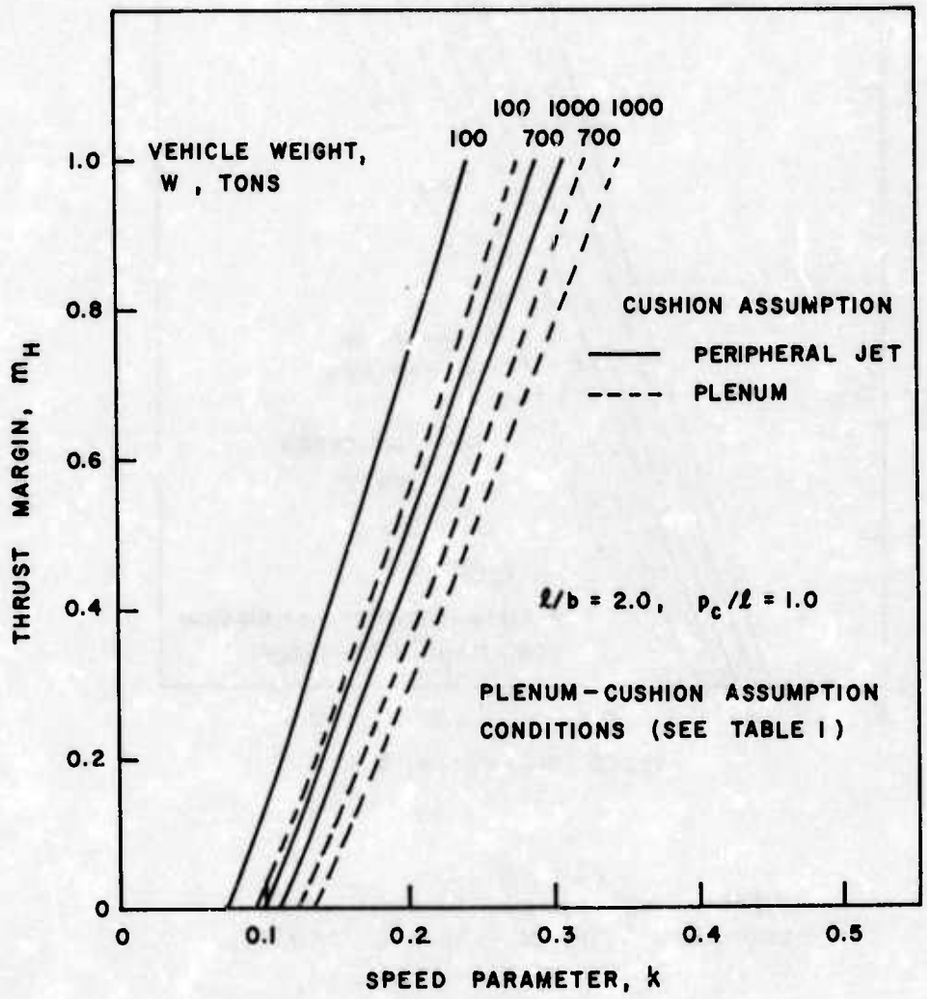


Figure 34
Effect of Cushion Assumption on Thrust Margin

## SUMMARY

As was stated in the Introduction, a summary of the results of the three analyses (power requirements, cargo loading, and thrust margin) and a definition of desirable operating regions will be attempted from the standpoint of vehicle powering. The total power analysis revealed that it was possible to summarize the results in terms of the speed parameter exclusively. The desirable range was between a speed parameter of 0.25 for minimum power to 0.42 for 10% more power, but lower cushion pressure under the plenum cushion assumption. This is shifted to a lower speed parameter with increasing range. In the case of constant power plant and fuel fraction, the results were not directly dependent on speed, vehicle weight, and cushion pressure. In the case of the cargo analysis it was found that, besides the cargo loading, the velocity also entered into the analysis. Figure 25 summarized the essential results of this analysis. Figure 35 replots these data along with the specific power results. It is at first surprising that the cargo study optimizes at a lower speed parameter than the minimum power, but it should be recalled from figure 22 that the payload fraction increases with increasing cushion pressure primarily because of the decreasing structural fraction. This in turn leads to lower cost at a lower speed parameter.

Also shown in figure 35 is the cargo loading limit of 100 $lb/ft^2$, below which most of the cargo is distributed. This limit indicates that design of vehicles is not warranted from an economic point of view for speeds in excess of 120 knots at a range of 1000 miles. In general, these high-speed vehicles optimize at a high cargo loading which is not of interest. By going to longer ranges the whole map can be shifted to lower cargo loadings and slightly lower speed parameters as shown in figure 36. The shift is a result of the additional required fuel which is subtracted from the payload but not the cargo area. At 3000 miles, one can carry payload with a cargo loading of less than 100 $lb/ft^2$ up to 150 knots and still operate near the optimum cost region. It should be noted that the cost parameter increases significantly with range (see figure 25). This problem is reflected somewhat by the behavior of the constant velocity curves at low speed parameters, as shown in figure 36. At a 3000-mile range the vehicle cannot carry any payload at a speed parameter below 0.04. At larger ranges this cutoff will be found to lie above the optimum cost area.

Previously, it was convenient to show the thrust margin results as a function of the pressure/length ratio and speed parameter. In order to make the results consistent with figure 35, it will now be of interest to eliminate the pressure/length ratio in terms of the vehicle velocity with the following equation:

$$\frac{P_c}{\ell} = \frac{1}{W_G^{1/2}\left(\frac{\ell}{b}\right)^{1/2}} \left(\frac{1/2\ \rho\ V^2}{k}\right)^{3/2} .$$

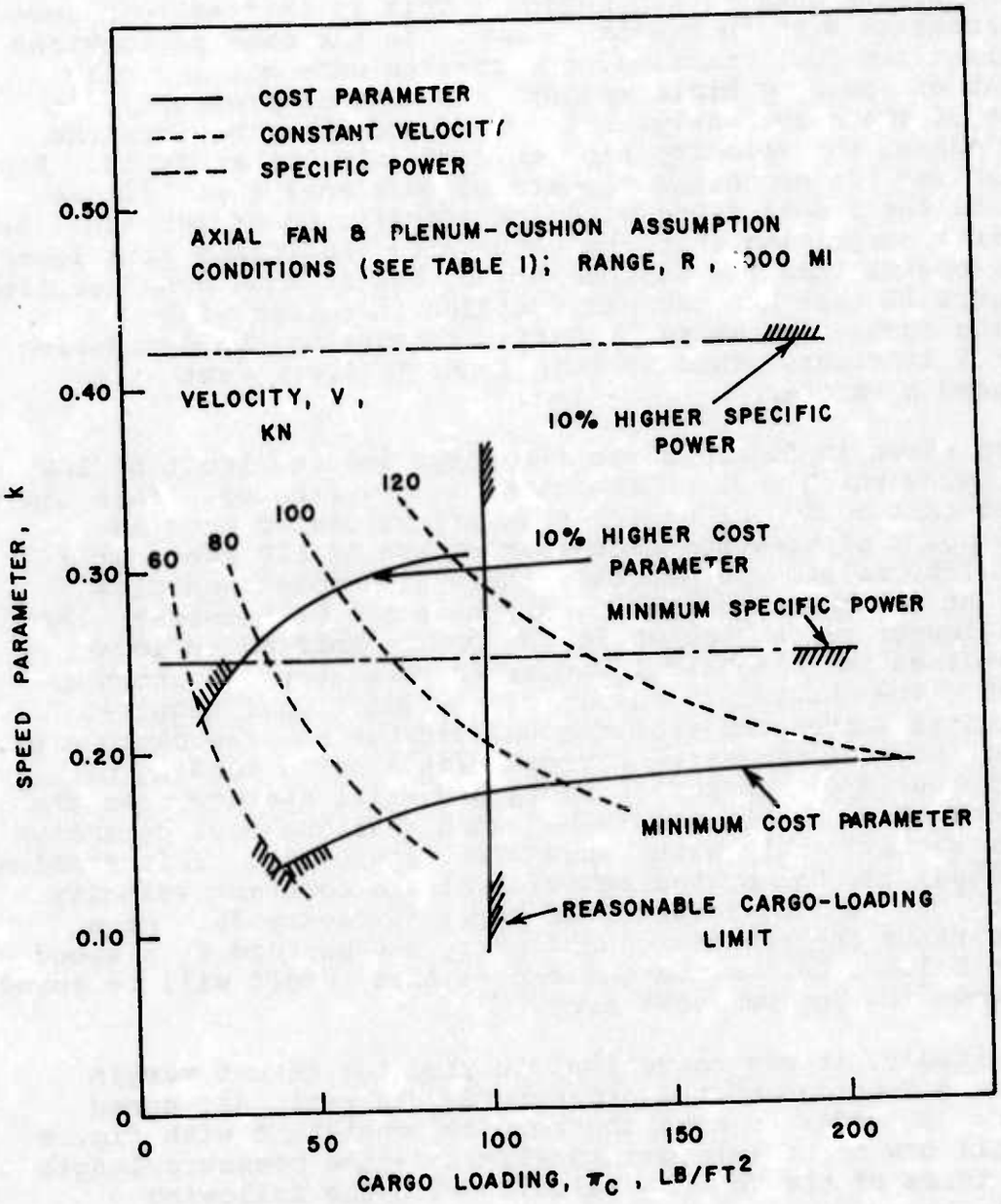


Figure 35
Specific Power/Cargo-Loading Summary

This equation was obtained with the help of equation (2). Figure 37 shows the speed parameter versus vehicle weight for a 50% thrust margin at both constant pressure/length ratio and constant velocity. For a constant pressure/length ratio the results are as previously noticed - that the larger vehicle requires a higher speed parameter. Also, for the smaller vehicles the cushion/propeller area ratio is independent of the vehicle weight due to the beam limitation on the propeller diameter (see figure 9). This results in a constant thrust coefficient and thrust margin which in turn results in a speed parameter independent of the vehicle weight.

The constant velocity results in figure 37 are first perplexing. At a constant velocity the smaller vehicle requires a higher speed parameter than a larger vehicle to reach 50% thrust margin. This is a result of the fact that a smaller vehicle with the same cushion pressure will have a higher pressure/length ratio than a larger vehicle and therefore less thrust margin. Then, in order to arrive at the same thrust margin, the speed parameter must be increased. Another discrepancy seems to be that higher speeds require higher speed parameters, but when one calculates the cushion pressure which goes along with each speed and speeds parameter, the cushion pressure increases with speed. This is indeed what was expected. It is just that the constant velocity plots are not the best way to view the results.

The thrust margin results for the 1000-ton vehicle are summarized with the cargo-loading results in figure 38, in terms of the more easily visualized cushion pressure and vehicle velocity. The figure again shows that, for reasonable cargo-carrying capability - that is, with cargo loading restricted to less than 100 $lb/ft^2$ - the cushion pressure must be restricted to less than 175 $lb/ft^2$. Vehicles designed to carry payload with lower cargo loading will require lower cushion pressures and also lower velocities. Reasonable thrust margins (72.5%) can be obtained between minimum and 10% higher cost factor regions. It should be remembered that various other assumptions discussed previously will shift the cargo-loading and thrust margin results. For instance, figure 28 shows that a longer range will shift the cargo-loading operation region to significantly higher cushion pressure and higher velocities, while the thrust margin will remain unaffected. The net result is that the thrust margin now becomes the limiting factor, forcing the designer to decrease the cushion pressure or increase the velocity.

Many more of these special aspects could have been covered in this report, but it would have expended a rather lengthy report even more. Other considerations, such as roll and directional stability, maneuvering forces, and cruise and dash considerations, also enter into a propulsion and lift-power tradeoff. Future studies should be performed which include additional considerations to help to determine parameters which could not be accomplished

in this analysis. For instance, a roll and directional stability tradeoff might help the determination of a desirable length/beam ratio.

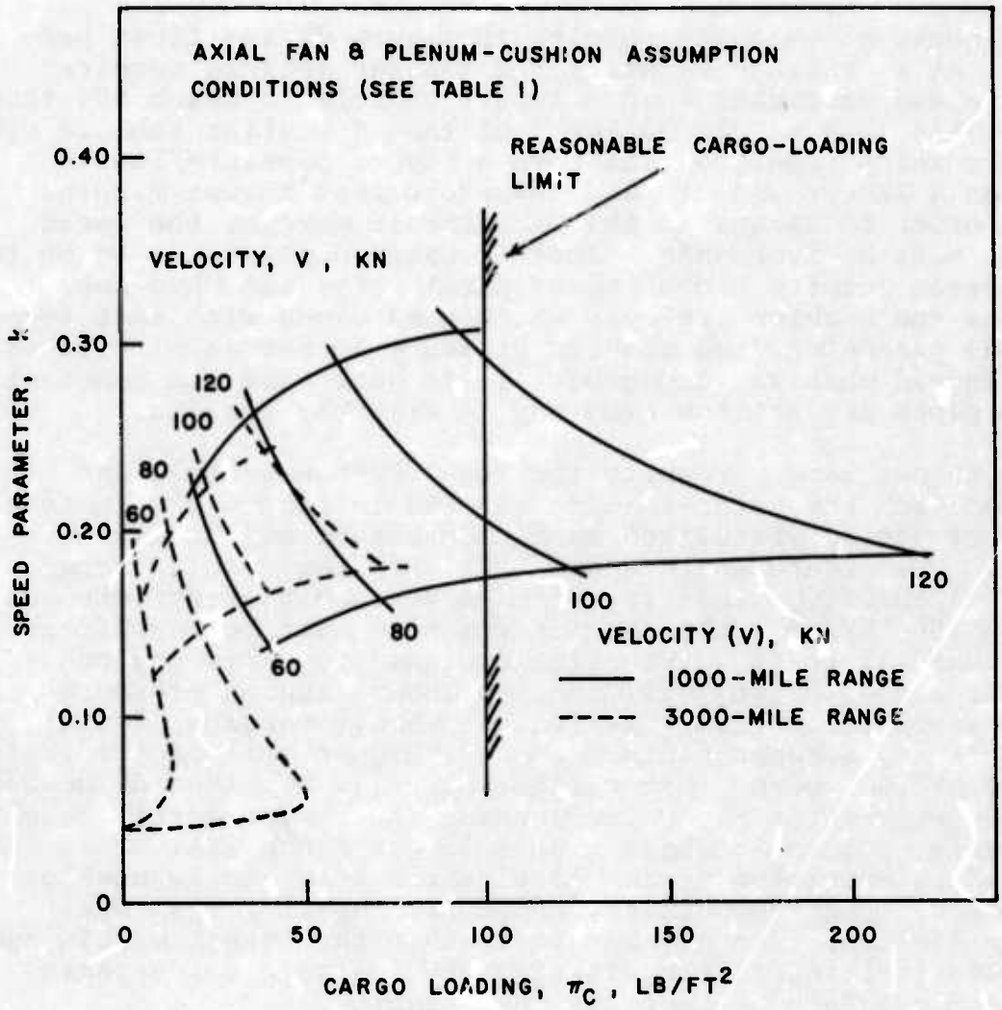


Figure 36
Cargo-Loading Summary,
1000- and 3000-Mile Ramge

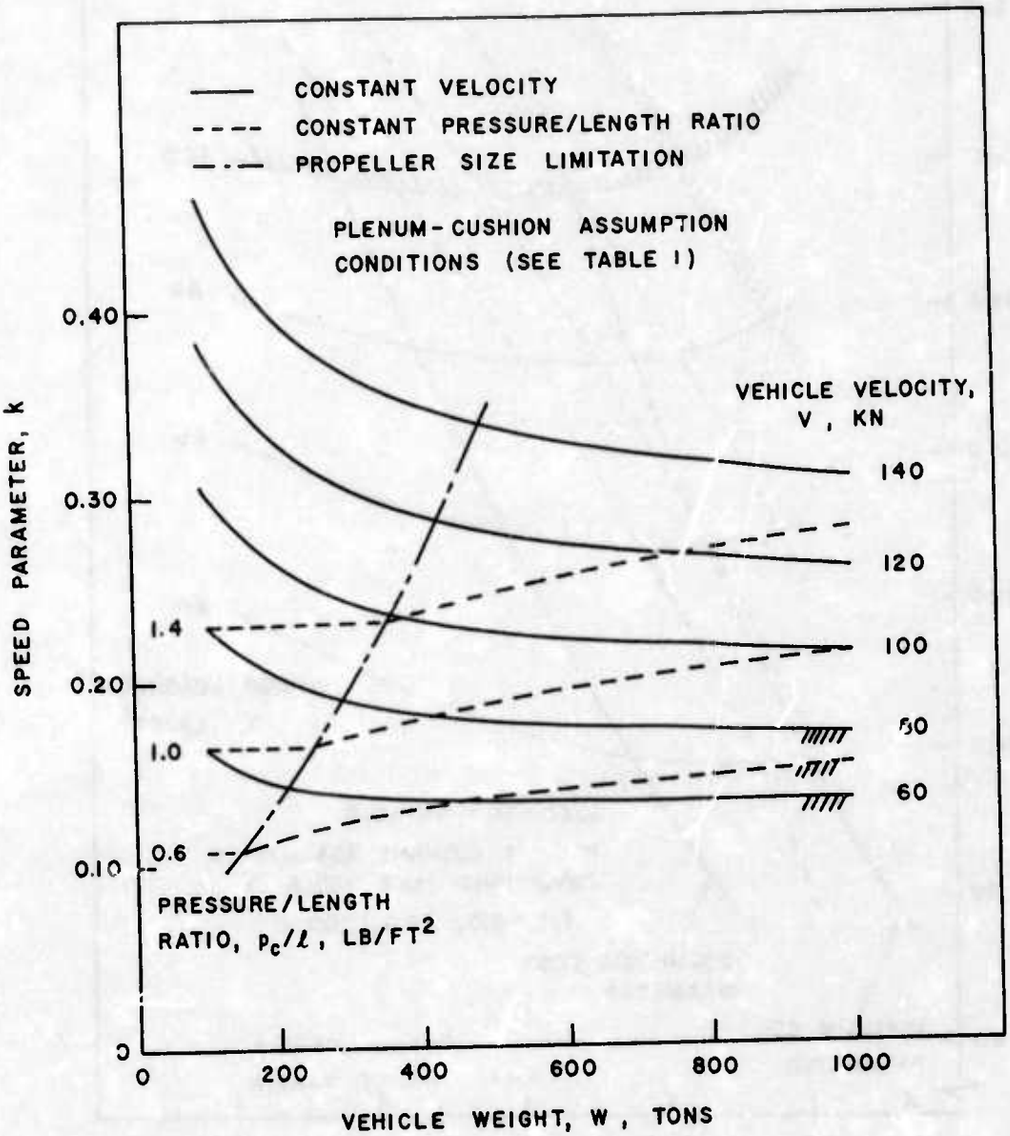


Figure 37
Thrust Margin Summary,
50% Thrust Margin

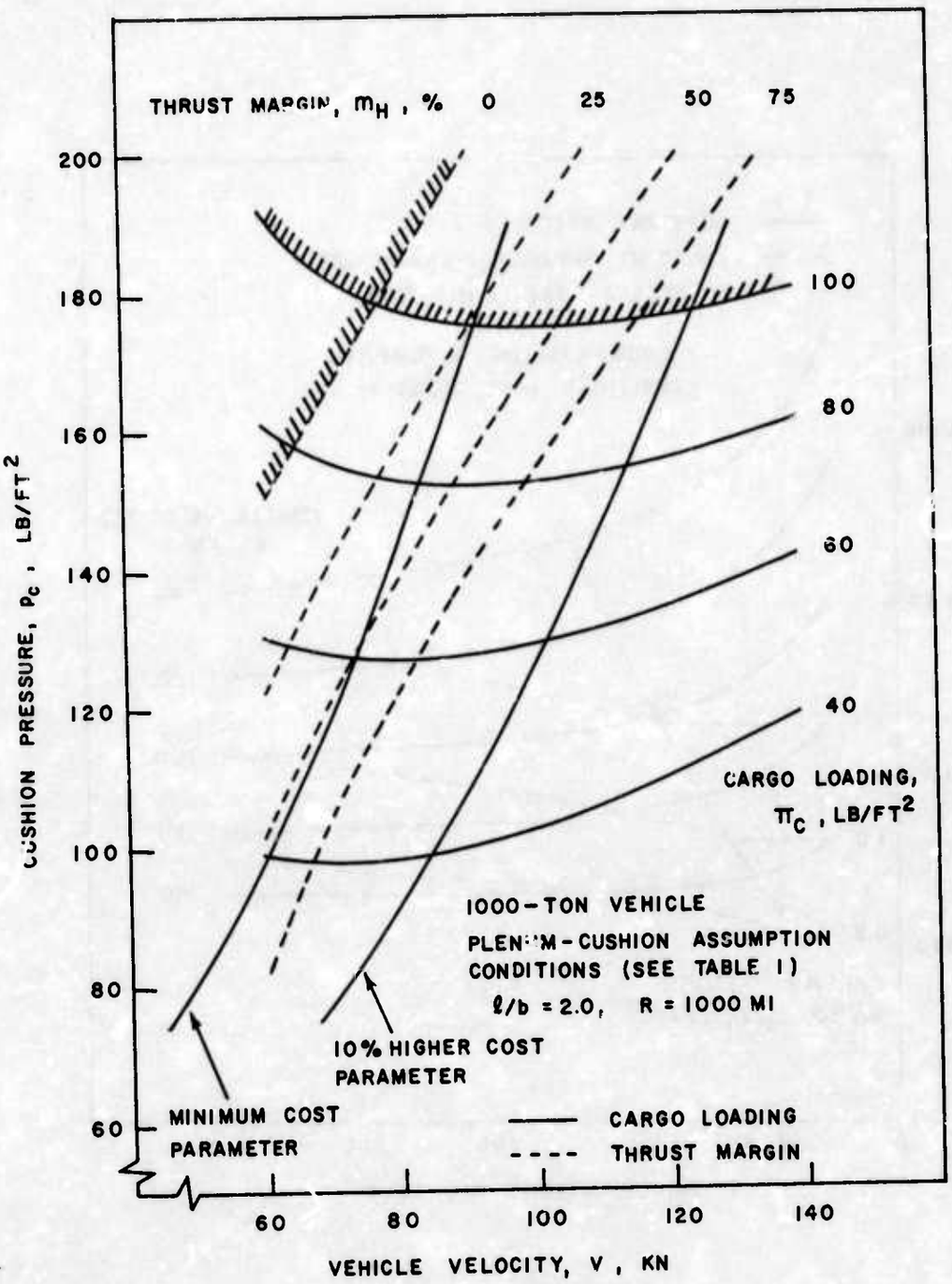


Figure 38
Cargo Loading and Thrust Margin Summary

## CONCLUSIONS

- There exists a minimum total specific power (P/WV) point for given conditions. Increasing the propulsion or decreasing the lift power shifts this minimum specific power to a higher speed parameter and vice versa.

- Lower cushion pressures can be traded off for higher total specific power. A 10% increase in specific power above its optimum will result in doubling the speed parameter or lowering the cushion pressure by 50%.

- The total specific power is most sensitive to the cushion mass flow and pressure coefficients. A 10% improvement of either of these results in a 8% decrease of the total power. A similar improvement in the drag coefficient or propulsion efficiency results in only 2% and 3% lower total power, respectively.

- The fuel fraction requirement of an SEV in general exceeds the results obtained with the Breguet range equation, since the specific power increases as the fuel is burned up and the vehicle becomes lighter. For some very low-speed parameters where the lift power is dominant, the fuel fraction will be less than obtained with the Breguet equation.

- The constant-propulsion/constant-lift power (separate lift and propulsion system) case has a very high fuel fraction requirement, since the constant lift power results in higher daylight clearances and therefore higher momentum drag as fuel is burned up.

- The constant total power/constant daylight clearance case requires a slightly higher fuel fraction for the high-speed parameters and a slightly lower fuel fraction for the lower speed parameters than the constant velocity case.

- Longer ranges shift the minimum fuel fraction point to lower speed parameters. As the range approaches zero, the minimum fuel fraction point approaches the minimum total specific power point.

- Fixing the fuel and power plant weight penalizes the high speeds and shifts the maximum range point to a lower speed parameter. The shift is approximately 10% compared with the constant fuel fraction case.

- High cushion pressure will optimize the vehicle for high cargo loading. Since the general cargo has a cargo loading less than 100 $lb/ft^2$, the cushion pressure is limited to 165 and 120 $lb/ft^2$ for axial and centrifugal fans, respectively.

- Longer ranges decrease the cargo loading at a given cushion pressure, while vehicle speed has only a small impact on the cargo-loading/cushion-pressure relationship.

- The minimum operating cost is found at a speed parameter between 0.12 and 0.19, with lower cargo loading, lower vehicle speeds, and longer ranges producing the lower value of the quoted speed parameter.

- Accepting higher operating cost will shift the desirable operating regime for a given velocity to lower cushion pressures and cargo loadings.

- Above a speed parameter of 0.2, one can obtain an acceptable thrust margin at the low speed drag hump. The thrust margin increases with increasing length/beam ratio, decreasing pressure/length ratio, and decreasing vehicle weight.

- The shrouded propeller has a 40% higher thrust margin than the free propeller.

- The cargo-loading limitation restricts the economic operation regime of the vehicle to below 120 knots at a range of 1000 miles. For longer ranges this maximum velocity increases.

- The thrust margin will become the limiting factor for long-range vehicles.

## RECOMMENDATIONS

- The cargo-loading analysis should be extended to cover other fan arrangements and also tradeoff fan size against efficiency.

- The cargo-loading analysis should include a more realistic fuel consumption formula and better machinery weight approximations.

- The cargo-loading analysis should include a more systematic economic analyis including such items as initial cost, maintenance, manning, etc.

- The specific power analysis should examine the effect of aerodynamic lift on the vehicle.

- The analysis should be expanded to include other considerations, such as roll stability and maneuvering requirements, to help determine the vehicle length/beam ratio and cruise and dash consideration to more realistically size the power plant.

## TECHNICAL REFERENCES


1 - Garrett, J. H., and R. K. Muench, "Analysis of Propulsion and Lift Power Requirements for the Arctic Surface Effect Vehicle," ASME Paper 72-GT-102 (Mar 1972)

2 - Mantle, P. J., "Some Design Aspects of Air Cushion Craft," presented at International Congress of Subsonic Aeronautics, New York, N. Y. (3-6 Apr 1967)

3 - Chaplin, H. R., and A. G. Ford, "Some Design Principles of Ground Effect Machines Section B - Air Cushion Mechanics," DTMB Rept 2121 B (Apr 1966)

4 - Barratt, M. J., et al, "Estimation of Power and Drag for Marine Hovercraft, Review of the State of Art in 1969," National Physical Lab., Hovercraft Unit Rept 10 (Sep 1969)

5 - Bodnaruk, A., and E. Quandt, "Performance Envelopes of Displacement Type Ships and Submarines Using Chemical Propulsion Systems," NSRDC/A Rept 7-781 (Jan 1972)

6 - Purnell, J. G., "Evaluation of Potential Fan Concepts and the Lift Fan Requirements for Large SEV's," NSRDC/A Rept 27-182 (Aug 1972)

7 - Baljé, O. E., and R. L. Binsley, "Axial Turbine Performance Evaluation, Part B - Optimization with and Without Constraints," ASME Paper 68-GT-14 (1968)

8 - Montes de Oca, R. A., and H. M. Simpson, "Nuclear-Powered Surface Effect Ships Design Problems," Journal of Aircraft, Vol. 2, No. 2, pp. 136-143 (Mar-Apr 1965)

9 - Ford, A. G., "Progress in Air Cushion Vehicles," NSRDC R&D Rept 2280 (Oct 1966)

10 - Shank, S. R., Jr., "Propeller Characteristics Related to the Design of Large, High-Speed Surface Effect Vehicles," NSRDC/A Rept 27-142 (June 1972)

11 - Nakonechney, B. V., "A Synthesis of Design Data Relating to Existing and Near-Future Air-Cushion Vehicles," NSRDC R&D Rept 3607 (Mar 1971)

12 - Anon, "Design Criteria for Large Surface Effect Ships," Bell Aerospace Co. Rept 7340-953014 (Jan 1970)

## APPENDIX A

## VEHICLE FUEL FRACTION APPROXIMATIONS

An approximation to the vehicle fuel fraction will be developed in this appendix. The approximation is based on the premise that the velocity change is small and can therefore be expanded and higher order terms can be neglected. Two cases will be treated: (1) the case of constant-propulsion/constant-lift power and (2) the case of constant total power/daylight clearance. The latter case represents the more interesting situation which might actually be encountered in an application.

### Constant-Propulsion/Constant-Lift Power

The specific propulsion power (equation (20) of the text of this report) is:

$$\frac{P_{PR}}{WV} = \frac{C_D}{\eta_{PR}} k + \frac{C_M}{\eta_{PR}} k^{1/2}. \qquad \text{(A-1)}$$

This can be rewritten in terms of constants and the velocity $(V/V_I)$ and weight ratio $(W/W_G)$ as shown in equation (24) of the text:

$$\frac{P_{PR}}{W_G V_I} = \frac{C_D}{\eta_{PR}} k_G \left(\frac{V}{V_I}\right)^3 + \frac{C_{MI}}{\eta_{PR}} k_G^{1/2} \left(\frac{W}{W_G}\right)^{-1} \left(\frac{V}{V_I}\right)^2$$

$$= \frac{C_D}{\eta_{PR}} k_G + \frac{C_{MI}}{\eta_{PR}} k_G^{1/2} = \text{constant}. \qquad \text{(A-2)}$$

Equation (17) of the text was used to substitute k in terms of $k_G$. Also, equation (23) was used to substitute $C_M$ which is affected by the changing weight, since it is required that the lift power remain constant. Now, expanding the velocity ratio in the following manner:

$$\frac{V}{V_I} = 1 + \frac{\Delta V}{V_I} + \cdots . \qquad \text{(A-3)}$$

Substituting this into equation (A-2), expanding the terms, and neglecting terms of $(\Delta V/V_I)^2$ and higher results in:

$$C_D k_G \left(1 + 3\,\frac{\Delta V}{V_I}\right) + C_M k_G^{1/2} \left(\frac{W}{W_G}\right)^{-1} \left(1 + 2\,\frac{\Delta V}{V_I}\right)$$

$$= C_D k_G + C_{MI} k_G^{1/2} \quad . \tag{A-4}$$

Now, solving for the velocity ratio:

$$\frac{V}{V_I} \cong 1 + \frac{\Delta V}{V_I} = 1 + \frac{\left(\frac{W}{W_G} - 1\right)}{3\,\frac{C_D}{C_M}\,k_G^{1/2}\left(\frac{W}{W_G}\right) + 2} \quad . \tag{A-5}$$

The velocity ratio can now be substituted into the range equation, equation (19) of the text, which in turn can be integrated between 1 and $W_X/W_G$:

$$Rc_F\left(\frac{P_T}{W_G V_I}\right) = -\frac{3\frac{C_D}{C_M}\,k_G^{1/2} + 1}{\left(3\frac{C_D}{C_M}\,k_G^{1/2}\right)^2} \left\{ \left(3\,\frac{C_D}{C_M}\,k_G^{1/2}\right)\left(\frac{W}{W_G}\right)\Bigg|_1^{\frac{W_X}{W_G}} + 2 \right.$$

$$\left. - \frac{6\left(\frac{C_D}{C_M}\,k_G^{1/2}\right) + 1}{\left(3\frac{C_D}{C_M}\,k_G^{1/2}\right)} \ln\left[\left(3\,\frac{C_D}{C_M}\,k_G^{1/2}\right)\left(\frac{W}{W_G}\right)\Bigg|_1^{\frac{W_X}{W_G}} + 2\right] \right\} .$$

Substituting the limits and the fuel fraction:

$$X_F = 1 - \frac{W_X}{W_G} \quad , \tag{A-6}$$

and simplifying the terms yields:

$$Rc_F\left(\frac{P_T}{W_G V_I}\right) = X_F + \frac{1}{3\left(\frac{C_D}{C_M} k_G^{1/2}\right)} \left\{ X_F + \frac{3\left(\frac{C_D}{C_M} k_G^{1/2}\right) + 2}{3\left(\frac{C_D}{C_M} k_G^{1/2}\right)} \right.$$

$$\left. \times \ln\left[ 1 - \frac{3\left(\frac{C_D}{C_M} k_G^{1/2}\right)}{3\left(\frac{C_D}{C_M} k_G^{1/2}\right) + 2} X_F \right] \right\}. \qquad \text{(A-7)}$$

If the results of equation (A-7) are compared with the exact results, one will find that differences are very small. This is a result of the small error incurred when expanding the velocity ratio. Figure 1-A shows that the maximum error of the velocity approximation is only 2% in the region of interest (fuel fraction from 0 to 0.5 and initial speed parameter from 0.5 to 1.0). This is not surprising, since in this region the maximum velocity ratio change is less than 17%.

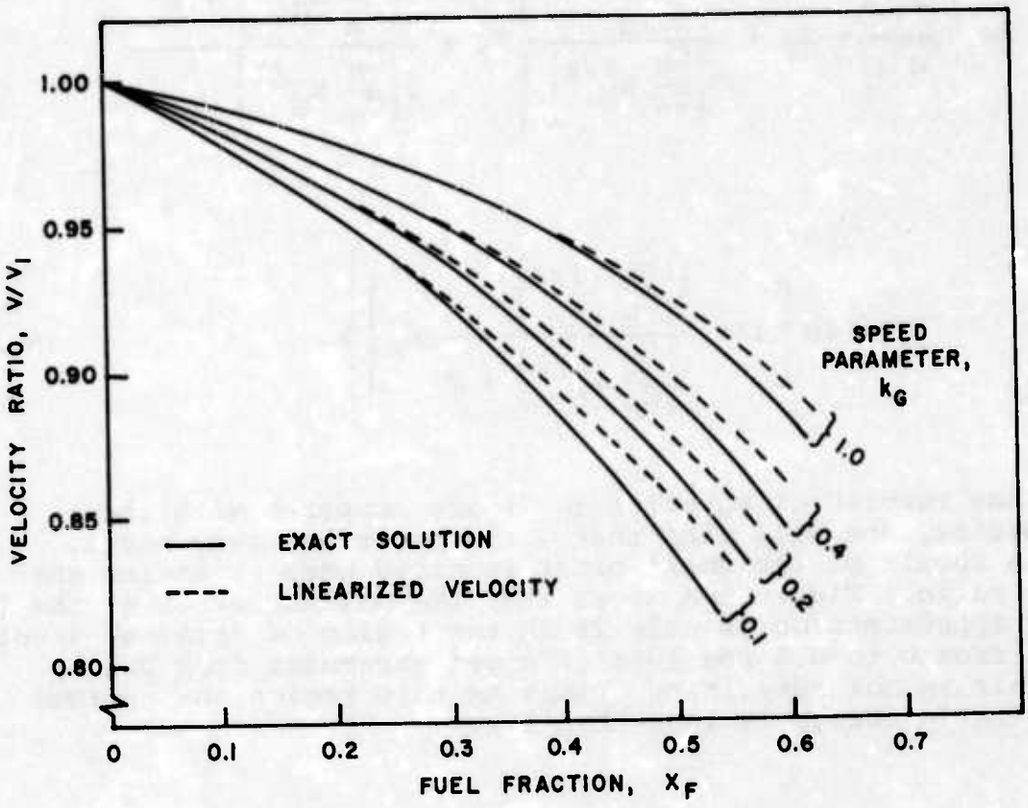


Figure 1-A
Comparison Between Exact and Linearized
Velocity Ratio for Constant-Lift/Constant-
Propulsion Power Case
(Standard Conditions - See Table 1 of the Text)

Constant Total Power/Constant Daylight Clearance

In this subcase the change in velocity ratio is significantly larger especially at a low speed parameter. If it is attempted to use a first order approximation, similar to the above approach, one finds that the velocity ratio will deviate very quickly from the exact solution (see figure 2-A). It will therefore be attempted to use the following second-order expansion for the velocity ratio in terms of the weight ratio ($\Delta W/W_G$):

$$\frac{V}{V_I} = 1 + A\,\frac{\Delta W}{W_G} + B\left(\frac{\Delta W}{W_G}\right)^2 , \qquad (A\text{-}8)$$

where

$$\frac{\Delta W}{W_G} = 1 - \frac{W}{W_G} \quad . \tag{A-9}$$

It should be noted here that the exact solution shown in figure 2-A is obtained via trial and error and is therefore not suitable for the fuel fraction determination.

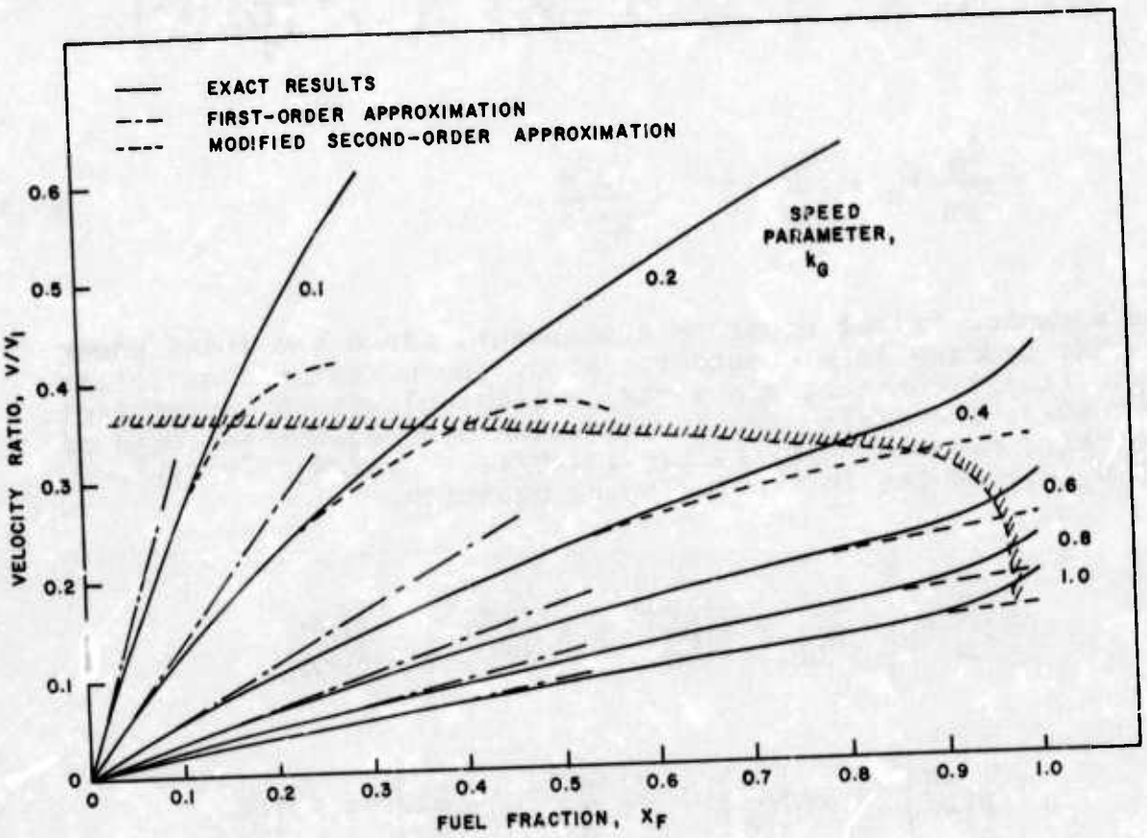


Figure 2-A
Comparison Between Exact and Approximate Velocity Ratio for the Constant-Power/Constant-Daylight Clearance Case
(Standard Conditions - See Table 1 of the Text)

The constants in equation (A-8) can be found after substitution into the equation for the total specific power:

$$\frac{P_T}{WV} = \frac{C_D}{\eta_{PR}} k + \frac{C_M}{\eta_{PR}} k^{1/2} + \frac{C_M C_P}{k^{1/2}} . \qquad \text{(A-10)}$$

Rewriting this similar to equation (A-2):

$$\frac{P_T}{W_G V_I} = \frac{C_D}{\eta_{PR}} k_G \left(\frac{V}{V_I}\right) + \frac{C_M}{\eta_{PR}} k_G^{1/2} \left(\frac{W}{W_G}\right)^{1/2} \left(\frac{V}{V_I}\right) + \frac{C_P C_M}{k_G^{1/2}} \left(\frac{W}{W_G}\right)^{3/2}$$

$$= \frac{C_D}{\eta_{PR}} k_G + \frac{C_M}{\eta_{PR}} k_G^{1/2} + \frac{C_P C_M}{k_G^{1/2}} . \qquad \text{(A-11)}$$

The equation is set equal to a constant, since the total power in this subcase is a constant. Also, the momentum coefficient ($C_M$) remains constant since the daylight clearance is constant. Performing the called-for substitution and neglecting terms of the third order or higher, i.e., $(\Delta V/V_I)^3$, $(\Delta W/W_G)(\Delta V/V_I)^2$, $(\Delta W/W_G)^3$, results in the following equation:

$$3 \frac{C_D}{C_M} k_G \left[ A\left(\frac{\Delta W}{W_G}\right) + B\left(\frac{\Delta W}{W_G}\right)^2 + A^2\left(\frac{\Delta W}{W_G}\right)^2 \right] - \frac{1}{2}\left(\frac{\Delta W}{W_G}\right)$$

$$- \frac{1}{8}\left(\frac{\Delta W}{W_G}\right)^2 + 2A\left(\frac{\Delta W}{W_G}\right) + 2B\left(\frac{\Delta W}{W_G}\right)^2 - A\left(\frac{\Delta W}{W_G}\right)^2 + A^2\left(\frac{\Delta W}{W_G}\right)^2$$

$$- \frac{C_P \eta_{PR}}{k_G} \left[ \frac{3}{2}\left(\frac{\Delta W}{W_G}\right) - \frac{3}{4}\left(\frac{\Delta W}{W_G}\right)^2 \right] = 0.$$

Now, equating the first- and second-order terms to zero gives the following expressions for constants A and B:

$$A = \frac{1}{2} \frac{1 + 3 \frac{C_P \eta_{PR}}{k_G}}{2 + 3 \frac{C_D}{C_M} k_G^{1/2}} \qquad \text{(A-12)}$$

$$\frac{A}{B} = \frac{1 - \left(1 + 3 \frac{C_D}{C_M} k_G\right) A + \frac{1}{8A}\left(1 - 3 \frac{C_P \eta_{PR}}{k_G}\right)}{2 + 3 \frac{C_D}{C_M} k_G^{1/2}} . \qquad \text{(A-13)}$$

Comparing this second-order approximation with the exact solution shows that it underestimates the velocity ratio almost as much as the first-order solution overestimates it. The second-order approximation was therefore modified to read:

$$\frac{V}{V_I} = 1 + A\left(\frac{\Delta W}{W_G}\right) + \frac{3}{4} B \left(\frac{\Delta W}{W_G}\right)^2 . \qquad \text{(A-14)}$$

This approximation is a significant improvement over the first-order approximation.

Substituting the above equation for the velocity ratio into equation 19 and performing the required integration results in:

$$Rc_F \frac{P_{TI}}{W_G V_I} = -\int_1^{\frac{W_X}{W_G}} \left(\frac{V}{V_I}\right)\frac{dW}{W_G} = \int_0^{X_F} \left(\frac{V}{V_I}\right) d \frac{\Delta W}{W_G}$$

$$= X_F + \frac{A}{2} X_F^2 \left(1 + \frac{1}{2} \frac{B}{A} X_F\right) , \qquad \text{(A-15)}$$

or

$$Rc_F \frac{P_{TI}}{W_G V_I} = X_F + \frac{1}{4} \frac{1 + 3 \frac{C_p \eta_{PR}}{k_G}}{2 + 3 \frac{C_D}{C_M} k_G^{1/2}} X_F^2 \left[ 1 + \frac{1}{2} \left( \frac{1}{2 + 3 \frac{C_D}{C_M} k_G^{1/2}} \right.\right.$$

$$- \frac{1}{2} \frac{1 + 3 \frac{C_D}{C_M} k_G^{1/2}}{2 + 3 \frac{C_D}{C_M} k_G^{1/2}} \frac{1 + 3 \frac{C_p \eta_{PR}}{k_G}}{2 + 3 \frac{C_D}{C_M} k_G^{1/2}}$$

$$\left.\left. + \frac{1}{4} \frac{1 - 3 \frac{C_p \eta_{PR}}{k_G}}{1 + 3 \frac{C_p \eta_{PR}}{k_G}} \right) \right] . \qquad \text{(A-16)}$$

As shown in figure 2-A, the approximation for the velocity ratio ($\Delta V/V_I$) can deviate significantly from the exact solution, but the resulting error of the fuel fraction parameter is much less. Due to the integration, the fuel parameter error is less than 0.5% and 2.0% when the velocity ratio ($\Delta V/V_I$) has an error of 10% and 20%, respectively. Difficulties will still be encountered with this approach for small values of the speed parameter. For instance, for a speed parameter of 0.1, the error in the fuel fraction calculation will exceed 10% for fuel fractions larger than 0.3.

INITIAL DISTRIBUTION

| Copies | | Copies | |
|---|---|---|---|
| 1 | OASN (Cdr A. Smith) | 1 | DOT, High Speed Ground Transportation (Mr. A. F. Lampros) |
| 1 | ONR (Code 415) | | |
| 4 | ARPA (Cdr B. Hannula)* | 1 | DOT, Office of Research and Technology |
| 1 | U.S. Marine Corps (RD&S) | 1 | SAMSO (LCol N. F. Finnegan) |
| 1 | U.S. Marine Corps (Dev. & Ed. Comm.) | 1 | NASA Hdqtrs |
| 5 | NAVSHIPS<br>1 (SHIPS 031)<br>1 (SHIPS 03Z2)<br>1 (SHIPS 03421)<br>2 (SHIPS 2052) | 1 | U.S. Naval Academy (J. F. Sladky, Jr.) |
| | | 2 | DDC |
| 1 | SESPO (PM 17) | 1 | Aerojet General Corp. (Mr. Shenfil) |
| 1 | NAVAIR (Code 303B) | 1 | Aerospace Corp. (Mr. R. T. Scott) |
| 1 | NAVSEC (SEC 6110.10) | 1 | Bell Aerospace Co. (Mr. Hite) |
| 1 | NELC (D. Forbes) | | |
| 1 | U.S. Army, MERDC (M&BD) (J. Sargent) | 1 | Boeing Co. (Mr. Miller) |
| 1 | U.S. Army, Res. Office (Dr. V. Zadnik) | 1 | Booz-Allen Applied Research, Inc. (Mr. Willard) |
| 1 | U.S. Air Force, FDL (FEM) (Dr. L. H. Digges) | 1 | Daedalean Associates (Mr. A. Thiruvengadam) |
| 1 | U.S. Air Force Academy (R. W. Gallington) | 1 | Goodyear Aerospace Corp. (Mr. Cross) |
| 1 | U.S. Coast Guard Hdqtrs (R&D) | 1 | Grumman Aerospace Corp. (Mr. Munz) |

*Addressee

27-497, September 1973

INITIAL DISTRIBUTION (cont)

| Copies | |
|---|---|
| 1 | Hamilton Standard (Mr. Deabler) |
| 1 | Oceanics, Inc. (Mr. Kaplan) |
| 1 | Science Applications, Inc. (Dr. C. Whittenberry) |
| 1 | Cornell Univ. (Dr. S. F. Shen) |
| 1 | Johns Hopkins Univ. Applied Physics Lab. (Mr. Paddison) |
| 1 | Univ. of Washington (G. Gray) |
| 1 | Dr. M. G. Bekker |
| 1 | Mr. R. S. Ross |
| 1 | USA, Cold Regions R&D Lab. (Dr. K. F. Sterrett) |
| 1 | Arctic Inst. of North America (Mr. R. Faylor) |

CENTER DISTRIBUTION

| Copies | Code |
|---|---|
| 1 | (11, W. M. Ellsworth) |
| 3 | (113, J. U. Kordenbrock) |
| 1 | (115, R. J. Johnston) |
| 1 | (118, M. W. Brown) |
| 1 | (1572, Mrs. M. Ochi) |
| 1 | (161, E. B. O'Neill) |
| 3 | (1735, R. G. Allen) |
| 1 | (272, Dr. E. Quandt) |
| 20 | (2721, R. K. Muench) |
| 1 | (2803, J. J. Kelly) |
| 30 | (5614) |
| 1 | (9401, Capt C. J. Boyd) |

UNCLASSIFIED

Security Classification

**DOCUMENT CONTROL DATA - R & D**

*(Security classification of title, body of abstract and indexing annotation must be entered when the overall report is classified)*

1. ORIGINATING ACTIVITY (Corporate author)

Naval Ship Research and Development Center
Annapolis, Maryland 21402

2a. REPORT SECURITY CLASSIFICATION

Unclassified

2b. GROUP

3. REPORT TITLE

Arctic Surface Effect Vehicle Program, Preliminary Propulsion and Lift-Power Tradeoff for a Large Surface Effect Vehicle

4. DESCRIPTIVE NOTES (Type of report and inclusive dates)

Research and Development

5. AUTHOR(S) (First name, middle initial, last name)

R. K. Muench

| 6. REPORT DATE | 7a. TOTAL NO. OF PAGES | 7b. NO. OF REFS |
|---|---|---|
| September 1973 | 97 | 12 |

| 8a. CONTRACT OR GRANT NO | 9a. ORIGINATOR'S REPORT NUMBER(S) |
|---|---|
| b. PROJECT NO. ARPA Order 2251 | 4153 |
| c. Program Code 3N10 | 9b. OTHER REPORT NO(S) (Any other numbers that may be assigned this report) |
| d. Work Unit 1-1130-272-20 | 27-497 |

10. DISTRIBUTION STATEMENT

Distribution limited to U.S. Government agencies only; Test and Evaluation; September 1973. Other requests for this document must be referred to Commander, Naval Ship Research and Development Center (Code 11), Bethesda, Maryland 20034.

| 11. SUPPLEMENTARY NOTES | 12. SPONSORING MILITARY ACTIVITY |
|---|---|
| | ARPA |

13. ABSTRACT

To determine the desirable speed and cushion pressure operating region of large surface effect vehicles, a propulsion and lift-power tradeoff study has been made for both overland and overwater operation. In addition, range has been examined as it is related to the associated fuel fraction and cargo-carrying capacity. The power tradeoff study examines the effect of the various drag components and efficiencies at the minimum power. The cargo-carrying study considers the effect of the available payload area and payload weight as a function of cushion pressure. The thrust margin study examines the impact on power requirement for the low-speed wave drag hump. The results generally indicate that cargo-carrying considerations restrict the maximum cushion pressure due to space and the maximum velocity due to cost consideration, while the overwater thrust margin study restricts the vehicle to low cushion pressure and high maximum velocity capability.

(Author)

DD FORM 1 NOV 68 1473 (PAGE 1)

S/N 0101-807-6801

UNCLASSIFIED

Security Classification

| 14 KEY WORDS | LINK A | | LINK B | | LINK C | |
|---|---|---|---|---|---|---|
| | ROLE | WT | ROLE | WT | ROLE | WT |
| Surface effect vehicles | | | | | | |
| Power | | | | | | |
| Cargo | | | | | | |
| Payload | | | | | | |
| Thrust margin | | | | | | |
| Cushion pressure | | | | | | |
| Equations | | | | | | |